2022

Review of Innovative Rehabilitation Techniques for Reinforced Concrete Buildings

Demetrius Karoubas
West Virginia University, dk00023@mix.wvu.edu

Review of Innovative Rehabilitation Techniques for Reinforced Concrete Buildings

Demetrius Karoubas

Problem Report submitted to the
Benjamin M. Statler College of Engineering and Mineral Resources
at West Virginia University
in partial fulfillment of the requirements
for the degree of

Master of Science
in
Civil Engineering

Udaya B. Halabe, Ph.D., P.E., Chair
Hema J. Siriwardane, Ph.D., P.E.
Leslie Hopkinson, Ph.D.

Wadsworth Department of Civil and Environmental Engineering
Morgantown, West Virginia

2022

Keywords: Seismic, Rehabilitation, Strengthening, Reinforced Concrete, Beam, Column, Beam-Column Joints

ABSTRACT

Review of Innovative Rehabilitation Techniques for Reinforced Concrete Buildings

Demetrius Karoubas

Building rehabilitation encompasses the act of repairing damaged structural elements, as well as the upgrading of older buildings to bring them up to modern standards. In recent years, due to the extreme economic and environmental cost of new construction, building rehabilitation is gaining ground as the most viable solution to the problem posed by damaged or substandard buildings. With the constant development of new materials with favorable properties and the improvement of our understanding of earthquakes, new rehabilitation techniques are being developed, improving on the efficiency and effectiveness of older ones.

Reinforced Concrete (RC) buildings are a type of building that emerged in the late 19th century and are designed to sustain controlled damage during earthquakes of certain magnitudes. Since most of the world's modern seismic design codes were developed in the 1980s or later, a large number of existing RC buildings are unable to handle design earthquake loads sufficiently and require seismic upgrading. Additionally, since RC buildings are designed to sustain damage under earthquakes of large magnitudes, they are also often in need of repair. Due to the above facts, the rehabilitation of RC buildings is a crucial part of their life cycle.

In this problem report, innovative rehabilitation techniques for RC buildings developed in recent years are reviewed and presented, including methods for global (structural level) seismic rehabilitation and the element level rehabilitation of RC beams, RC columns, and RC beam-column joints.

ACKNOWLEDGEMENTS

First, I would like to thank my academic and research advisor, Dr. B. Udaya Halabe, for his critical guidance and support towards the achievement of my academic and professional goals, as well as for his assistance in the completion of my Problem Report. I am honored to have had Dr. Halabe as an advisor for my Master of Science in Civil Engineering (MSCE) degree and as an instructor for the "Matrix Method for Statically Indeterminate Structures" course.

I would also like to thank Dr. Hema J. Siriwardane and Dr. Leslie Hopkinson for serving as members of my Advisory and Examining Committee and supporting me in furthering my academic education.

I would like to express my gratitude towards my colleagues Navid Mardmomen, Vladyslav Machul's'ki, Prabal Shrestha, and Joseph R. Virga for their camaraderie and for helping create an environment conducive to study.

I would like to thank the Professors who acted as my course instructors for their contributions to my educational experience. I also wish to acknowledge the Wadsworth Department of Civil and Environmental Engineering and the Statler College at West Virginia University for the financial support I received in the form of tuition waivers during my MSCE degree program.

Finally, I would like to thank my family members, Konstantinos Karoubas, Anastassia Ioannidu, and Emily Karouba, for their indispensable emotional and financial support towards my efforts in furthering my education.

TABLE OF CONTENTS

LIST OF FIGURES

LIST OF TABLES

1 INTRODUCTION

1.1 BACKGROUND

Building rehabilitation is the act of bringing up a damaged or substandard building to a satisfactory level of performance to extend its service life. In recent years, building rehabilitation has been on the rise compared to the construction of new buildings, partly due to the environmental cost but mostly due to the enormous economic cost associated with new construction. In comparison, building rehabilitation is cheaper, less time-consuming, and less intrusive (on the residents' day-to-day lives) solution to the problem posed by damaged or substandard buildings.

Reinforced concrete (RC) buildings are usually multi-story residential, commercial, or public buildings, and they are the most prevalent type of building in high seismic hazard zones of the world, such as southern Europe, Southeast Asia, Japan, and the California region of the U.S.A but can be found all over the world. While modern seismic building codes emerged towards the end of the 20^{th} century and continue being updated, many reinforced concrete buildings were built before that and require strengthening or seismic rehabilitation. Additionally, reinforced concrete buildings are designed to undergo plastic deformations under heavy earthquake loads and require repairs to be brought to their original condition or better. Finally, steel rebar in reinforced concrete structures is susceptible to corrosion, which can significantly reduce the material's strength and needs to be addressed. For the above reasons, the development of efficient and effective rehabilitation methods for RC buildings is essential for their existence.

In this problem report, modern research on strengthening or repairing reinforced concrete structures is presented. The report is divided into the following categories: 1. Global (Structural Level) Seismic Rehabilitation, 2. Rehabilitation of Beams, 3. Rehabilitation of Columns, 4. Rehabilitation of Beam-Column Joints.

1.2 RESEARCH OBJECTIVES

In recent years, a lot of research has been conducted on the topic of building rehabilitation, and multiple innovative rehabilitation methods have been developed. The research objectives for this problem report are as follows:

- To conduct a literature review that highlights interesting new developments on the rehabilitation of RC buildings and their structural elements.
- To provide a compilation of recent advancements in building rehabilitation that can be used for future research and field applications.

1.3 ORGANIZATION

This problem report is organized into six chapters. Chapter 1 presents the introduction to building rehabilitation, highlights its rising importance in the construction industry, and lists the objectives of this report. Chapter 2 presents innovative global (structural level) seismic rehabilitation methods for RC buildings. Chapters 3, 4, and 5 present innovative techniques for the rehabilitation of RC beams, RC columns, and RC beam-column joints, respectively. Chapter 6 presents the conclusions of the literature review and recommendations for future implementation.

2 GLOBAL SEISMIC REHABILITATION TECHNIQUES FOR REINFORCED CONCRETE BUILDINGS

2.1 INTRODUCTION

The process of strengthening certain elements of a building or entire buildings to make them conform with current seismic codes is commonly referred to as seismic rehabilitation. Gkournelos et al. (2021), in their state-of-the-art review, divide the measures for seismic upgrading for RC buildings into local and global (Figure 2.1), and depending on the goals of the seismic rehabilitation, either type of measures, or a combination of the two can be used.

Local measures involve increasing a member's strength and ductility by jacketing them with a variety of materials such as RC, steel, fiber-reinforced polymers (FRP), textile reinforced mortars (TRM), or hybrid jacketing. Compared to RC and steel jacketing, which are more traditional jacketing methods, FRP jacketing offers higher installation speeds, a high strength-to-weight ratio, and a minimum effect on the geometry of the members.

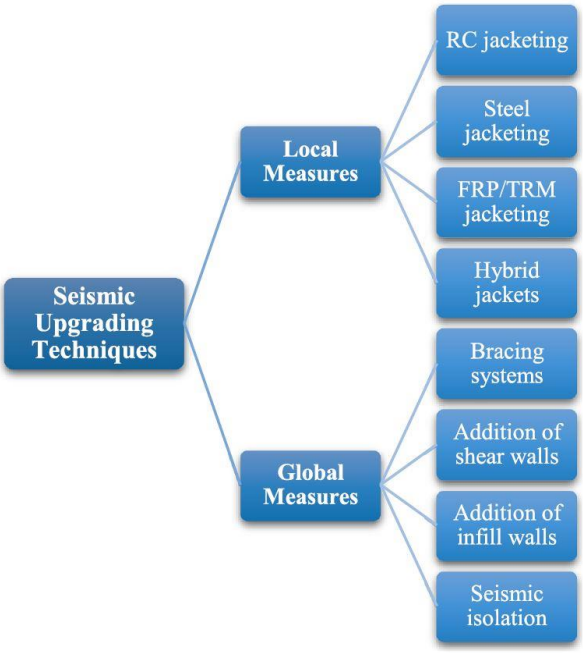

Figure 2.1 Seismic Upgrading Techniques (Gkournelos et al. 2021)

The global measures are focused on either increasing the structure's stiffness and load capacity or reducing the loads on the structure. Methods associated with the first approach involve the addition of structural elements such as concentric and eccentric braces, post-tensioned cables, steel plate shear walls, exoskeletons, RC shear walls, and RC or masonry infill walls. Methods associated with the second approach include seismic base isolation and passive and active energy dissipation systems (Gkournelos et al. 2021).

In this chapter, innovative methods for global seismic rehabilitation measures will be covered, divided into the following subchapters: (a) Masonry infill walls, (b) Seismic dampers, (c) Exoskeletons, (d) Base isolation, while local seismic rehabilitation measures will be covered in subsequent chapters.

2.2 MASONRY INFILL WALLS

2.2.1 INTRODUCTION

The presence of masonry infill walls in RC buildings can have both positive and negative effects on their seismic behavior. Infill walls are non-load bearing walls that are typically used between rooms as separation, and as outer walls to protect the building from the environment (Figure 2.2). The addition of infills to a frame contributes positively to the seismic behavior of the frame by increasing its lateral stiffness, lateral strength, and energy dissipation.

Figure 2.2 Masonry infill wall (Sharbatdar and Tajari 2021)

However, it also increases the total earthquake load applied to the building and can cause the brittle shear failure of columns due to increasing the shear column demand at the column-end region or due to causing short column effects (Pardalopoulos et al. 2018). With careful planning, the addition of masonry infill walls to a building can lead to an upgrade in seismic performance, as well as in thermal performance if the appropriate insulation is applied. The four recent studies presented in this chapter propose methodologies for seismic and thermal retrofitting of RC buildings by adding, replacing, or jacketing masonry infill walls.

2.2.2 SEISMIC REHABILITATION OF SUBSTANDARD R.C. BUILDINGS WITH MASONRY INFILLS (PARDALOPOULOS ET AL. 2018)

Pardalopoulos et al. (2018) studied the effect of adding masonry infills to RC buildings as a rapid seismic rehabilitation measure and developed design charts for calculating the total area of masonry walls that need to be added for several scenarios. This measure can be particularly effective for older pilotis-type RC structures, where the structure has no infill walls at the perimeter of the ground level, and the difference in stiffness between different floors is significant.

The authors' design charts are based on the Inter-story Drift Spectra (IDS) representation, developed by Thermou and Pantazopoulou (2011), which is a tool for relating the drift demand and the required stiffness under the lateral movement of the building. The authors developed equations that relate the Inter-story Drift of the 1^{st} floor, the Peak Ground Acceleration of the seismic motion, and the composite floor area ratio of vertical members of the 1^{st} floor, by using the type I elastic spectrum of the Eurocode (EN 1988-1, 2004), the conservative soil class B, and algebraic manipulations. By using the above equations and the Peak Ground Acceleration (a_g) associated with the 3 seismic zones in Greece, with a_g=0.16g for Zone 1, a_g=0.24g for Zone 2, and a_g=0.36g for Zone 3, the authors were able to develop the following design charts.

The charts in Figure 2.3 (Left) can be used for analysis or rehabilitation purposes, either to determine the Inter-story Drift for a given composite floor area ratio of vertical members (RC columns and masonry walls) or to determine the area of masonry walls that need to be added to achieve the desired Inter-story Drift. The charts in Figure 2.3 (Right) can be used to determine the required area of masonry walls that needs to be added to a given area of columns, to achieve a desired Inter-story Drift for a two-story building.

To test their method, the authors performed dynamic analysis, using the OpenSees finite element software, on 8 multi-story pilotis-type RC buildings built in the early 1980s in Greece, before and after the addition of masonry infill walls at the first story level. The buildings were tested against the acceleration data of a group of 10 strong earthquakes that occurred in Greece between 1978 and 2014. The authors' goal when planning the rehabilitation of these buildings was to have the Inter-story Drift of the first floor not exceed 0.5%. The results of the analysis were that in the 49 cases where the ID1 of the as-built buildings exceeded 0.5% and rehabilitation was required, only in 6 cases the ID1 of the rehabilitated building exceeded 0.5%. Even in those cases, however, ID1 did not exceed 0.6%.

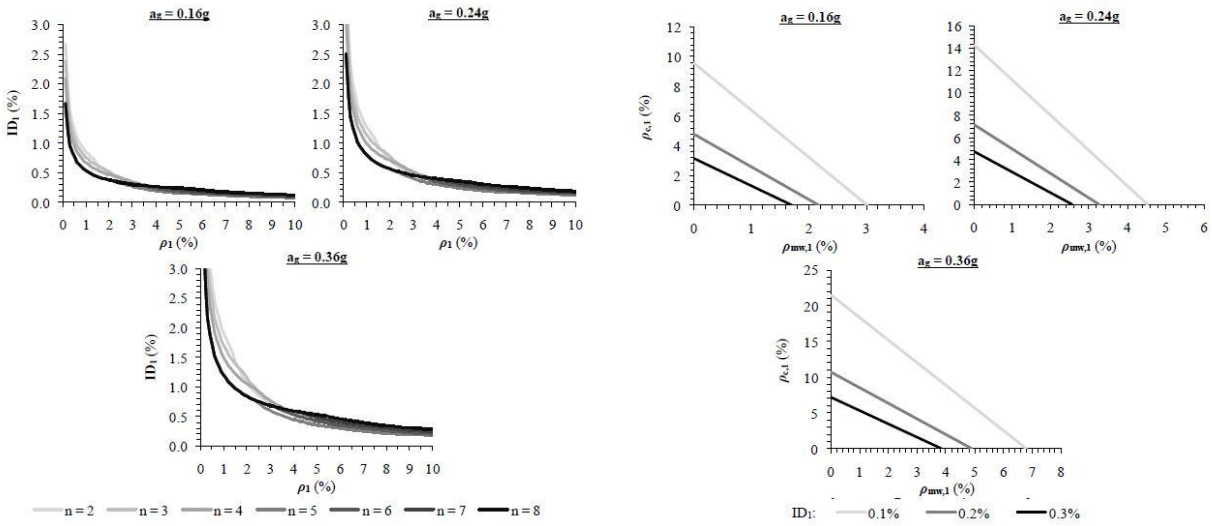

Figure 2.3 Left: Design charts that relate the required composite floor area ratio of vertical members to the inter-story drift demand ratio for a mass per unit area of the floor, γ=1.0 t/m^2, for ag=0.16, 0.24, and 0.36g (Pardalopoulos et al. 2018)

Right: Design charts that relate the various combinations between $\rho_{c,1}$: column area ratio, and $\rho_{mw,1}$: masonry wall area ratio, for target inter-story drift values ranging between 0.1 and 0.3%, for n=2, γ=1.0 t/m^2 and ag=0.16, 0.24 and 0.36g. (Pardalopoulos et al. 2018)

Based on the results of the analysis, Pardalopoulos et al. (2018) believe that their method is a cost-efficient and effective way of rehabilitating pilotis-type RC buildings, but propose further studies to be made on the contribution of masonry infill walls in triggering local shear failures in the adjacent RC columns.

2.2.3 SEISMIC STRENGTHENING AND ENERGY EFFICIENCY: TOWARDS AN INTEGRATED APPROACH FOR THE REHABILITATION OF EXISTING RC BUILDINGS (MANFREDI ET AL. 2018)

Manfredi et al. (2018), motivated by the need for seismic and thermal rehabilitation in more than 75% of the buildings in Italy, studied the mechanical and thermal properties of infill walls and worked on developing an integrated thermal and seismic rehabilitation method for RC buildings. They observed that while older masonry materials had low thermal transmittance (U) and compressive strength (f_c) values, newer materials, with sufficient thickness, have significantly higher U and f_c values. They proposed a combined thermal and seismic rehabilitation program, where the following three configurations are considered for the target building:

- C1: as-built;
- C2: replacing the existing infill walls with more energy-efficient ones;
- C3: adding new external RC frames and connecting them to the existing ones.

They applied their proposal by analyzing, according to Italian regulations, the above three configurations for a six-story Italian building (Figure 2.4), built post-1971 with two-layer brick masonry infill walls. Concerning the masonry wall properties, their total thickness was 30 cm, their Thermal Transmittance was approximately U = 1.50 W/m^2K, and their compressive strength was approximately f_c = 2.0 MPa (290 psi).

The Italian energy efficiency regulations require for infill walls, a thermal transmittance value between 0.45 and 0.28 (W/m^2K) depending on the climatic zone of the building. The Italian seismic design regulations assign a seismic demand for Damage Limitation (DLLS) and Life Safety (LSLS) Limit States based on the seismic zone the structure is located in, while the seismic capacity of the structure in both directions and Limit States can be evaluated with the Incremental Dynamic Analysis (IDA), where the structure is subjected to accelerograms of increasing intensity up to collapse.

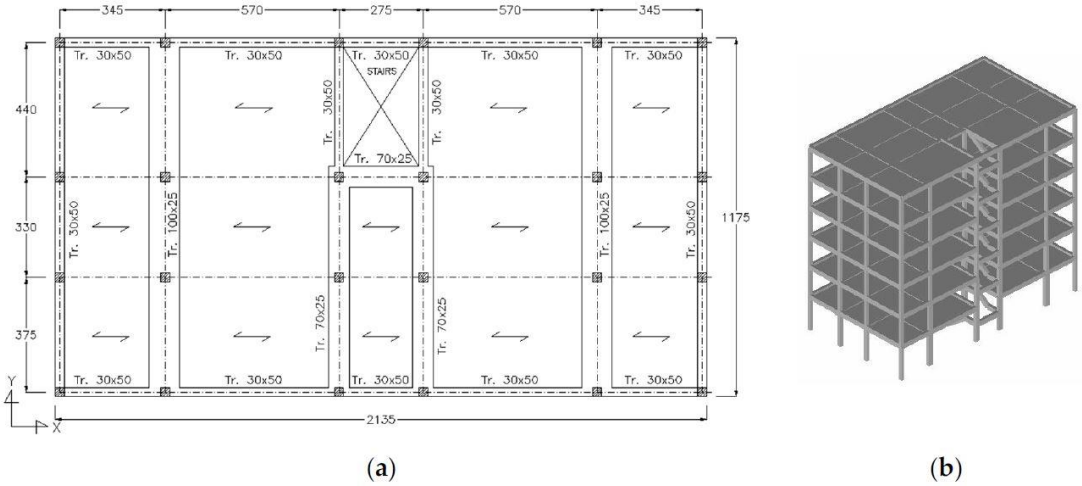

Figure 2.4 (a) Floor plan of the building of study, (b) 3D view of the model. (Manfredi et al. 2018)

For configuration C2 the authors replaced the existing two-layer brick infill walls with a modern 20cm thick cored brick with 8cm glass wool insulation, that has a thermal transmittance U = 0.28 (W/m^{2}K) and compressive strength f_c = 4.0 MPa (580 psi), while for configuration C3 they added new RC frames along the north, east and west faces of the building, infilled with the same type of masonry as configuration C2.

The results of the analysis showed that the as-built configuration (C1) had insufficient thermal performance and insufficient seismic capacity for the mid and high seismic zones, configuration C2 had sufficient thermal performance and seismic capacity for low and mid seismic zones, and configuration 3 had sufficient performance in all cases.

The authors concluded that according to the results of the analysis, both seismic and thermal rehabilitation can be achieved by replacing old masonry infill walls with newer ones, in all cases but the ones with the highest seismic demand. They also suggested that further studies need to be carried out on the effect of adding stiffer infill walls on existing RC beams, columns, and beam-column joints.

2.2.4 SEISMIC REHABILITATION OF RC BUILDINGS BY JACKETING MASONRY INFILL WALLS (KOUTAS ET AL. 2015), (POHORYLES ET AL. 2020), AND (SHARBATDAR AND TAJARI 2021)

Jacketing masonry infill walls of RC buildings can have a positive impact on their seismic performance. Koutas et al. (2015) studied the effect of jacketing masonry infill walls on the seismic performance of substandard RC buildings by testing two nearly full-scale three-story RC frames under lateral cyclic loading, with and without TRM jacketing of the infills. The strengthening procedure that they applied to the infills and the end sections of the columns can be seen in Figure 2.5. Each TRM layer applied on the faces of the infills had a thickness of approximately 3 mm and was comprised of polymer-coated e-glass fiber 10x10 mm (3/8" x 3/8") rovings with a tensile strength of 115 kN/m (7.88 kip/ft) and ultimate strain of 2.5% and a fiber-reinforced cement-based mortar with a compressive strength of 18.9 MPa (2.74 kip) and a flexural strength of 4.3 MPa (624 psi).

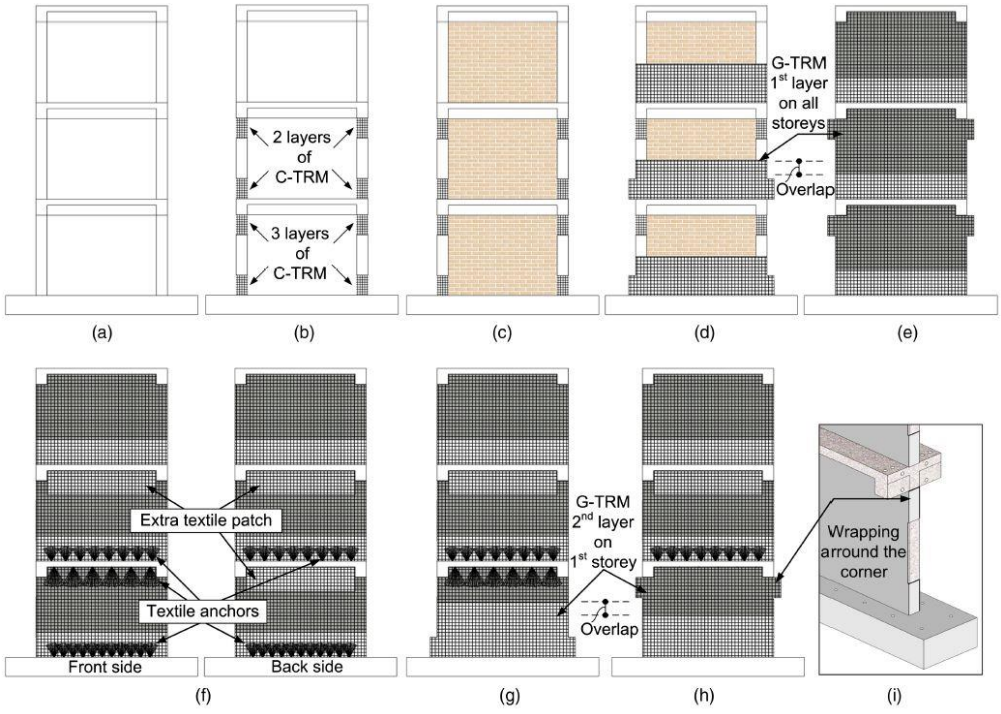

Figure 2.5 Strengthening scheme application steps: (a) bare frame; (b) shear strengthening of first and second story columns at shear-critical regions; (c) infilling with masonry; (d) application of first TRM layer on the face of masonry infills, bottom part of the textile; (e) application of first TRM layer on the face of masonry infills, top part of the textile; (f) application of textile anchors and extra textile patches on the front and back side of the specimen,

respectively; (g) application of second TRM layer on the faces of first story masonry infill, bottom part of the textile; (h) application of second TRM layer on the faces of first story masonry infill, top part of the textile; (i) wrapping of the overhanging textile parts around the column corner (Koutas et al. 2015)

The results of the lateral cyclic loading tests showed a 56% increase in the lateral load capacity, a 52% higher deformation capacity at the top of the frame, and a 22.5% increased energy dissipation in the strengthened frame, compared to the reference frame. Koutas et al. (2015), in their conclusion, noted the importance of a sufficient connection existing between the infill wall and the frame, such as the textile anchors used in their study, since it delays or even prevents the debonding of TRM.

Pohoryles et al. (2020) based on the previous study by Koutas et al. (2015), investigated the viability of a combined thermal and seismic retrofitting method for buildings, considering the European Union's energy saving and decarbonization goals for 2030 and 2050. After studying the climate and earthquake data of twenty big European cities, as well as the age and type of most of their buildings, they proposed a combination of TRM jacketing and thermal insulation with mineral wool or polystyrene layers, to be applied on the masonry walls of masonry and RC buildings. While their research was mostly focused on the thermal aspect of the rehabilitation, they conducted an economic analysis of a combined thermal and seismic rehabilitation by weighing the total cost of the rehabilitated buildings against the energy savings and the reduction in expected annual losses due to earthquake damage, in 2030, in all seismic and climate zones in their study. They concluded that the combined rehabilitation approach paid back its investment faster than either individual seismic or thermal rehabilitation in every case.

Sharbatdar and Tajari (2021) considered using engineered cementitious composites (ECC), which are a type of high-performance fiber-reinforced cementitious composites with a low fiber volume fraction (<2%), for the seismic rehabilitation of infill masonry walls of RC buildings (Figure 2.6 Left). They tested four 1/3 scale, low ductility RC frames under cyclic lateral loading, of which the first one was not infilled (BF), the second one had a plain masonry infill wall (IF-E0), and the other two had a masonry infill wall reinforced with ECC, in one (IF-SF-E20) and in both (IF-SF-E20-2) of its faces respectively. The ECC used for reinforcing the walls was a mixture of type II, developed by Kim et al. (2003) with a fiber volume fraction of V_f = 1.5% Polyvinyl Alcohol (PVA) fibers, a mean compressive strength of f_c = 26.86 + 2.23 MPa (3900 + 320 psi), and a mean tensile strength of f_t= 2.84 MPa (410 psi) at first crack. Before

applying the 20 mm (7/8”) ECC layers to the reinforced frames, the authors drilled holes in the infill walls and the concrete beams and columns and installed screws and shear dowels (Figure 2.6 Right) to provide sufficient anchoring between the frame and the ECC layers.

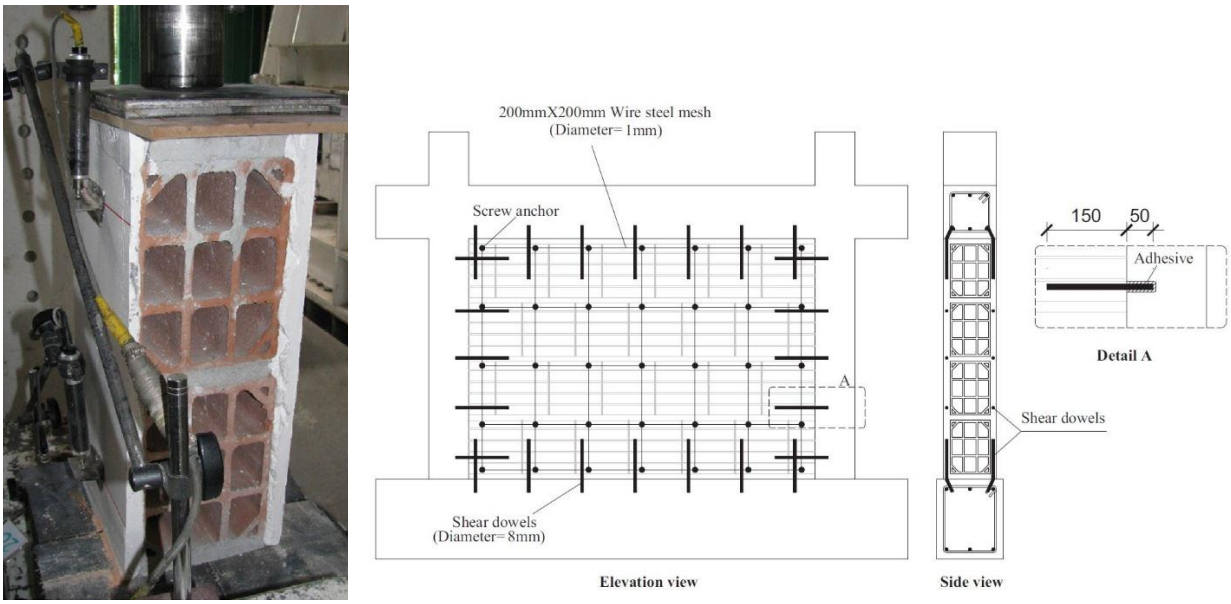

Figure 2.6 Left: ECC jacketed masonry. Right: Retrofit design of the infilled RC frames. (Sharbatdar and Tajari 2021)

The results showed that, compared to the unreinforced infilled frame IF-E0, the reinforced frames IF-SF-E20 and IF-SF-E20-2, had 1.89 and 3.21 times the lateral load capacity, 1.00 and 1.32 times the initial lateral stiffness, and 0.86 and 2.02 times the cumulative energy dissipation respectively (Figure 2.7). The reduced energy dissipation of the IF-SF-E20 frame was due to an early shear failure of the infill wall (Figure 2.8), which also led to a reduced maximum displacement of 13.16 mm (4/8”) compared to 19.86 (6/8”) of the IF-E0, while the IF-SF-E20-2 had 28.90 mm (1 1/8”).

The ECC reinforcement also caused a reduction in the deterioration of the lateral stiffness of the frames, prevented severe local damages, and partially maintained the infill wall’s integrity. Finally, the authors compared their test results with different analytical models for estimating an RC frame’s initial stiffness and lateral load capacity and concluded that the Masonry Standard Joint Committee, the FEMA (2000), and the New Zealand seismic assessment standard methods had sufficient accuracy in predicting the initial stiffness, while the ASCE/SEI 41 (2017) method accurately predicted the lateral load capacity, but heavily overestimated the initial lateral load capacity.

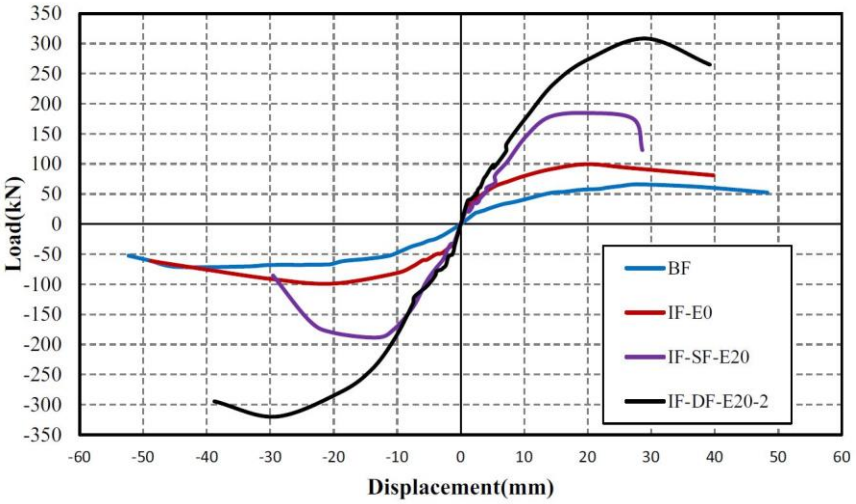

Figure 2.7 Load-displacement curves of test specimens. (Sharbatdar and Tajari 2021)

Figure 2.8 Left: Early shear failure of specimen IF-SF-E20. Right: Specimen IF-DF-E20-2 at failure. (Sharbatdar and Tajari 2021)

2.3 EXOSKELETONS

2.3.1 INTRODUCTION

Much like an animal's exoskeleton, which is the external armor that protects the internal organs, a building's exoskeleton consists of structural elements located in its perimeter that protect the building by insulating it and carrying vertical and lateral loads. According to the state-of-the-art review by Di Lorenzo et al. (2020), exoskeletons have been used for the seismic retrofit of buildings since the 1980s by increasing their lateral strength and stiffness.

In contrast with all other global seismic rehabilitation methods, which involve the addition of structural elements within the perimeter of the building, exoskeletons are added externally, giving them unique advantages and disadvantages. The greatest disadvantage of exoskeletons is that their installation depends on the availability of sufficient space since they increase the volume of the building. They alter the external image of a building, which is an architectural choice, desirable in some cases and undesirable in others, while also providing an opportunity for upgrading the building's energy performance. Their biggest advantage is that since they are applied externally, they do not inhibit the usage of the building during installation.

In this chapter, three innovative methods of seismic rehabilitation with the use of steel and RC exoskeletons will be presented.

2.3.2 SEISMIC RETROFIT OF RC BUILDINGS USING SELF-CENTERING PC FRAMES WITH FRICTION-DAMPERS (ELDIN ET AL. 2020)

Eldin et al. (2020) proposed the use of pre-cast, post-tensioned concrete frames, equipped with friction dampers, attached externally to the perimeter of RC buildings, as a seismic rehabilitation measure. According to the authors, the use of post-tensioned concrete gives the frame a self-centering ability, which allows it to behave elastically under a design-level earthquake, reduces residual drift, and, in combination with the energy dissipation provided by seismic dampers, produces an ideal flag-shaped hysteresis curve. To validate their method, they tested an RC frame under lateral cyclic loading, before and after retrofit, and used finite element software to analyze a three-story, a five-story, and an eight-story RC building before and after being retrofitted by their method.

The proposed pre-cast concrete (PC) frame includes two columns and two beams, at both ends of the columns, connected between them by post-tensioned steel tendons and reinforced grout at their interface (Figure 2.9 Left). The PC frame is equipped with rotational friction dampers at the beam-column joints of the top beam and connected to the RC frame with horizontal anchor rods that penetrate the beam-column joints of both frames.

The lateral cyclic loading test was conducted on an RC frame with 300x300x2850 mm (1x1x9.35 ft) columns and 300x350x2100 mm (1x1-2x6-11 ft) beams made of concrete with a compressive strength of 22 MPa (3.2 ksi), strengthened by a PC frame with columns and beams of similar dimensions, made of concrete with a compressive strength of 40 MPa (5.8 ksi) (Figure

2.9 Right). The steel reinforcement of the RC frame for both columns and beams, consisted of eight 22 mm (#7) diameter 400 MPa (58 ksi) steel rebar, while for the PC frame it was twelve 22 mm (#7) diameter 500 MPa (72 ksi) steel rebar and two seven-wire steel tendons for each PC beam, with 15.2 mm (5/8") diameter, 1600 MPa (232 ksi) yield strength, and 146 kN (33 kip) pre-tensioning force.

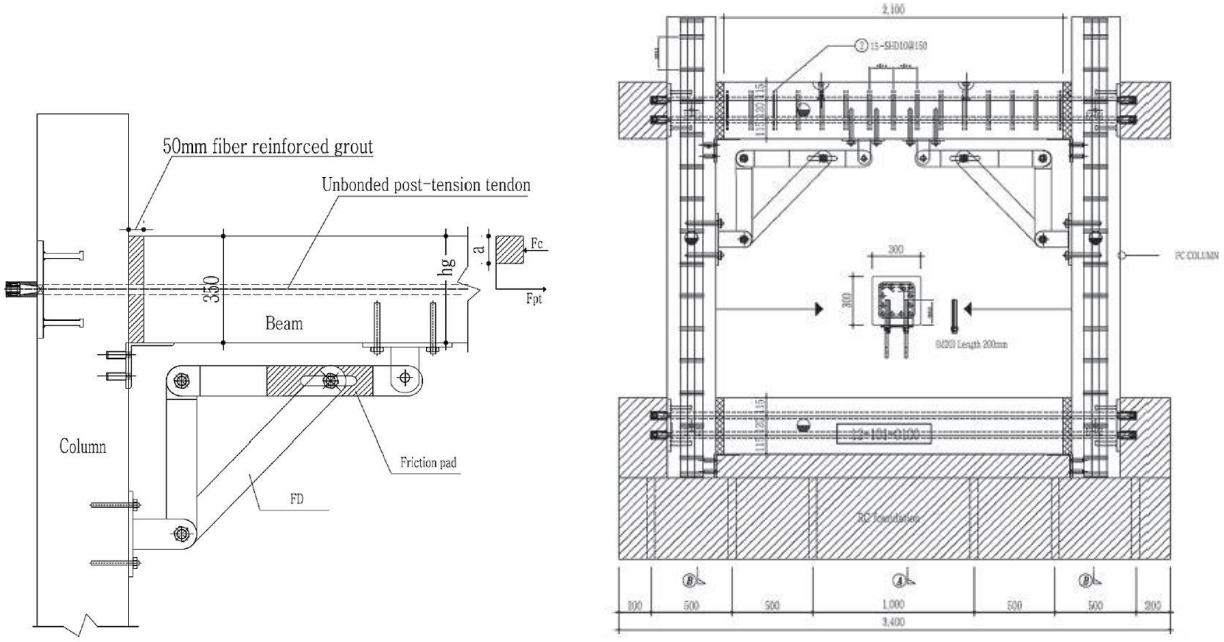

Figure 2.9 Left: Sketch of the beam-column joint of the PC frame (Eldin et al. 2020)
Right: Configuration of the PC frame of the test specimen (Eldin et al. 2020)

The friction dampers consisted of friction pads at the slotted and knee parts, held together by clamping forces of 135 kN (30 kip) and 100 kN (22.5 kip) respectively, that achieved a yield force of about 50 kN (11 kip). The results of the strengthened frame compared to the bare RC frame showed an increased lateral stiffness, a 40% increased lateral strength, a similar yield strain at 30 mm deformation, and a 20% higher ultimate strain at 60 mm, which indicate a higher ductility and energy dissipation.

They then used the OpenSees finite element software to model a three, five, and eight-story RC building, with and without the proposed retrofit measure, and conducted non-linear dynamic analyses with records from seven earthquakes and incremental dynamic analyses with records from thirty earthquakes. Intending to reduce inter-story drift below 2%, the rehabilitation procedure involved installing the self-centering PC frames with friction dampers in the perimeter

of the modeled buildings, with the optimal yield strength of the friction dampers at each story of the buildings determined by a genetic algorithm. The results of the non-linear dynamic analyses showed the desirable flag-shaped hysteresis curve (Figure 2.10) and a significant reduction in the inter-story drift of the first floor in all cases, achieving the goal of the rehabilitation in all but the three-story building affected by the Northridge earthquake, where the inter-story drift of the first floor was reduced from 4% to 2.5%. The results of the incremental dynamic analyses showed improved fragility curves for the retrofitted buildings, with lower probabilities of reaching 1, 2, and 3% inter-story drift in all cases.

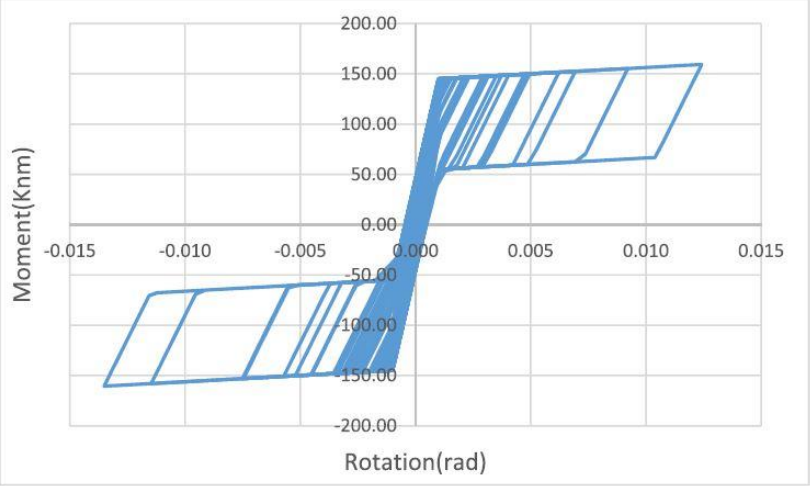

Figure 2.10 Flag-shaped hysteresis curve of the first floor of the 5-story building under the Loma Prieta earthquake. (Eldin et al. 2020)

The authors conclude by bringing attention to the fact that, while their method can reliably reduce the inter-story drift of the superstructure, it also causes an increase in dead loads at the foundation and earthquake loads at the base of the building. When their method is applied, they suggest the safety of the foundation be checked and reinforced if needed.

2.3.3 SEISMIC PERFORMANCE OF EXOSKELETON STRUCTURES (REGIO ET AL. 2019)

Regio et al. (2019) studied the behavior and viability of exoskeleton structures as a form of seismic rehabilitation, focusing on a rigid connection between the exoskeleton and the existing building, as opposed to the more commonly studied dissipative connection. While the goal of

exoskeletons with a dissipative connection is to limit the damage to the existing structure by absorbing the energy of the seismic motion through the relative movement between the primary structure and the exoskeleton, the goal of exoskeletons with a rigid connection is to be sacrificial structural members that absorb the seismic loads in order to protect the primary structure. The authors first define how the coupled structure should be modeled and then apply their design to a substandard RC building located in a high seismicity area in Italy.

The general form of the model proposed by the authors is that of two oscillators: one primary (existing building) and one secondary (exoskeleton), coupled by a rigid connection (K→∞) as can be seen in Figure 2.11.

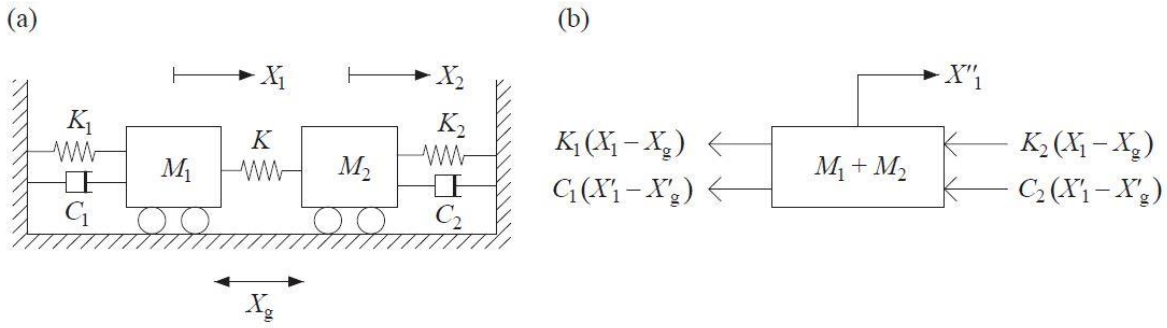

Figure 2.11 Coupled primary-secondary oscillator system (a) Structural model, (b) Free body diagram in case of K→∞. (Regio et al. 2019)

Assuming a rigid connection, a constant mass ratio for the secondary oscillator μ=0.05 and damping ratios ζ1=ζ2=0.05 for both oscillators, analysis of the displacement and acceleration response of the system revealed that frequency ratios of value α>1 cause a decrease in the displacement response and an increase in the acceleration response of the coupled system. In terms of transmitted force, values of frequency ratios α>1 cause an increase in the total transmitted force in the coupled system and a decrease in the force transmitted through the primary oscillator (existing building) when compared to the uncoupled primary oscillator. Further analysis showed that increasing the mass ratio μ, as well as the frequency ratio α of the secondary oscillator causes an additional decrease of the force transmitted through the primary oscillator and an increase of the force transmitted through the secondary oscillator.

The object of the case study is a 4-story, 4-by-2 bay RC building with substandard earthquake detailing that the authors decided to rehabilitate by adding an S235 steel exoskeleton

of HE100A columns and 114.3mm×5mm (4 4/8”x1/8”) diagonal beams (Figure 2.12). The uncoupled and coupled building models were developed with the OpenSees FEM module within the CDS WIN structural analysis software, with the exoskeleton being connected to the existing building by rigid connections at each floor level in the coupled building model.

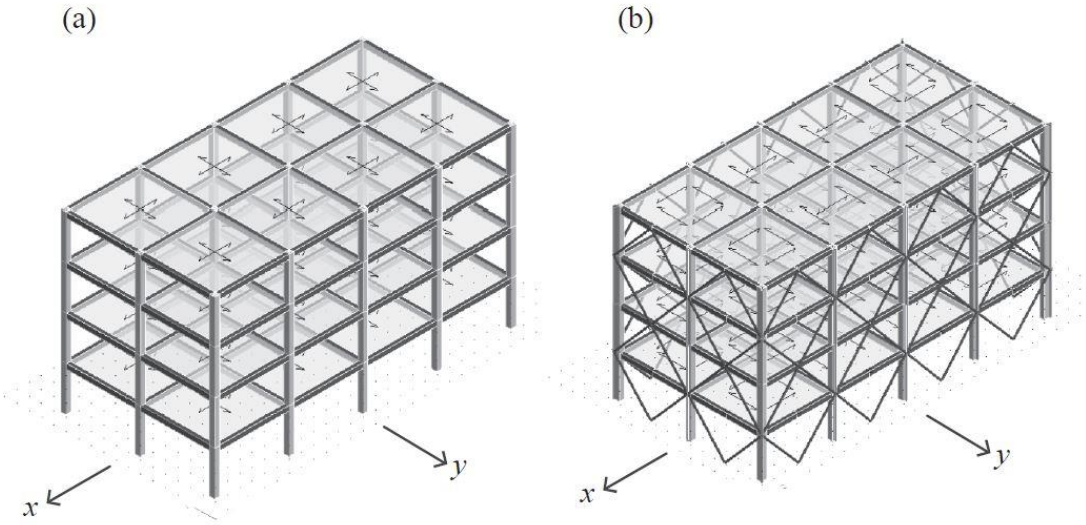

Figure 2.12 3D views of the FE models of (a) Primary building, (b) Coupled primary-exoskeleton building. (Regio et al. 2019)

The mass and frequency ratios of the exoskeleton in the x-direction are μ=0.0087 and α=19.10, while in the y-direction they are μ=0.0085 and α=13.50. Seismic input for the analysis was selected as defined by the Italian Building Code for high seismicity areas: ag=0.082g for the Damage Limitation (DLLS) and a_g=0.249g for the Life Safety (LSLS) Limit States.

The results of the analysis for the coupled primary-exoskeleton building were a decrease in displacements and inter-story drift, an increase in the total shear force applied to the coupled system with a decrease in the force applied to the primary building, and an increase in the peak acceleration in all floor levels. The displacement reductions are particularly significant since they were 40-50% on average, while the reductions in inter-story drift reached up to 75%. The increase in peak acceleration is the expected trade-off for the displacement reduction and should be taken into consideration during design. The authors conclude by pointing out that while their research proved the effectiveness of exoskeletons with rigid connections as a seismic rehabilitation measure, further research, with multi-objective optimization for cost and performance, needs to be performed to determine its efficiency.

2.3.4 THE HIGH-PERFORMANCE DISSIPATING FRAME (HPDF) SYSTEM FOR THE SEISMIC STRENGTHENING OF RC EXISTING BUILDINGS (MANFREDI ET AL. 2021)

Manfredi et al. (2021), motivated by the need for seismic rehabilitation for a large portion of the RC building stock in Italy, proposed a rehabilitation method involving a pre-cast RC exoskeleton with enhanced dissipating capabilities due to the addition of shear and flexural dampers.

The pre-cast RC exoskeleton proposed in this article, referred to as the High-Performance Dissipating Frame (HPDF), is based on an original solution patented by the authors and presented in a previous article (Manfredi et al. 2018). The original solution consisted of pre-cast RC beam-column joint elements, with each element carrying half the span of its respective beams and columns and connecting with other elements through rigid steel connections. The exoskeleton would be based on a new foundation, independent from the existing structure's and it would be connected to the existing structure via shear connectors with epoxy resin at the beam-column joints (Figure 2.13 Left). The newer, improved solution replaces certain rigid connections with dissipating ones, namely the ones at the midspan of the beams with shear hinges and the ones at the base of the columns with flexural hinges while keeping the rest of the original solution intact (Figure 2.13 Right).

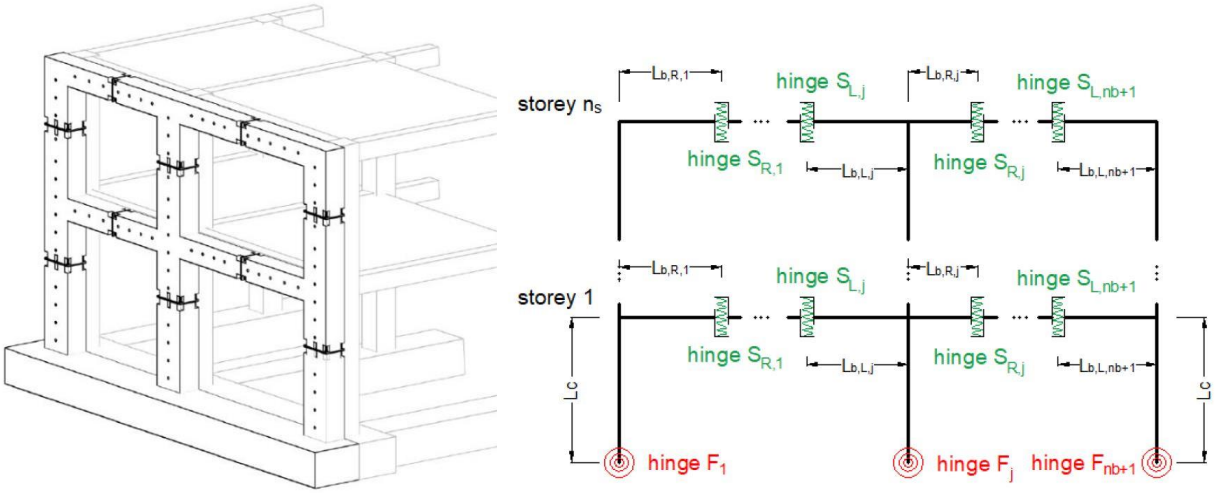

Figure 2.13 Left: 3D view of the exoskeleton of the original solution (Manfredi et al. 2021)
Right: Locations of the shear (green) and flexural (red) hinges for a multi-bay multi-story HPDF frame (Manfredi et al. 2021)

The authors explain that, while the load capacity of the exoskeleton can be determined by the design of the pre-cast RC members, the stiffness and the inter-story drift of the exoskeleton and the retrofitted existing building depend on the yield point of the flexural and shear hinges. The displacement-based procedure they propose for the design of the hinges is summarized in Figure 2.14 and uses an iterative procedure along with results from non-linear static analyses (push-over) of the existing and the rehabilitated building in order to determine the actual damping ratio of the building for a given yield point of the hinges.

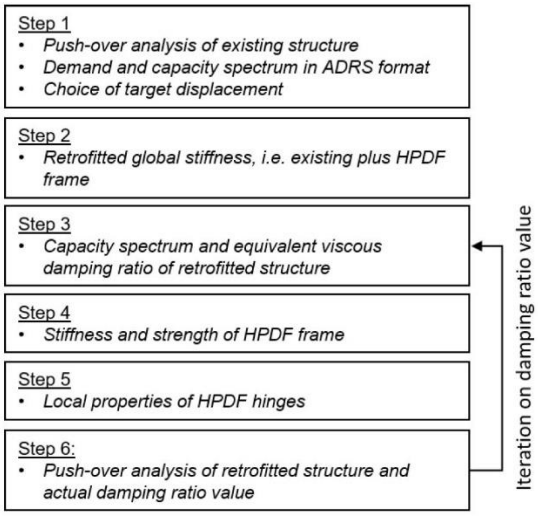

Figure 2.14 Design procedure for the HPDF (Manfredi et al. 2021)

They simulated a simple single-bay, single-story HPDF rehabilitated RC building using the FEM OpenSees software and observed that, when using the same amount of normalized stiffness for both flexural and shear hinges, the amount of energy dissipated by the shear hinges was double that of the flexural ones, highlighting the influence of shear hinges on the effectiveness of the proposed method. The authors conclude by mentioning that laboratory testing, as well as application to real buildings, is needed for the validation of their method and that it is planned for the near future.

2.4 SEISMIC DAMPERS

2.4.1 INTRODUCTION

Seismic dampers are mechanical components whose purpose is to absorb seismic energy in place of the structural elements and to reduce the deformations of a building during an earthquake. Depending on the principles by which they work, seismic dampers are divided into the following categories (Hamakareem 2019):

i. Viscous Dampers, which absorb energy using a silicon-based fluid passing through a piston-cylinder arrangement and are commonly used in high-rise buildings,
ii. Viscoelastic Dampers, which use layers of viscoelastic materials between steel plates sliding against each other to convert mechanical energy into heat, and are commonly used in medium-height buildings,
iii. Friction Dampers, which use friction pad materials between steel plates sliding against each other to dissipate seismic energy,
iv. Yielding Dampers, which consist of a metal component that absorbs energy by plastically deforming,
v. Magnetic Dampers, which consist of two racks, two pinions, a copper disk, and rare-earth magnets, and
vi. Tuned Mass Dampers (Vibration Dampers), which are passive control devices, consisting of a mass mounted on springs in a specific location of a building in order to reduce the amplitude of the building's vibration, and are used in high-rise buildings.

With the exception of Tuned Mass Dampers, seismic dampers are placed within structural frames and are usually connected to them with steel braces. Compared to other seismic rehabilitation methods, seismic dampers focus on reducing displacements and inter-story drift instead of increasing lateral load capacity and stiffness. Outside of rehabilitation purposes, seismic dampers are often used in the original construction of buildings as a way to control building deformations during earthquakes. In this chapter, three innovative seismic rehabilitation techniques, utilizing different seismic damper types will be presented.

2.4.2 SEISMIC REHABILITATION OF DAMAGED REINFORCED CONCRETE FRAMES USING COMBINED METALLIC YIELDING PASSIVE DEVICES (OINAM ET AL. 2017)

Oinam et al. (2017) studied the effectiveness of combined metallic yielding devices (CMDs), for the seismic rehabilitation of damaged RC frames, and analyzed the behavior of CMD strengthened RC frames. CMDs are metallic dampers that yield in both flexure and shear, proposed by Taraithia et al. (2013), comprising one shear and two flexural plates with a gap between them to allow for unconstrained deformations (Figure 2.15 Left). The authors tested two reduced scale single-story, single-bay frames under lateral cyclic loading, both in their undamaged condition and after applying two different strengthening configurations, and analyzed their cyclic behavior.

The two frames: S-1 and S-2 were identical in their dimensions and materials, with the exception of the plastic hinge regions of the columns and beam-column joints of frame S-2, which had steel fiber reinforced concrete (SFRC) instead of normal concrete. Both frames were tested under lateral cyclic loading up to 4.5% drift level and sustained damages to their beams and columns. The exact details of the test can be found in the report by Oinam R. et al. (2014). The frames were then retrofitted, as can be seen in Figure 2.15 (right), by adding the CMD device and concentric steel bracing, with the RS-1 variation having additional full column steel jacketing and the RS-2 variation having only local steel collar strengthening of the columns. The strengthened frames RS-1 and RS-2 were then subjected to lateral cyclic loading up to 6.0% drift level, and a summary of the test results can be seen in Table 2.1

Table 2.1 Summary of cyclic loading test results (Oinam et al. 2017)

Parameters	*S-1*	*S-2*	*RS-1*	*RS-2*
Yield drift (%)	.5	.75	1.0	.75
Initial stiffness (kN/mm)	2.5	3.1	17.0	3.6
Peak load (kN)	57.0	75.0	136.0	125.0
Energy dissipation (kNm)	3.5 @3.5% drift	5.6 @4.5% drift	16.3 @3.5% drift	14.3 @4.5% drift

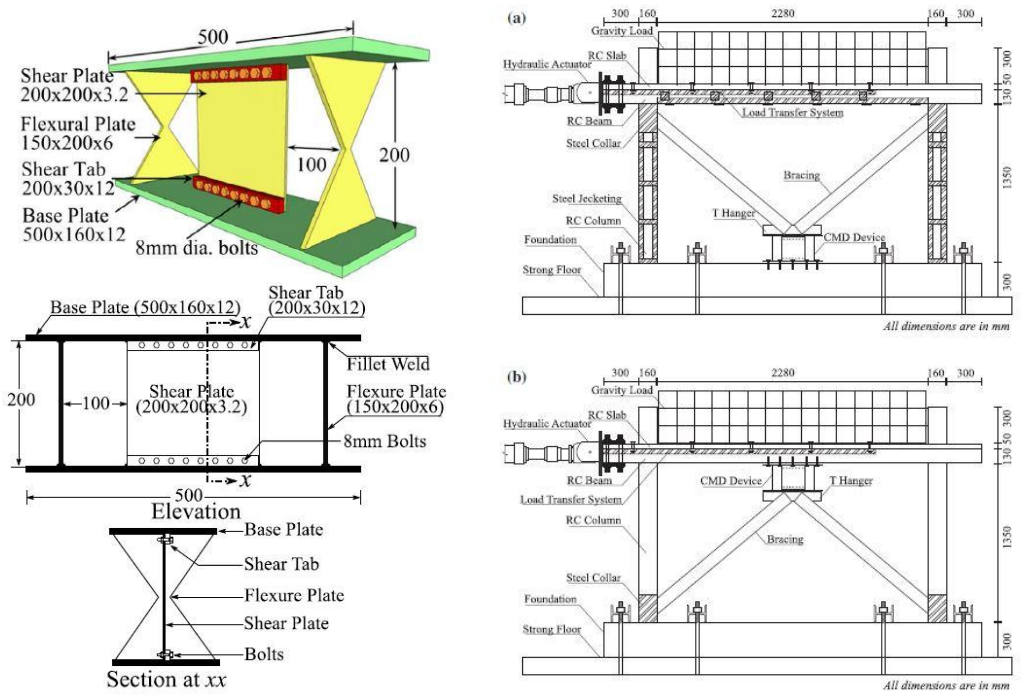

Figure 2.15 Left: Schematic with dimension details for the CMD (Oinam et al. 2017)
Right: Details of the rehabilitated frames (a) frame RS-1 strengthened by CMD and steel jacketing of columns, (b) frame RS-2 strengthened by CMD and local column strengthening. (Oinam et al. 2017)

The rehabilitation caused a significant increase in the initial lateral stiffness of frame RS-1 and an increase of 140% of the maximum lateral load-carrying capacity for frame RS-1 and 70% for frame RS-2. Lateral load capacities had sudden drops at 1.4% and 2.2% drift levels for frames RS-1 and RS-2 due to inelastic buckling of the shear plate of the CMDs. The energy dissipation, which is the area enclosed by the hysteretic response graph, was lower than expected for frame RS-2, 14.3 kN-m (10.5 ft-kip) as compared to 16.3 kN-m (12 ft-kip) for frame RS-1, due to a failure in the anchor bolts between the CMD and a column of frame RS-2 at 4.5% drift level. The lateral load carried by the CMDs was measured by strain rosettes installed in the shear platers and strain gauges installed at the flexure plates. The shear plates carried a maximum lateral load of 15 kN (3.4 kip) and 20 kN (4.5 kip) for frames RS-1 and RS-2, while each pair of flexure plates carried a maximum lateral load of about 20kN (4.5 kip). Frame RS-1 exhibited only minor cracks in its beams and columns until the 6% drift level, where major cracks were formed in the beam-column joints, while frame RS-2 exhibited severe damage to its

unstrengthened columns along with major cracks in the beam-column joints. Regardless of the damages, none of the strengthened frames completely collapsed at a 6% story drift level.

The flexural plates in CMD dissipate energy mostly by inelastic deformations, while shear plates undergo yielding, followed by inelastic buckling. According to the authors, the contribution of the CMDs to the lateral load resisting capacity of the frames in either the post-buckling or the yielding stage of shear plates can be calculated by adding the ultimate strength of the flexural plates to either the ultimate or the yield strength of the shear plate. The maximum lateral strength of the strengthened frame can be predicted by adding the yielding stage contribution of the CMD to the lateral strength of the original RC frame. By using this method, the authors were able to predict a maximum lateral strength of 149.1 kN (33.5 kip) for frame RS-1 against the observed 136 kN (30.6 kip), which is a reasonably accurate prediction, considering that the full lateral strength of the RC frame would not be utilized due to the strengthening elements.

Based on the test results and the accuracy of their analysis, the authors believe that seismic rehabilitation of RC frames with CMD can be an effective and reliable way to increase peak lateral strength, lateral stiffness, and energy dissipation, especially if coupled with the strengthening of the columns, and if adequate anchorage between the CMD and the existing RC frame is provided.

2.4.3 SEISMIC RETROFIT OF SOFT-FIRST-STORY STRUCTURES USING ROTATIONAL FRICTION DAMPERS (JAVIDAN AND KIM 2019)

Javidan and Kim (2019) developed a new type of rotational friction damper for the seismic strengthening of soft-story RC buildings that are commonly found in Korea and investigated its effectiveness by testing a retrofitted steel frame under cyclic lateral loading and by analyzing a four-story RC building, before and after retrofit, with finite element software.

The rotational friction damper developed by the authors consists of three steel links, connected between them by pins with friction pads that control the rotation, mounted on a steel beam-column system that is connected to the RC frame (Figure 2.16). This rehabilitation method was developed with RC frame buildings without infills on the first floor (pilotis) in mind, and as such, its installation and function do not interfere with the first floor’s utility, which is most often a parking space. The purpose of the steel beam-column system, to which the dampers are

mounted, is to provide sufficient relative displacement for the dampers to be able to dissipate energy, and to avoid the application of point loads to the RC columns and beams, as would be the case if the dampers were mounted directly on them.

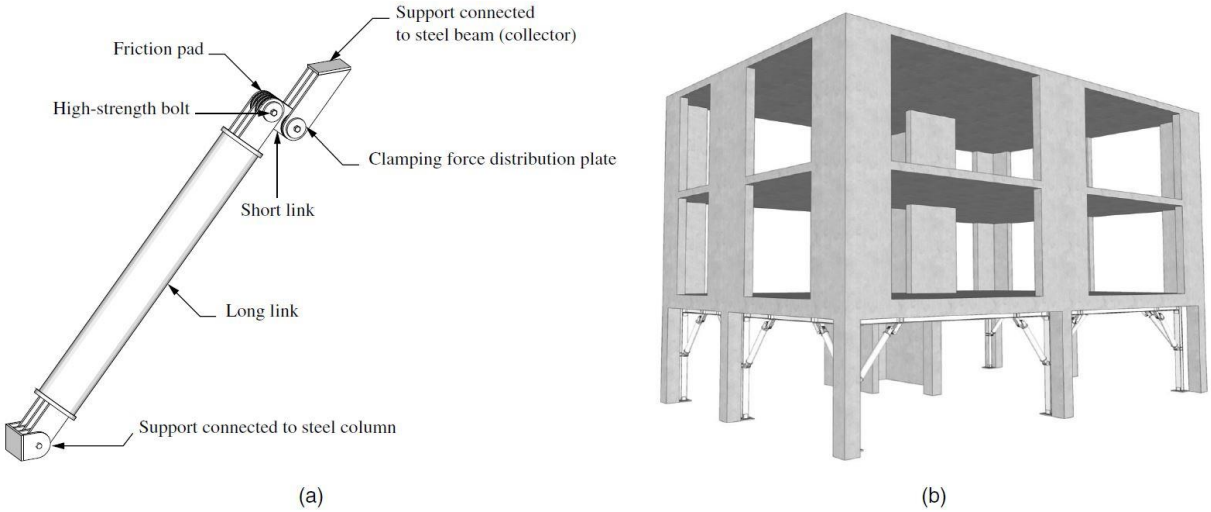

Figure 2.16 Proposed retrofit system (a) details of the damper, (b) installation scheme. (Javidan and Kim 2019)

The authors tested a one-story, one-bay steel frame, equipped with two of the proposed rotation friction dampers, under lateral cyclic loading (Figure 2.17), with 10, 5, and 3 cycles at 0.25, 0.5, and 1.0 times the device displacement, which corresponded to 1.5% inter-story drift.

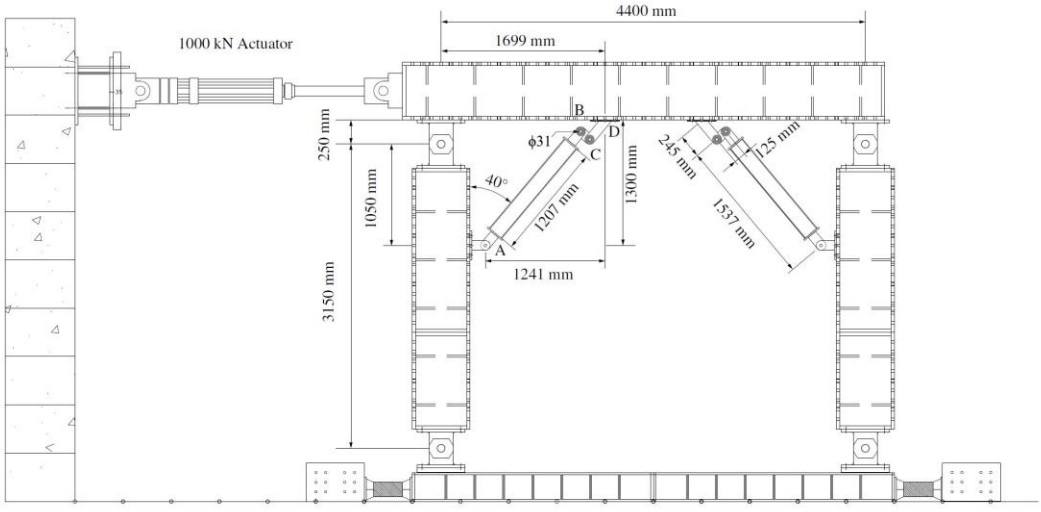

Figure 2.17 Test setup (Javidan and Kim 2019)

For this test, the dimensions of the links were chosen as 125x250x1500 mm (5”x10”x4’-11”), in order to maximize the rotation of the links compared to the inter-story drift, which is referred to as the amplification factor, while the hinges connecting the links were each equipped with four 100 mm (4”) diameter circular friction pads and a 30 mm (1 2/8”) diameter high-strength bolt with approximately 80 kN (18 kip) pretension to apply compression on the friction faces. Other than an early loss of bolt pretension leading to a slight loss of lateral strength, which according to the authors can be prevented by using special washers or by increasing the pretension force, the hysteretic behavior results showed broad loops, which are an indicator of good energy dissipation capabilities (Figure 2.18).

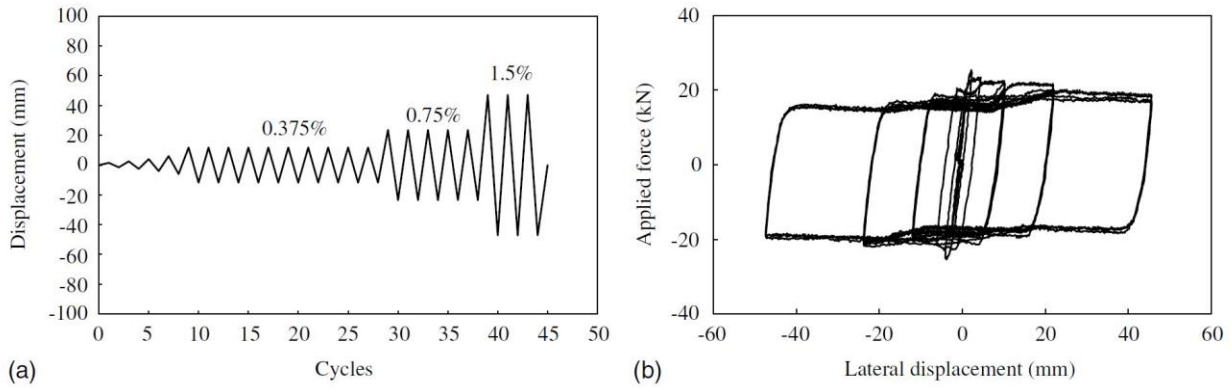

Figure 2.18 Hysteretic behavior of test specimen. (Javidan and Kim 2019)

They then used the OpenSees finite element software to model a pilotis type four-story RC building (Figure 2.19), representative of buildings in Korea, before and after retrofitting it with rotational friction dampers and studied its behavior against seven earthquakes from the PEER database, scaled to meet the maximum considered earthquake in Korea. The rehabilitation aimed to reduce the inter-story drift of the first floor below 1.0%. While the unretrofitted version of the building exhibited maximum inter-story drifts mostly above 1.5%, reaching up to approximately 3.8% (Figure 2.20), the retrofitted version, with rotational friction dampers applied to a two-bay frame, exhibited maximum inter-story drifts below 1.0%, with the exception of two earthquakes where the maximum drift was 1.2% and 1.7% (Figure 2.21).

Supported by the results of the tests, the authors concluded that their proposed rotational friction dampers are a viable seismic rehabilitation measure that can reduce inter-story drift, without altering the utility, or reducing the usable space of the building.

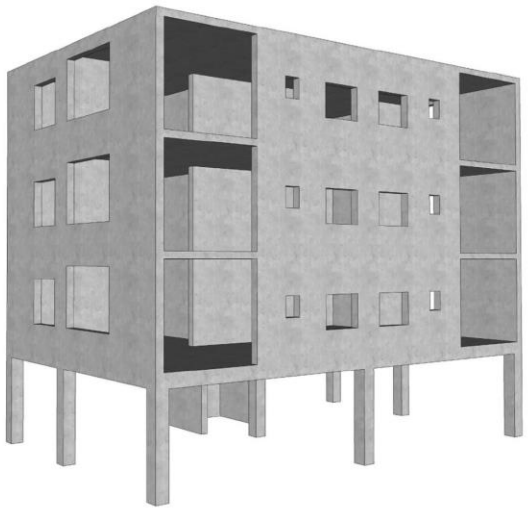

Figure 2.19 Four-story pilotis building model. (Javidan and Kim 2019)

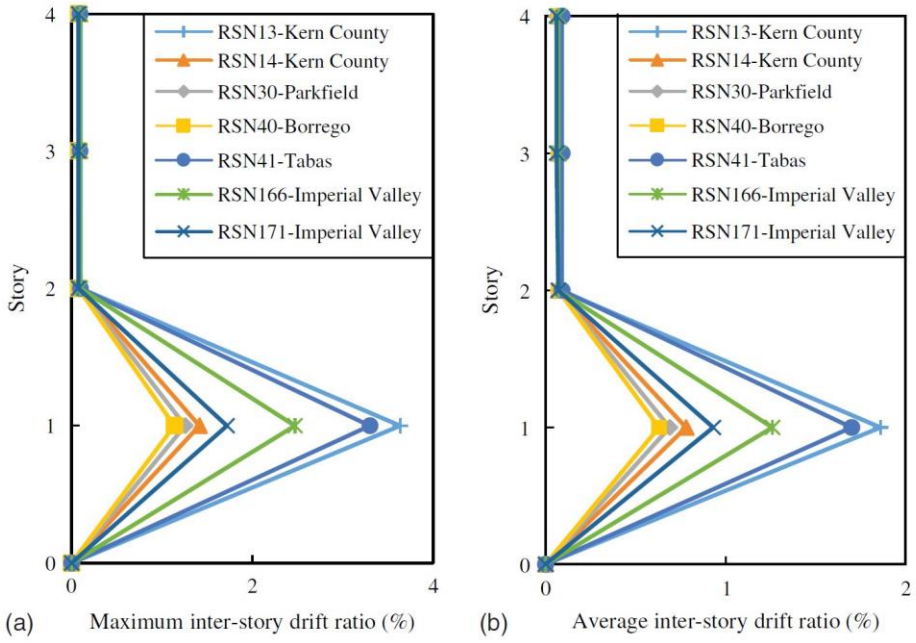

Figure 2.20 Interstory drifts before retrofit. (Javidan and Kim 2019)

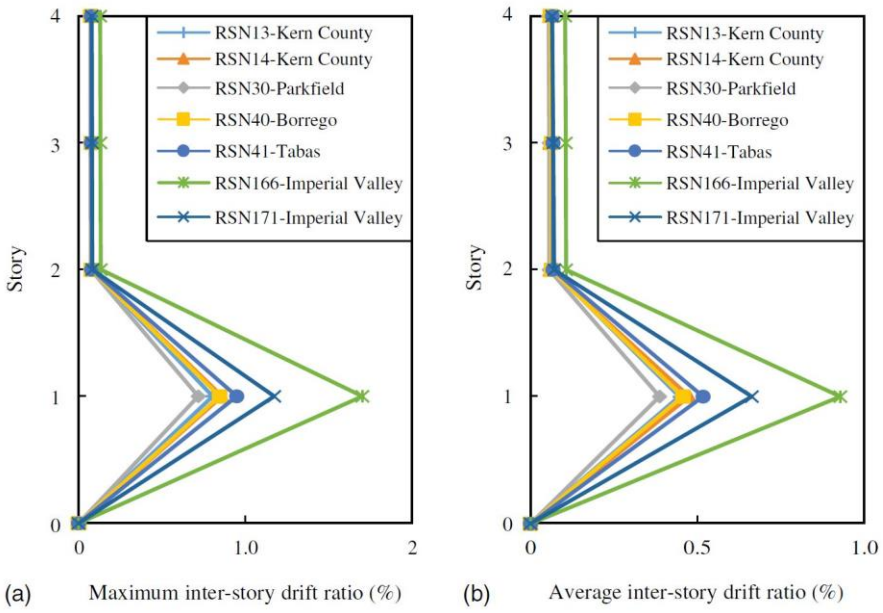

Figure 2.21 Interstory drifts after retrofit. (Javidan and Kim 2019)

2.4.4 SEISMIC STRENGTHENING OF RC STRUCTURES USING WALL-TYPE KAGOME DAMPING SYSTEM (HUR ET AL. 2022)

Hur et al. (2022) studied the effectiveness of a Kagome truss damper used for the seismic rehabilitation of RC buildings. For that purpose, they developed a method for estimating the truss's shear strength and shear modulus, they tested a small-scale RC frame under lateral cyclic loading, with and without reinforcement by a wall-type Kagome damping system (WKDS), and they performed non-linear static and dynamic analyses on an existing RC school building strengthened by their proposed method.

Kagome trusses differ from conventional trusses in that they form tri-hexagonal patterns instead of triangle ones (Figure 2.22), offering better resistance to buckling, higher strength to weight ratio, and lower anisotropy, and they have been used as vibration dampers in mechanical, naval, and aerospace engineering. While the bending and compressive strength, as well as the elastic modulus of 3D Kagome trusses, had been determined in past research as a function of the properties of the steel, the diameter of the wire, and the geometry of the truss, the formulas for shear strength and shear modulus had yet to be developed. The authors estimated the shear strength and modulus of Kagome trusses by simplifying their structure into two ideal tetrahedrons and generating the appropriate formulas.

The wall-type installation system for the Kagome truss damper developed by the authors, referred to as the WKDS, consists of two identical steel walls made of rectangular steel pipes, with one of them connected to the upper girder and the other to the lower one, transferring the frame's loads to the Kagome truss damper located between them. This system was chosen by the authors as opposed to others, such as diagonal bracing or K-bracing, due to its minimal effect on the aesthetics of a building's façade.

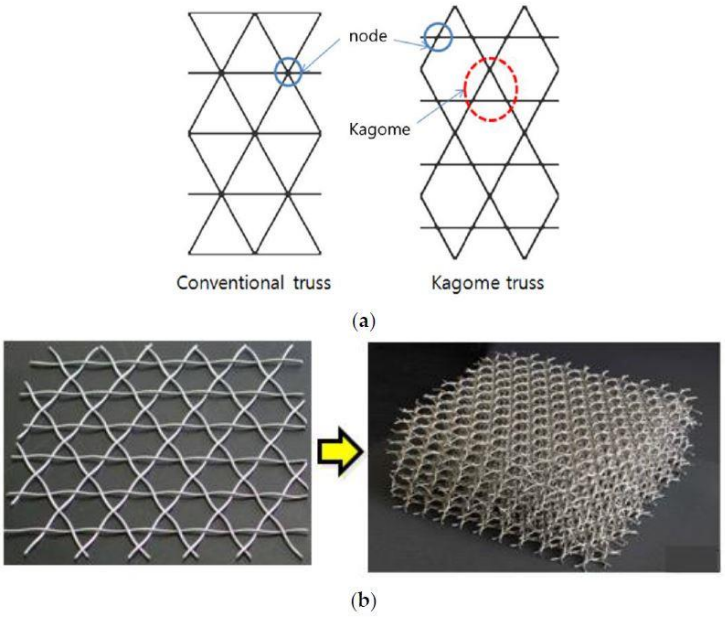

Figure 2.22 (a) Comparison of a conventional and a Kagome truss; (b) 2D and 3D Kagome trusses (Hur et al. 2022)

Based on an RC frame of a school building built in 1986 in South Korea, they constructed a frame at 60% the size of the original, and tested it under lateral cyclic loading, with and without the WKDS reinforcement. The RC frame had the dimensions shown in Figure 2.23 and was designed to yield at 96 kN (21.6 kip) lateral load and 6.7 mm (2/8") displacement, while the Kagome damper was designed to yield at 50 kN (11.2 kip) and 0.67 mm (1/32") displacement, which is 10% of the yield displacement of the original frame. The results showed a 50% increase in lateral strength from 147 kN (33.0 kip) to 234 kN (52.6 kip), an increase in maximum displacement from 33.6 mm (1 2/8") to 42.0 mm (1 5/8"), and a 200% increase in energy dissipation at maximum displacement from approximately 1900 kN-mm (1.41 ft-kip) to approximately 6500 kN-mm (4.8 ft-kip).

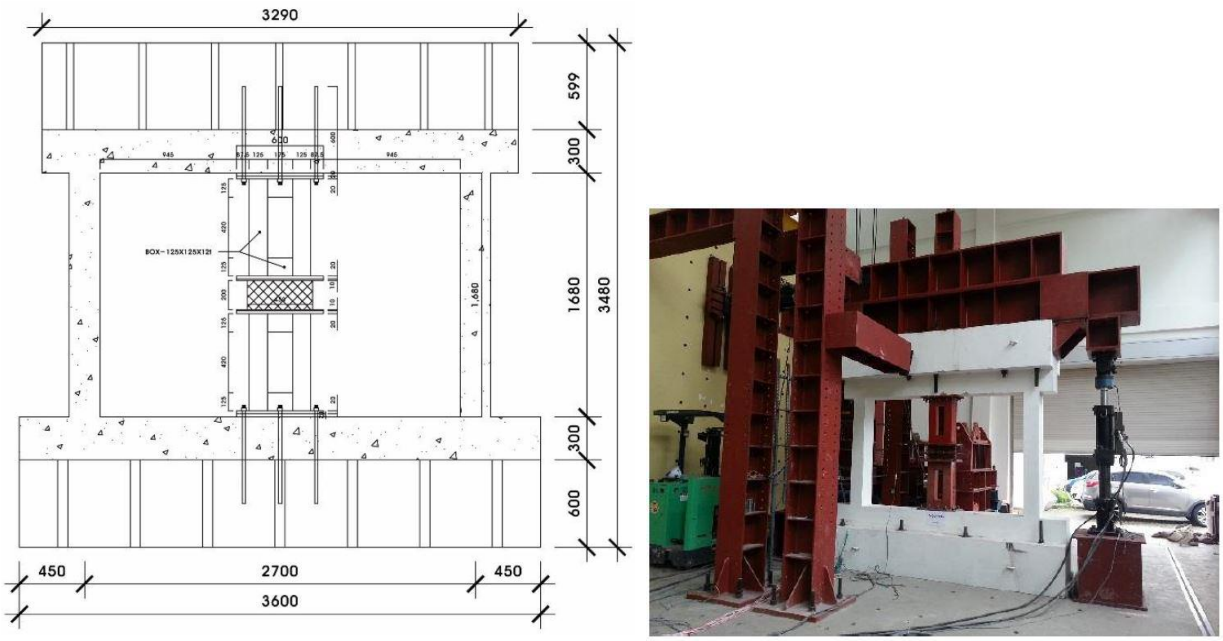

Figure 2.23 Left: Schematic with the dimensions of the test frame with the WKDS. Right: Photograph of the test frame with the WKDS (Hur et al. 2022)

To verify the effectiveness of their method, they modeled an existing four-story school building with the PERFORM-3D software and conducted non-linear static and dynamic analyses on the model, before and after retrofitting it with six WKDS on each of the first two stories. The non-linear static analysis, considering effective ground accelerations of 0.146 g for the Design Based Earthquake (DBE) and 0.22 g for the Maximum Considered Earthquake (MCE), gave inter-story drift ratio values of 0.8% at the DBE and building collapse at the MCE for the original building, while it gave drift ratios of 0.37% at the DBE and 0.74% at the MCE for the retrofitted building. The non-linear dynamic analysis, using the time-history data of 14 earthquakes scaled to the design level earthquake, gave a significantly lower peak displacement (54%) and drift ratio (47%) for the retrofitted building, as well as a slightly reduced peak acceleration (92%) and peak base shear (74%).

The authors conclude that their proposed WKDS is an effective measure for seismic rehabilitation of RC buildings since it can reduce the displacement and drift response of buildings, as well as increase their maximum displacement and lateral strength, leading to significant increases in energy dissipation capacity.

2.5 BASE ISOLATION

2.5.1 INTRODUCTION

Base Isolation Systems (BIS) for buildings are based on the concept of the ideal separation of the superstructure from the ground with the use of rubber bearing devices or friction pendulums. The goal of BIS is to modify the original, fixed base system, and create a two-degree of freedom (2DOF) system with higher vibration periods and lower relative displacements.

De Luca et al. (2019) reviewed the history and evolution of BIS, and divided them into three generations, covering the periods between 1984-1994, 1995-2004, and 2005-2018. With rubber bearing devices (Figure 2.24 Left) being by far the most popular choice for base isolation, the authors noticed the trend of decreasing the number of isolators and increasing their dimensions, in order to achieve higher vibration periods. While first-generation rubber bearing isolators had diameters of 40-60 cm, were designed for up to 25 cm lateral displacements, and achieved vibration periods of up to 2.5 seconds, third-generation ones have diameters of 100-150 cm, are designed for lateral displacements of 60 cm, and can achieve vibration periods of up to 10 seconds.

Friction pendulums (Figure 2.24 Right) are sliding steel-PTFE systems that dissipate seismic energy through friction generated by the relative movement of two elements and determine the vibration period of the isolated building solely through the curvature and diameter of their sliding surfaces. While experimental testing indicates that friction pendulums can provide efficient base isolation, they are not widespread and have not been as tested by earthquakes in the field as rubber bearing isolators.

Since 1984, BIS have been used both in the original construction and as a seismic retrofit measure of masonry, RC, and steel buildings all over the world. Weaknesses of BIM: 1. Additional space needed to avoid collision with neighboring buildings. 2. Utilities such as pipelines and cables need to have flexible connections that can handle large deformations.

Figure 2.24 Left: Rubber bearing isolator with a diameter of 1300 mm, tested at the University of California, Berkeley (De Luca et al. 2019)
Right: Bottom surface of friction pendulum with a diameter of 4 meters, used in the Benicia-Martinez bridge, California (De Luca et al. 2019)

In the following section, an innovative technique for Base Isolation by De Domenico and Ricciardi (2017) will be presented.

2.5.2 AN ENHANCED BASE ISOLATION SYSTEM EQUIPPED WITH OPTIMAL TUNED MASS DAMPER INERTER (TMDI) (DE DOMENICO AND RICCIARDI 2017)

The inerter, or J-damper is a 2-terminal device consisting of an arrangement of racks, pinions, and gears that can produce an apparent mass up to 200 times its physical mass. De Domenico and Ricciardi (2017) inspired by the inerter's success in the automotive sector and its possible application in structural dynamics, aimed to improve the viability and performance of Base Isolation Systems (BIS) by proposing the combined use of a BIS along with a Tuned Mass Damper Inerter (TMDI). In the above combination, the BIS separates the structure from the ground while the TMDI dampens the earthquake-induced vibrations in the BIS and the structure while requiring only a fraction of the mass that a conventional Tuned Mass Damper (TMD) would need. The authors first determined the optimal BIS and TMDI properties and assessed the effectiveness of their proposed method for simple SDOF buildings, and then attempted to do the same for a multi-story MDOF building.

The proposed solution can be represented by a 3DOF system consisting of the BIS, the TMDI, and the structure (Figure 2.25). By studying the system's governing equations of motion,

the authors reasoned that increasing the TMDI's apparent mass ratio β_t is more beneficial for the system than increasing its actual mass ratio μ_t because it increases the TMDI's inertia without increasing the seismic load on the system.

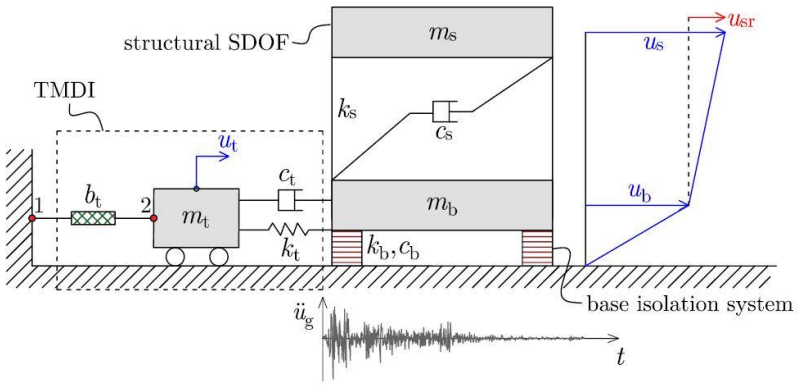

Figure 2.25 Sketch of the 3DOF system representing the proposed solution applied to a one-story SDOF building. (De Domenico and Ricciardi 2017)

To determine the optimal TMDI properties, the authors set fixed β_t and μ_t values and used objective functions to optimize ζ_t (damping ratio) and v_t frequency ratio $v_t = \omega_t / \omega_b$). Of the three objective functions available, each related to displacements, accelerations, and the seismic energy passing from the TMDI to the structure respectively, the last one was deemed as the best, since by minimizing the seismic energy, the displacements and accelerations are minimized as well. According to their analysis, the BIS damping ratio should be low (ζ_b=0.1), the TMDI apparent mass should be high (β_t = 0.4), and the TMDI actual mass should be as low as possible (μ_t=0.01), giving an optimal TMDI damping ratio of ζ_t=0.25 and an optimal frequency ratio v_t=0.35.

In order to evaluate the effectiveness of their proposed solution, they conducted a numerical application on a SDOF building using data from eight past earthquake accelerograms and the following two scenarios: a) with a TMDI with β_t=0.4 and μ_t=0.01, b) with a TMD with μ_t=0.41. The results showed that the TMDI led to smaller displacements in all eight accelerograms, both for the structure (u_s) and the TMD/TMDI itself (u_t), with reductions of 27.2% and 30% of max values on average respectively.

Finally, they conducted a numerical application of their proposed system on a 5-story symmetric MDOF building and studied the following four scenarios: a BIS with (a) TMDI (β_t=0.4 and μ_t=0.01), (b) conventional TMD (μ_t=0.10), (c) a non-conventional TMD (μ_t=0.41),

and (d) without a TMD/TMDI. The results showed that the scenario with the TMDI (a), outperformed both TMD scenarios (b and c) in terms of BIS displacement, global kinetic energy, and base shear, with reductions of 50%, 66%, and 43% respectively compared to the bare BIS scenario (d). the non-conventional TMD (c) performed well, and in some cases outperformed the TMDI, the enormous amount of mass needed for its construction makes it an inefficient solution.

The authors conclude that their proposed TMDI-enhanced BIS is an efficient and effective base isolation method, capable of reducing BIS and superstructure displacements with a significantly low mass requirement for damping purposes. While the authors have planned for future research focused on more accurate modeling of the BIS, they believe that the optimal BIS and TMDI properties they derived in the current research can be a reasonable assumption for preliminary design purposes.

2.6 SUMMARY

This chapter has presented 12 innovative global seismic rehabilitation techniques that utilize masonry infill walls and exoskeletons to increase a structure's lateral stiffness and capacity, as well as seismic dampers and base isolation to reduce the seismic loads on the structure. Techniques involving the addition, replacement, and jacketing of masonry walls with TRM and ECC, capable of increasing a structure's lateral stiffness and strength, as well as its thermal insulation are presented in sub-chapter 2.2. Techniques involving the addition of steel and RC exoskeletons, capable of increasing a structure's lateral stiffness and capacity while also dissipating seismic energy and reducing the lateral loads of the existing structure are presented in sub-chapter 2.3. Sub-chapter 2.4 presents techniques able of reducing earthquake loads to structures with the use of yielding and friction dampers, while sub-chapter 2.5 presents a novel technique that utilizes base isolation combined with a tuned mass damper inerter, able of reducing a structure's earthquake loads more efficiently than conventional base isolation.

Each group of techniques offers unique advantages and disadvantages, and the optimal seismic rehabilitation technique cannot be determined universally in terms of effectiveness and efficiency but depends on the individual structure's needs and considerations.

3 REHABILITATION TECHNIQUES FOR RC BEAMS

3.1 INTRODUCTION

RC beams are structural elements subjected mostly to flexural stresses at their midspans and shear stresses at their ends and are designed to be the first elements that fail under a design-level earthquake, with beam failure defined as exceeding the beam's shear or flexural stress capacity. Additionally, it is not uncommon for rebar in beams exposed to the environment to become corroded and for spalling to occur in the concrete. As such, it is important to be able to repair and strengthen damaged and inadequate RC beams efficiently and effectively. While traditional methods of RC beam rehabilitation involved the concrete or steel jacketing of the members, modern methods involve jacketing, or externally bonding (EB) with the use of newer materials such as FRP (Fiber Reinforced Polymer) composites, FRCM (Fiber Reinforced Cementitious Materials), TRM (Textile Reinforced Mortars) and ECC (Engineered Cementitious Composites), as well as the Near Surface Mounting (NSM) of FRP rebars.

FRP jacketing is the most popular of the modern RC beam rehabilitation methods, capable of repairing and restoring damaged RC beams to their original strength and strengthening RC beams in flexure and shear to up to twice their original load capacity, if premature FRP debonding failure can be avoided (Siddika et al. 2019). An alternative method for rehabilitating RC beams with FRP is the NSM method, which involves the cutting of grooves on the surface of the concrete and inserting FRP rebars along with epoxy, and has proven to have a higher resistance to premature debonding failure compared to FRP jacketing due to its increased generation of interfacial stress (Bilotta et al. 2011, Bilotta et al. 2015, and Lundqvist et al. 2005).

FRP's weaknesses, namely its high cost and its poor performance under high temperatures, are addressed by FRCM, TRM, and fiber-reinforced ECC jacketing, which utilize mortars instead of epoxies as a matrix for their fibers and are a lower-cost alternative that performs well under high temperatures. However, these jacketing methods aren't directly superior to FRP jacketing since they are less effective than FRP in increasing load capacities. According to Raoof et al. (2017), TRM jacketed RC beams achieve flexural load capacities in a range between 47-80% of the respective FRP jacketed ones, depending on various factors such as the quality of the mortar used and the number of layers used, with more layers leading to higher load capacities.

In this chapter, seven innovative techniques concerning the flexural and shear rehabilitation of RC beams will be presented.

3.2 FLEXURAL REHABILITATION OF RC BEAMS

3.2.1 REHABILITATION OF REINFORCED CONCRETE STRUCTURES USING FRP AND WOOD (GRACIDE ET AL. 2020)

Gracide et al. (2020) studied the possibility of using wood to repair and strengthen RC beams and compared its effectiveness to that of commonly used reinforcements such as Carbon Fiber Reinforced Polymer (CFRP) and Flax Fiber Reinforced Polymer (FFRP) bands. To compare the new wood reinforcement method with more common methods, they tested 6 beams with different external reinforcement materials under four-point bending, and to analyze the effect of each component on the performance of the wood reinforcement, they tested 10 beams with different wood reinforcement configurations under four-point bending.

The beams were made of C30/37 concrete (5.4 ksi), with a length of 2.3 meters (7'-6 4/8") and a cross-section of 15x25 cm (6"x10"), while the materials used for the external reinforcement were the following.

- CFRP band with 65% fiber volume fraction, a thickness of t = 0.48 mm (1/64") and f_t = 1700 MPa (247 ksi),
- FFRP band with a thickness of t = 2.1 mm (1/16") and f_t = 160 MPa (23 ksi),
- CFRP rod with f_t = 1500 MPa (218 ksi),
- C24 lumber with bending strength $f_{m,k}$ = 24 MPa (3.5 ksi) and tensile strength $f_{t,0,k}$ = 14 MPa (2 ksi).

For the first test, they tested one reference beam with no external reinforcement, three beams with one, two, and four CFRP layers, one beam with two FFRP layers, and one beam with 45 mm (1 6/8") thick wood reinforcement and a 9 mm (3/8") diameter CFRP bar (Figure 3.1).

The reference beam had a maximum load capacity of 45.6 kN (10.2 kip), the CFRP reinforced beams had 65.1 kN (14.6 kip), 78.2 kN (17.6 kip), and 87.7 kN (19.7 kip) for one, two, and four layers respectively, the FFRP reinforced beam had 82.0 kN (18.4 kip), and the wood reinforced beam had 151.1 kN (34 kip), which is a 230% increase in capacity compared to

the reference beam. The results of the test validated the expected gradual increase in capacity along with the increase in CFRP layers, showed that FFRP reinforcement can be on par with CFRP, and motivated the further study of the wood reinforcement.

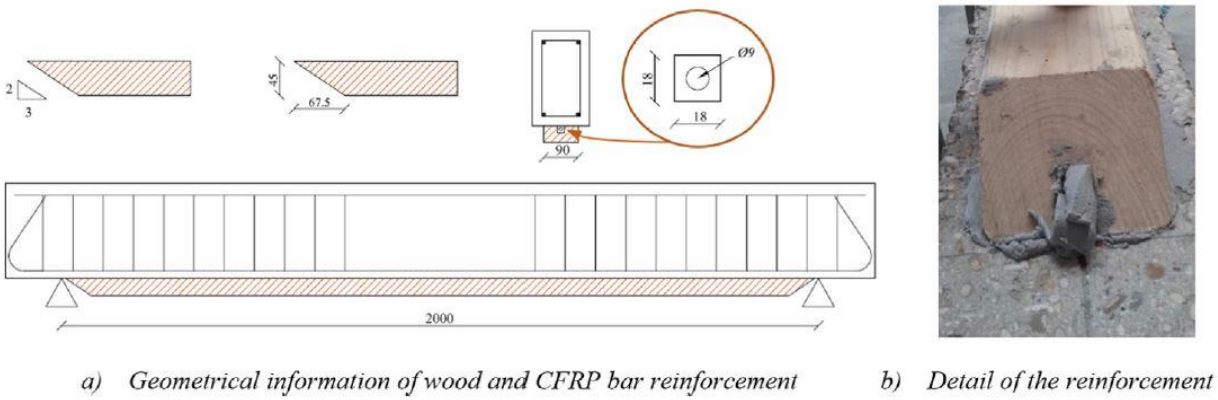

a) Geometrical information of wood and CFRP bar reinforcement *b) Detail of the reinforcement*

Figure 3.1 Details of the wood reinforcement with the CFRP bar. (Gracide et al. 2020)

For the second test, 10 RC beams with different configurations of wood reinforcement, with and without FRP bars were tested in four-point bending. To determine the effect of the wood's thickness, two beams with 25 mm (1") thick wood reinforcement (W25) and two beams with 45 mm (1 6/8") thick wood reinforcement (W45) were tested without the use of FRP bars, and to determine the effect of the type and diameter of the FRP bar, five beams with 45 mm thick wood reinforcement were tested, two of which included a 9 mm (#3) diameter CFRP bar (W45_CFRP9), one included a 9 mm (#3) GFRP bar (W45_GFRP9) and two included a 14 mm (#4) GFRP bar (W45_GFRP14). The tenth beam was a reference beam with no additional wood reinforcement.

Compared to the maximum load capacity of the reference beam, which was 48.3 kN (10.8 kip), all wood reinforced beams exhibited an increase in capacity in the range of 40-130%. There was a large discrepancy in the capacity of the two W25 beams, with the first one having a capacity of 72 kN (16.2 kip) and the second having 108 kN (24.3 kip), suggesting that any imperfections in the 25 mm (1") thick wood reinforcement heavily influence the beam's load capacity. The W45 beams had capacities of 119.2 kN (26.8 kip) and 113.2 kN (25.4 kip), which is not a significant increase compared to the higher value of the W25 beam, but the smaller discrepancy suggests that they are more reliable. The addition of the FRP bar in the wood reinforcement did not cause a significant increase in capacity, with the largest capacity found in

one of the W45_GFRP14 beams, at 122.5 kN (27.5 kip), but increased the brittleness of the beams, especially when GFRP bars were used. Three different failure types were observed among the test subjects, namely (a) failure of the wood on the tensile side, which occurred to the W25 beams, (b) shear failure with concrete cover debonding, which occurred to W45 beams, and (c) composite debonding from the end of the element, that occurred to all beams with FRP bars.

The authors conclude by pointing out the economic and environmental benefits of their method. They also suggest further research to focus on wood reinforcement without the use of FRP bars, and to consider the use of anchor sockets between RC and wood in addition to epoxy, to improve the bonding between the materials.

3.2.2 FLEXURAL REHABILITATION AND STRENGTHENING OF REINFORCED CONCRETE BEAMS WITH BFRP COMPOSITE (DUIC ET AL. 2018)

Motivated by the availability and low cost of Basalt Fiber Reinforced Polymer (BFRP) composites, as well as the limited amount of current research on the topic, Duic et al. 2018 studied the feasibility of BFRP as a material for flexural strengthening and rehabilitating corroded and uncorroded RC beams. For that purpose, they conducted two-point loading (four-point bending) tests on seven beam specimens with different amounts of steel reinforcement, corrosion levels, and BFRP layers, and compared their results.

The seven beam specimens were constructed with f'_c=37 MPa (5360 psi) concrete, with five longitudinal f_y=430 MPa (62 ksi) steel rebars, and were 3200 mm (10’-6”) long, 275 mm (11”) wide, and 500 mm (20”) deep. The BFRP reinforcement was applied on the beams with the dry lay-up method and had 0.33 mm (1/8”) thickness per layer, ultimate stress f_u=493 MPa (71.5 ksi), ultimate strain ε_u=2.52%, and Young’s Modulus E_f=20.4 GPa (2.9 msi). The authors divided the testing procedure into two phases, the first of which evaluated the strengthening effect of the BFRP reinforcement on uncorroded beams, while the second evaluated its effectiveness in rehabilitating corroded beams. For the first phase, four beams were tested, two of which were control beams with 10 mm (#3) and 15 mm (#5) diameter rebars respectively, and the other two were identical to the first, but with the addition of 3 layers of BFRP reinforcement using the midsection cross-strapping scheme. For the second phase, three beams using 20% corroded 15 mm (#5) diameter rebars were tested, including a control beam and two beams with 8 layers of BFRP reinforcement, using the midspan and the bottom cross-strapping schemes

respectively (Figure 3.2). The effect of corrosion was simulated by removing 20% of the rebar area by machining, while the effect of spalling due to corrosion was simulated with missing patches of concrete achieved by adding insulation foam boards in the formwork during concrete casting. All the beam specimens were simply supported at their ends and subjected to two-point loading until flexural compression failure.

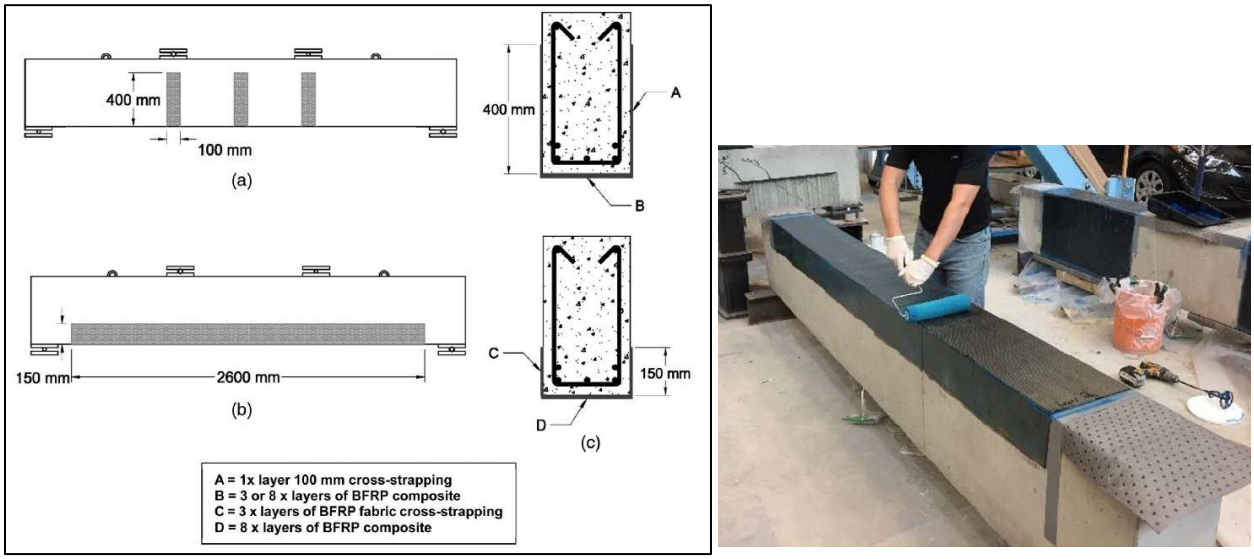

Figure 3.2 Left: BFRP reinforcement configurations (a) midspan scheme; (b) bottom scheme; (c) sections. Right: Installation of BFRP Sheets for the bottom cross-strapping scheme. (Duic et al. 2018)

The authors evaluated the crack pattern development, the load-deflection ratio, the ductility, the moment capacity, and the failure modes for all the beams tested and compared the BFRP reinforced beams with their control beams. The results showed that, compared to the control beams, the BFRP reinforced beams didn't exhibit different crack patterns, and achieved 3.8 times higher post-yield load-deflection ratios in phase 1 and 5.6 times higher in phase 2. In terms of failure modes and moment capacity, both phase 1 beams failed with rupture and achieved a 25% increase, and of the phase 2 beams, the one with mid-span cross-strapping failed with debonding and achieved a 15% increase, while the one with bottom cross-strapping failed with rupture and achieved a 30% increase. Additionally, consistent with other literature, all BFRP reinforced beams showed a 30% decrease in ductility approximately.

The authors conclude that BFRP is a viable material for flexural strengthening and rehabilitation of RC beams, and can be a more affordable alternative to CRFP and GFRP.

Finally, they remind the reader of the ductility reduction caused by the BFRP reinforcement, as well as the possibility of debonding failure occurring instead of rupture failure, for which they advise the use of the bottom cross-strapping scheme.

3.2.3 IMPREGNATED CARBON FABRIC-REINFORCED CEMENTITIOUS MATRIX COMPOSITE FOR REHABILITATION OF THE FINALE EMILIA HOSPITAL ROOFS: CASE STUDY (NOBILI ET AL. 2017)

Nobili et al. (2017) studied the performance of concrete beams strengthened by an impregnated Carbon Fabric-Reinforced Cementitious Matrix (CFRCM) composite, with the goal of seismically rehabilitating the poorly reinforced roof beams of a previously damaged hospital in Finale Emilia, Italy. They developed two rehabilitation procedures with CFRCM that could be applied to the hospital's beams on-site and tested them on 7 pairs of beams taken directly from the hospital.

The hospital was severely damaged due to the 2012 northern Italy earthquake and, at the time of the study, was in need of seismic rehabilitation in its entirety, including its roof beams. The roofs of the subject hospital in their majority consisted of hollow blocks supported by poorly reinforced RC beams that were cast on a thin layer of clay tiles (Figure 3.3). For their study, the authors removed a single 8-meter (26'-3") long RC roof beam from the hospital and did not remove the thin layer of clay tiles bonded to the bottom of the beams, due to the high cost of removing it, and in order to study the layer's effect on the beams' rehabilitation.

The authors considered two procedures for rehabilitating the beams using CFRCM, differing in the way the composite reinforcement is applied to the beams. The first procedure, termed Cycle A, follows the below steps:

1. A liquid adhesion promoter is applied with a brush to the clay tile substrate.
2. The first 5 mm (2/8") thick mortar bed is laid.
3. Unidirectional carbon fabric reinforcement sheets are impregnated with the adhesion promoter through immersion.
4. The first carbon fabric reinforcement sheet is placed on the mortar bed and rolled to eliminate air bubbles.
5. The second carbon fabric reinforcement sheet is placed in a similar manner.

6. The second 5 mm (2/8”) thick mortar bed is placed on top.

According to the second procedure, termed Cycle B, which was considered in order to provide a faster and easier installation at the cost of performance, the adhesion promoter, instead of being applied to the carbon fabric reinforcement sheets through immersion, is applied with a brush after they are already placed on the mortar bed.

The mortar the authors used had a compressive strength of f_c = 6.5 MPa (0.95 ksi) and an Elastic Modulus of E = 11 GPa (1600 ksi), while the carbon fabric had an ultimate tensile strength of 2.0 GPa (290 ksi), an ultimate strain of ε_{uf} = 2.1%, Elastic Modulus of E_f = 210 GPa (30.5 msi) and a cross-section area per unit width of 0.88 mm^2 /cm. The above mortar type was chosen, despite its low strength, due to its good compatibility with the clay tile’s mechanical properties and because it has been proven to develop strong bonds with carbon fabric.

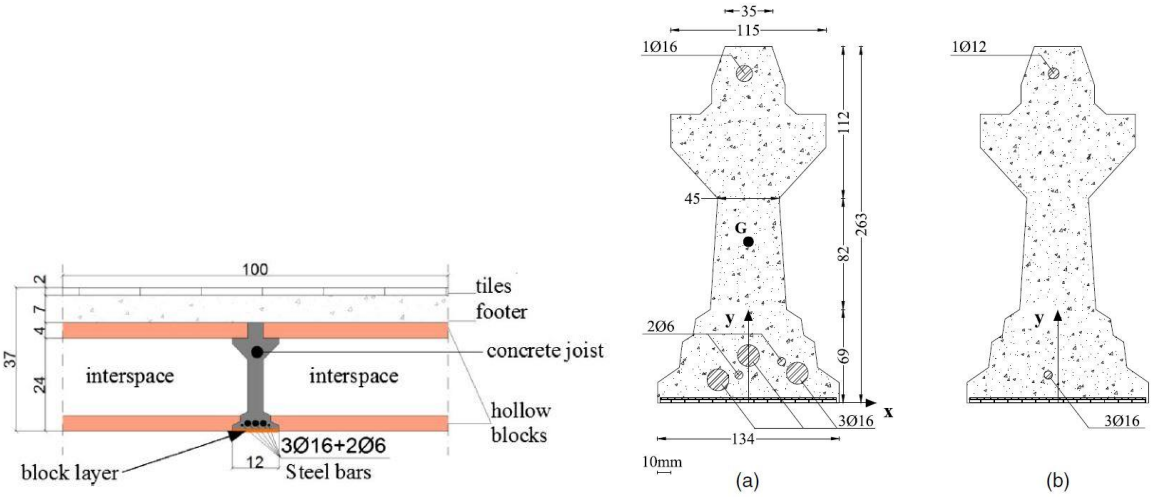

Figure 3.3 Left: Cross-section of a typical hospital roof; Right: Cross-section of a typical hospital beam (Nobili et al. 2017)

For the test procedure, the single 8-meter (26’-3”) long beam taken from the hospital roof was cut into 15 pieces of 400 mm (1’-3 6/8”) length each. In order to avoid shear failure in the specimens due to the low amount of shear reinforcement detected in them, the beam pieces were connected in pairs by steel hinge devices and subjected to a four-point bending test as seen in Figure 3.4. Three of the pairs were rehabilitated according to Cycle A and four according to Cycle B.

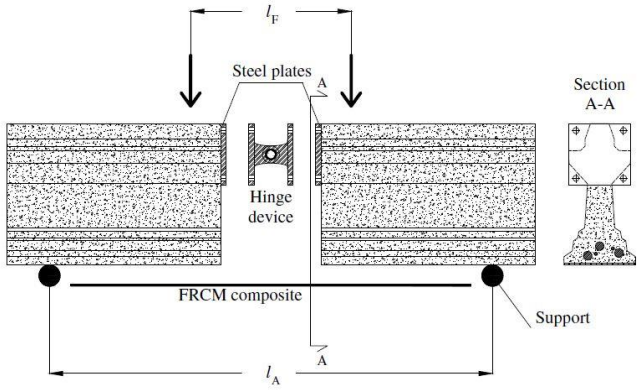

Figure 3.4 Schematic of beam test l_F = 300 mm, l_A = 900 mm (Nobili et al. 2017)

The results of the test showed that the three beam pairs of Cycle A failed due to either cohesive fracture in the thin tile layer, or due to tensile failure in the concrete, with load capacities exceeding 60 kN (13.5 kip), while the four beam pairs of Cycle B failed due to delamination of the fabric at the matrix-fabric interface, with load capacities below 50 kN (11.2 kip). Additional calculations on the theoretical flexural strength of the beams showed that while the existing beams were adequately reinforced for static loads both at the midspan and end sections, they would not be able to handle a moment sign inversion due to an earthquake. Application of the composite reinforcement would increase the moment capacity of the end-sections from 12.6 kN-m (9.3 ft-kip) to 21.9 kN-m (16.1 ft-kip) in case of a moment sign inversion.

Based on the results of the tests and their calculations, the authors concluded that CFRCM composite reinforcement applied on the clay tile layer below the RC beams of the Finale Emilia hospital is a safe and economic way to repair and strengthen them against earthquakes. Finally, they bring to attention the importance of fabric impregnation and suggest it be done through immersion since it led to 1.5 times higher load capacities compared to expedited impregnation with a brush.

3.2.4 STRENGTHENING OF RC BEAMS USING BOTTOM AND SIDE NSM REINFORCEMENT (SABAU ET AL. 2018)

Near Surface Mounted (NSM) reinforcement is a technique for flexural strengthening RC beams and columns, alternative to jacketing or External Bonding (EB), where a shallow groove

is cut on the concrete surface of the member for a reinforcing bar to be placed and secured inside, along with an adhesive material. Research by Bilotta et al. (2011), Bilotta et al. (2015), and Lundqvist et al. (2005), has shown that compared to EB, NSM can achieve higher interfacial stress capacity, and thus provide higher resistance to debonding failures. The two different NSM techniques for beams that exist currently are Bottom NSM (BNSM), where the reinforcement is applied on the bottom surface of the beam, and Side NSM (SNSM), where the reinforcement is applied on the sides of the beam. Sabau et al. (2018) motivated by the lack of recent research on the behavior of SNSM, studied the behavior of seven RC beams with different configurations of BNSM and SNSM reinforcements under four-point bending and compared their results.

Of the seven RC beams tested, one had no external reinforcement and acted as the control beam, three had BNSM reinforcement and the other three had SNSM reinforcement. The beam dimensions were 200x300x4000 mm (8”x12”x13’-1 4/8”), with f'_c=50 MPa (7000 psi) concrete, and four 16 mm diameter (#5) longitudinal bars (two top-side, two bottom-side) made of f_y=578 MPa (84 ksi) steel. Both groups of NSM reinforced beams were reinforced with two rectangular 10x10 mm (3/8”x3/8”) CFRP bars, with an ultimate strength of f_u=3300 MPa (480 ksi) and Young’s modulus of E_f =210 GPa (30.5 msi). The three beams of each group had cut-off lengths of 300, 250, and 200 mm (8”, 10”, and 12”) for their CFRP reinforcements on one end, in order to better study the development of cracks and failure mechanisms (Figure 3.5).

The results showed that the BNSM reinforced beams had 117-128% increased yield load and 122-136% increased ultimate load compared to the control beam and failed due to Clear Cover Debonding (CCD), with the CFRP bars achieving 45-47% of their ultimate strain. The SNSM reinforced beams had 83-98% increased yield load and 122-127% increased ultimate load compared to the control beam and failed due to concrete compressive crushing first and Intermediate Crack Debonding (ICD) later, with the CFRP bars achieving 51-54% of their ultimate strain. Other than a slight increase in ultimate lateral load at lower cut-off lengths for the BNSM beams, the variation in cut-off lengths didn’t produce any significant differences in behavior.

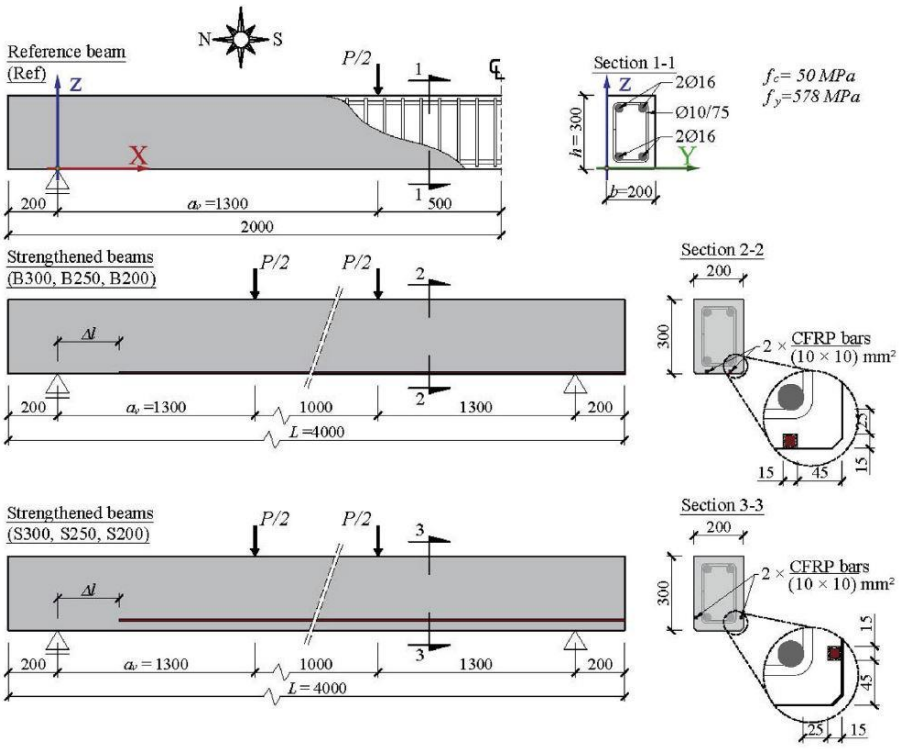

Figure 3.5 Test specimen details (Sabau et al. 2018)

Overall, the BNSM reinforced beams had a 13% higher crack load and a 23% higher yield load and achieved similar ultimate loads to the SNSM reinforced beams, which can be explained by the longer lever arm utilized by the BNSM reinforcement. However, since the SNSM reinforced beams exhibited a more ductile failure mode than the BNSM ones, they had 31-46% higher deflection at failure and 88% higher average energy dissipation as a result (Figure 3.6). Concerning crack propagation, in BNSM reinforced beams, horizontal cracks developed below the steel reinforcement level that grew in size and led to CCD failure (Figure 3.7 Left), while in SNSM reinforced beams, horizontal cracks developed above the steel reinforcement level but didn't lead to failure (Figure 3.7 Right), possibly due to the resisting effect of the shear reinforcement (stirrups).

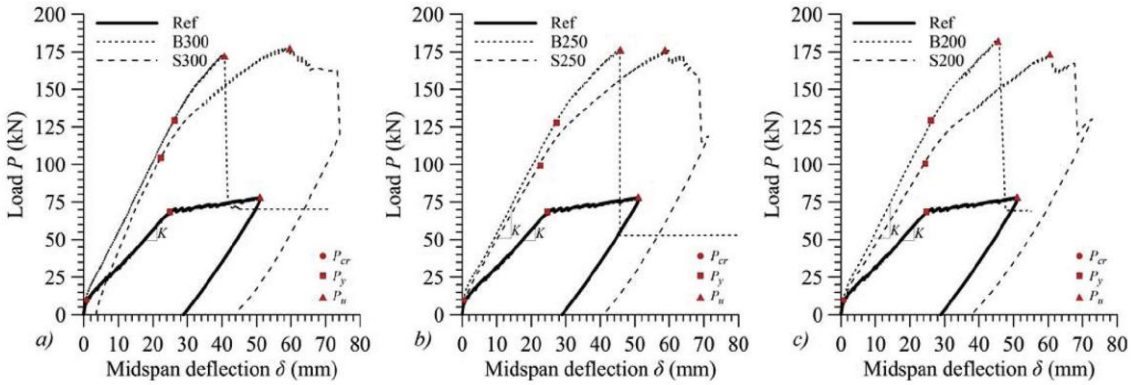

Figure 3.6 Load-deflection curves for BNSM and SNSM specimens. (Sabau et al. 2018)

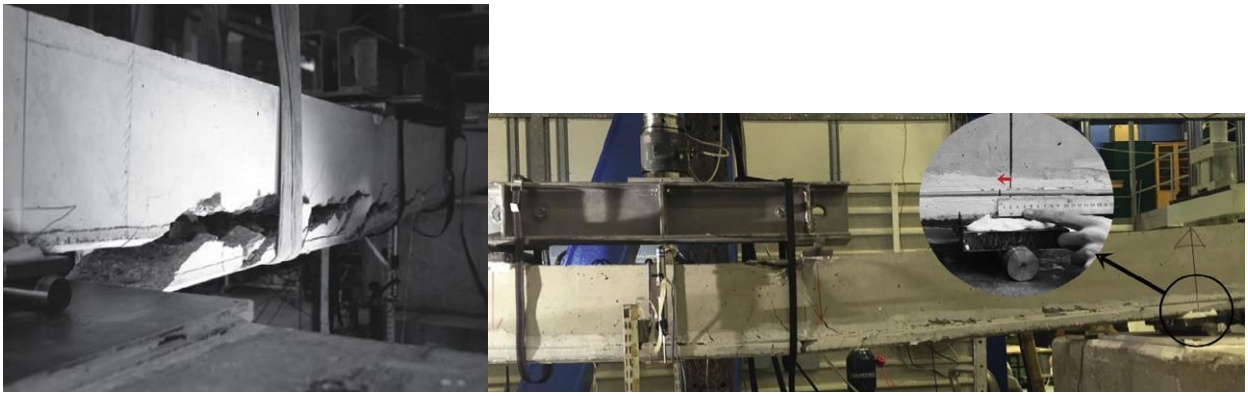

Figure 3.7 Left: Clear cover debonding failure in BNSM reinforced beam. Right: Horizontal cracks in SNSM reinforced beam. (Sabau et al. 2018)

The authors concluded that SNSM reinforcement can be used to strengthen RC beams, providing similar capacity to BNSM reinforcement while achieving increased ductility and energy dissipation. They advise further research to address the possibility of CCD or other failure modes in SNSM reinforcement, as well as the effect of other parameters, such as clear cover depth and flexural and shear reinforcement ratios on SNSM reinforcement.

3.3 SHEAR REHABILITATION OF RC BEAMS

3.3.1 SHEAR STRENGTHENING OF REINFORCED CONCRETE BEAMS USING CFRP WRAPS (MHANNA ET AL. 2019)

For the rehabilitation of RC beams with Externally Bonded (EB) FRP wraps, the full and partial (U) wrapping schemes are considered. While full wrapping is considered the superior scheme due to failing in rupture instead of brittle debonding, it is not always possible to apply it

due to obstructions such as slabs at the top of the beam. Mhanna et al. (2019) studied the behavior of six RC beams with different geometries and strengthening schemes in shear loading and compared the results of the fully wrapped beams with the U-wrapped ones.

The authors conducted 1-point loading (3-point bending) tests on six, 2-meter (6'-6 6/8") long beams, two of them being T-beams and four of them being rectangular. Of the T-beams with 250 mm (9 7/8") web depth, 350 mm (1'-1 6/8") total depth, one had CFRP U-wrapped reinforcement, and the other was an unreinforced control beam, while of the rectangular beams two had CFRP full wrapped reinforcement and 250 mm (9 7/8") and 350 mm (1'-1 6/8") depths respectively, and the others were not reinforced control beams. The beams were constructed using f'_c=45.9 MPa (6.67 ksi) concrete and f_y=460 MPa (66.7 ksi) steel rebars, while the CFRP laminate used as the EB reinforcement had ultimate tensile strength f_u=1034 MPa (150 ksi), Young's modulus E_f=73.77 GPa (10.7 msi), and strain to failure ε_f=1.4%. The CFRP EB reinforcement consisted of six 1-ply wraps, 100 mm (4") wide and at 150 mm (6") spacing, impregnated with epoxy using rollers and applied to the beam near the supports. To ensure shear failure occurs on one end of the beams, stirrups were placed only on one side of the beams. The beam geometry and reinforcement details can be seen in Figure 3.8.

The results of the tests showed an increase in load capacity as well as deflection at failure for all strengthened beams. Specifically, in the T beams load capacity was increased from 148.3 kN (33.3 kip) to 318.6 kN (71.6 kip), and deflection at failure from 4.22 mm (1/8") to 10.07 mm (3/8"). Similarly, in the 250 mm (9 7/8") deep rectangular beams load capacity improved from 101 kN (22.7 kip) to 171 kN (38.4 kip), and deflection at failure from 5.43 mm (2/8") to 19.88 mm (6/8"), while the 350 mm (1'-1 6/8") deep rectangular beams showed an increase from 118.6 kN (26.5 kip) to 357.6 kN (80.2 kip) in load capacity and 3.43 mm (1/8") to 34.46 mm (1 3/8") in deflection at failure.

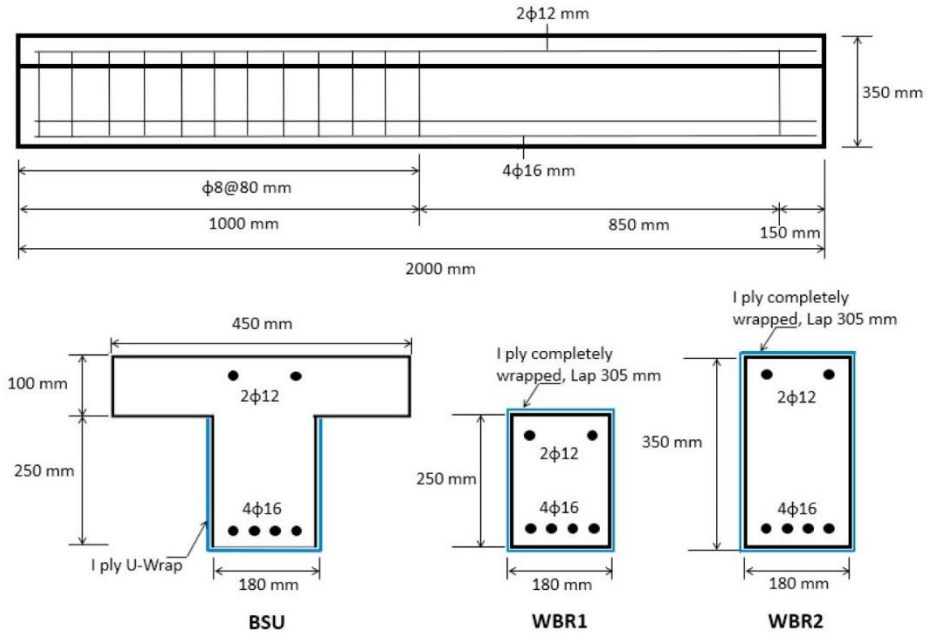

Figure 3.8 Side view and cross-section of reinforcement detailing of beams (Mhanna et al. 2019)

While the strengthened T-beam showed a higher load capacity than its 250 mm (9 7/8") rectangular counterpart due to its greater depth and total concrete compression area, the 350 mm (1'-1 6/8") fully wrapped rectangular beam managed to surpass it. The main difference in the behavior of the U-wrapped and the fully wrapped beams was the failure mode, which was debonding in the U-wrapped T-beam and concrete crushing and CFRP rupture in the fully wrapped beams. This difference in failure mode led to a much higher ductility for the fully wrapped beams, as can be seen by the deflection at failure results.

The authors concluded that fully wrapping clearly outperforms U-wrapping of EB reinforcement in shear strength and ductility due to failing in rupture instead of debonding. Since full wrapping of beams is not always possible, anchoring the EB reinforcement to the beam in order to resist debonding is their recommended solution, as well as the subject of their future research.

3.3.2 DIFFERENT FRCM SYSTEMS FOR SHEAR-STRENGTHENING OF REINFORCED CONCRETE BEAMS (YOUNIS ET AL. 2017)

Fiber Reinforced Cementitious Materials (FRCM) are becoming popular as a strengthening material for concrete due to several advantages over their main competitor: FRP,

which include higher compatibility with concrete, higher heat resistance, and the ability to use recycled cementitious materials. While a large amount of literature is available concerning the use of FRCM as a strengthening material for concrete elements, few studies compare the effect of different fibers in FRCM or the effect of anchoring the FRCM reinforcement for shear strengthening. With that in mind, Younis et al. (2017) studied the shear behavior of 16 RC beams, strengthened with different configurations of FRCM reinforcement, with the goal of enriching the literature with comparisons of the performance of different FRCM fibers, different reinforcement orientations, and reinforcement anchoring.

The authors tested 16 RC beams with 2100 mm (6'-10 5/8") length, 150 mm (5 7/8") width, and 330 mm (1'-1") depth, in one-point loading. Of the 16 beams, one had no additional reinforcement and was the control beam, and the rest of the beams were reinforced by three different materials and five different reinforcement schemes. The materials were Carbon (C-FRCM), polyparaphenylene benzobisoxazole (PBO-FRCM), and Glass (G-FRCM), while the strengthening configurations covered the shear critical zone of the beam and included (a) a full/continuous scheme, (b) two intermittent schemes with 90° and 45° orientations, and (c) two schemes identical to the previous with the addition of anchorage (Figure 3.9). The FRCM reinforcement was applied on the sides of the beam, consisting of two fiber fabric layers and three mortal layers, and had approximately 15 mm (5/8") thickness. The intermittent strips were 120 mm (4 6/8") wide and were spaced 95 mm (3 6/8") from each other, while the anchorage was achieved by mechanically fixing two FRP plates on the top and bottom parts of the FRCM reinforcement (Figure 3.10). The beams were constructed with f'_c=30 MPa (4.3 ksi) concrete and f_y=600 MPa (87 ksi) steel, while the different FRCM materials were tested in tension and were assigned the properties shown in Table 3.1.

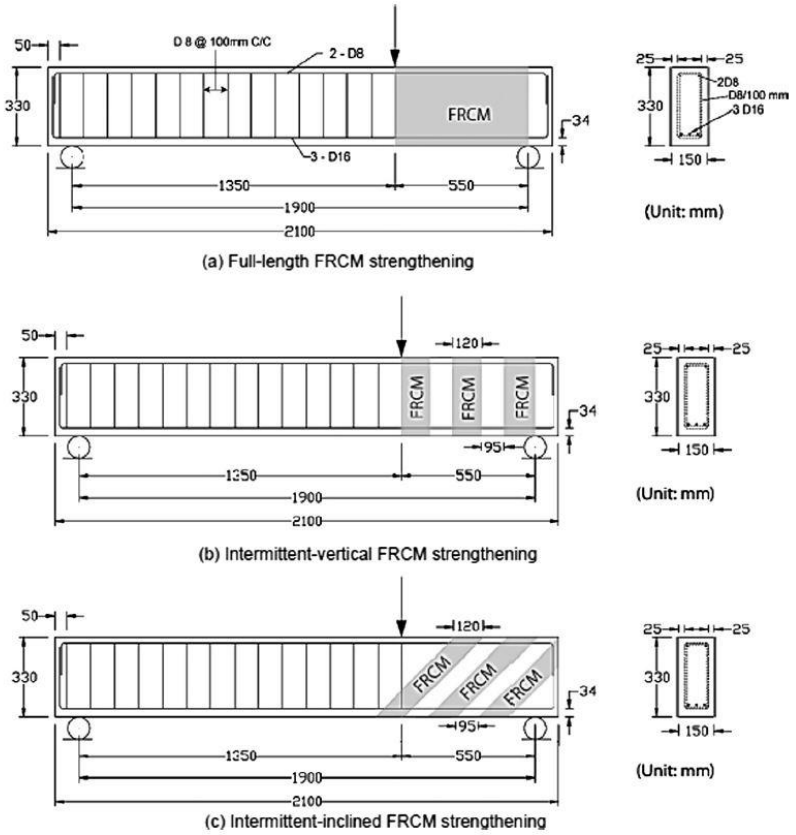

Figure 3.9 Side view and cross-section of the steel reinforcement detailing and the three different FRCM strengthening schemes used in the study (Younis et al. 2017)

Table 3.1 Derived properties of the three FRCM materials (Younis et al. 2017)

FRCM type	σ_{fu} (MPa)	ε_{fu} (%)	E_f (GPa)	Mode of failure
C–FRCM	1178	1.04	135	Fabric slippage
PBO–FRCM	1235	1.06	112	Fabric slippage
G–FRCM	767	0.93	60	Fabric rupture

Figure 3.10 Application of the anchorage for the FRCM reinforcement. (Younis et al. 2017)

The results of the one-point loading tests showed a 51% increase in load capacity, a 60% increase in deformation at failure, and increased energy absorption on average for the strengthened beams compared to the control beam. Among the different materials, C-FRCM outperformed PBO-FRCM and G-FRCM in load capacity, deformation at failure, and energy absorption. Among the configurations, the full/continuous scheme performed better than the others, due to its higher amount of total reinforcement, with a 101.6% increase in load capacity, 138% increase in deformation at failure, and 328% increase in energy absorption for the C-FRCM variant, which was the overall highest performer. Among the intermittent schemes, however, the 90° orientation performed better for the C-FRCM and the G-FRCM, while the 45° orientation performed better for the PBO-FRCM. One possible explanation given by the authors is that the PBO fibers were utilized better against shear when oriented at 45° since their fabric was one-directional, while the Carbon and Glass fiber fabrics were unidirectional. The anchored variants had a slightly higher performance than their counterparts. However, all beams, including the anchored ones, failed due to debonding and shear beam failure, which means that the anchorage used in this study failed its purpose.

Finally, they studied a parameter named axial stiffness κ_f, which is a unique FRCM characterization, and depends on (a) the amount of FRCM applied in the beam's critical area, (b) the amount of fabric utilized in the FRCM, and (c) the cracked elastic modulus of the FRCM. They determined with high statistical accuracy that the load capacity and energy absorption of the strengthened beam are proportional to the axial stiffness κ_f of the FRCM reinforcement.

The authors summarize their findings as follows: (a) the FRCM reinforcement was able to efficiently raise shear load capacity by 51% on average, deformation at failure by 60% on average and energy absorption up to 328% (b) all beams failed due to debonding of the FRCM reinforcement and shear beam failure, so the anchoring used in this study wasn't effective, and (c) fiber orientation should be considered when deciding on FRCM reinforcement orientation.

3.3.3 SHEAR STRENGTHENING OF RC BEAMS WITH FRP GRID-REINFORCED ECC MATRIX (YANG ET AL. 2020)

Fiber Reinforced Cementitious Materials (FRCM), along with their variant TRM (Textile Reinforced Mortars), are increasingly being used in externally bonded (EB) strengthening of reinforced concrete members due to their advantages over FRP, which include better

performance in high temperatures, better compatibility with concrete, and a lower cost. Engineered Cementitious Composites (ECC), which are cementitious materials reinforced with a low fiber volume, are also gaining ground due to their high load capacity and ductility as well as their strain hardening behavior. FRP Grid Reinforced ECC Matrix (FGREM) is a material obtained by using ECC as the cementitious material in FRCM, that utilizes the advantages of both materials and could be an ideal material for strengthening RC members. Yang et al. (2020) inspired by recent studies showing the effectiveness of FGREM in the flexural strengthening of RC members, investigated its effectiveness in shear strengthening, by studying the behavior of 12 shear-critical RC beams under one-point loading with different configurations of FGREM reinforcement.

The 12 shear-critical beams were tested in one-point loading at a rate of 1.5 mm/minute until failure and had a width of 150 mm (5 7/8”), a depth of 300 mm (11 6/8”), and a length varying between 1500 mm (4’-11”) and 1900 mm (6’-2 6/8”). They were constructed with f'_c=30 MPa concrete and f_y=400 MPa steel, and were strengthened with different combinations of the following matrices and FRP grids:

- ECC matrix with Polyethylene (PE) fibers
- Polymer Modified Mortar (PMM) matrix
- Carbon FRP grid
- Basalt FRP grid

All the materials used in the study were tested by the authors and the results of the tests can be seen in Table 3.2, while the reinforcement details can be seen in Figure 3.11.

Table 3.2 Material properties. (Yang et al. 2020)

Material	Yield stress (MPa)	Yield strain (%)	Ultimate strength (MPa)	Rupture strain (%)	Elastic modulus (GPa)
Tensile steel bar	467	0.242	628	–	193
Compressive steel bar	467	0.242	628	–	193
Stirrup	453	0.227	567	–	200
CFRP grid	–	–	1400	1.40	100
BFRP grid	–	–	1760	2.20	80
Material	Compressive strength (MPa)	Tensile strength (MPa)	Ultimate tensile strain (%)	Elastic modulus (GPa)	
Concrete	32.7	2.62	–	28.9	
ECC	25.0	7.22	16.0	16.9	
PMM	37.0	11.9	0.13	9.0	

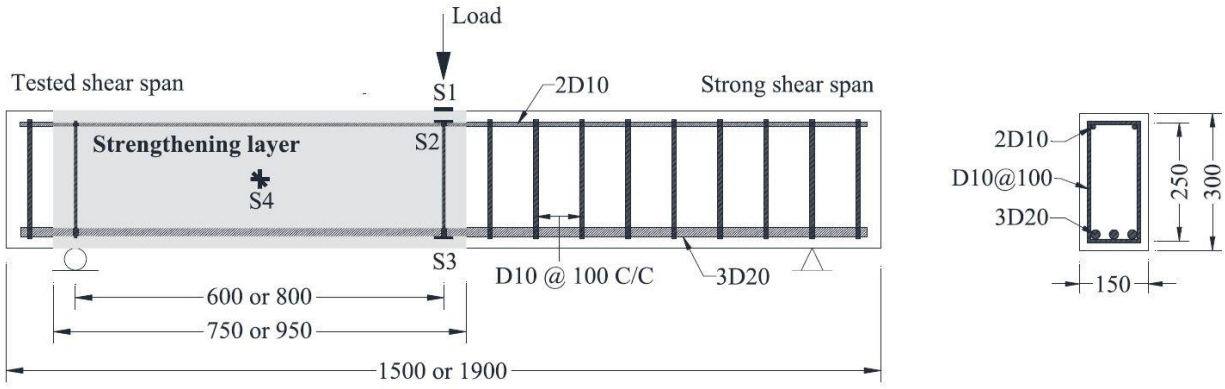

Figure 3.11 Beam dimensions and reinforcement details (Yang et al. 2020)

The two different beam lengths were selected in order to give the beams two different characterizations according to ASCE: the 1500 mm (4'-11") length beams had a span-to-depth ratio a/d=2.26 which is less than 2.5 and are considered short beams, while the 1900 mm (6'-2 6/8") length beams had a/d=3.02 and are considered ordinary shallow beams.

The strengthening layers were applied on both sides of the beams and were all 20 mm (6/8") thick but varied in their installation methods. The two installation methods used were (a) Prefabricated, where the strengthening layers were cast in the laboratory, wet cured for seven days, and glued to the beam with the use of an epoxy (Figure 3.12) (b) Cast-in-place, where the strengthening layers were applied manually to the beams with a thin latex layer between them in order to improve adhesion.

Figure 3.12 Installation of prefabricated strengthening layers. (Yang et al. 2020)

In summary, the 12 tested beams were divided into three groups of 4 beams each, the details of which can be seen in Table 3.3:

- Group A, where the beams were 1500 mm (4'-11") long and the strengthening layers were composed of matrices without FRP grids.
- Group B, where the beams were 1500 mm (4'-11") long and the strengthening layers included FRP grids.
- Group C, where the beams were 1900 mm (6'-2 6/8") long and were strengthened with and without the use of FRP grids.

Table 3.3 Design parameters of the tested beams (Yang et al. 2020)

Series	Specimen code	Shear span-to-effective depth ratio	Type of matrix	Type of FRP grid	Reinforcement ratio of FRP grid (‰)	Installation method
a	*a*-0	2.26	–	–	–	–
	a-N-E-Cast		ECC	–	–	Cast-in-place
	a-N-E-Pre		ECC	–	–	Prefabricated
	a-N-M-Pre		PMM	–	–	Prefabricated
b	*b*-B-E-Cast	2.26	ECC	BFRP	1.69	Cast-in-place
	b-B-E-Pre		ECC	BFRP	1.69	Prefabricated
	b-C-E-Pre		ECC	CFRP	3.52	Prefabricated
	b-B-M-Pre		PMM	BFRP	1.69	Prefabricated
c	*c*-0	3.02	–	–	–	–
	c-N-E-Cast		ECC	–	–	Cast-in-place
	c-N-E-Pre		ECC	–	–	Prefabricated
	c-C-E-Pre		ECC	CFRP	3.52	Prefabricated

The detailed results of the test can be seen in Table 3.4, and showed that all the beams except one failed in shear (Figure 3.13) and that the strengthened beams had a load capacity increase ranging between 51% and 161%. More specifically, the control beams failed by crack-induced shear, the cast-in-place strengthened beams failed by debonding of the strengthening layer, and the prefabricated layer strengthened beams failed due to separation caused by cracks in the substrate concrete. The authors believe that the increased stiffness at the sides of the beams due to the prefabricated layers caused stress concentrations and increased interfacial stress, while the epoxy glue used with the prefabricated layers was strong enough that it caused the beam's concrete substrate to fail first. The one beam that didn't fail in shear was the 1900 mm (6'-2 6/8") long beam, strengthened by prefabricated CFRP-ECC layers, and it failed due to separation caused by flexural cracks in the concrete substrate.

Table 3.4 Detailed results of the three-point bending test (Yang et al. 2020)

Summary of test results.

Name	P_{cr} (kN)	P_u (kN)	Gain in P_u (%)	δ_u (mm)	$\delta_{0.8u}$ (mm)	$D = \delta_{0.8u}/\delta_u$	Failure mode
a-0	40.6	58.0	–	1.93	2.01	1.04	Major shear crack
a-N-E-Cast	50.0	90.1	55.3	2.23	3.04	1.36	Interfacial debonding
a-N-E-Pre	70.9	125.0	115.5	3.89	5.78	1.49	Separation of concrete side cover
a-N-M-Pre	65.0	121.0	108.6	3.65	3.94	1.08	Separation of concrete side cover
b-B-E-Cast	68.0	95.5	64.7	3.03	4.40	1.45	Interfacial debonding
b-B-E-Pre	92.4	147.6	154.5	4.03	5.00	1.24	Separation of concrete side cover
b-C-E-Pre	76.5	142.4	145.5	3.91	4.35	1.11	Separation of concrete side cover
b-B-M-Pre	55.0	114.6	97.6	2.93	3.68	1.26	Separation of concrete side cover
c-0	34.7	49.5	–	1.93	2.08	1.08	Major shear crack
c-N-E-Cast	34.0	74.7	50.9	3.92	5.09	1.30	Interfacial debonding
c-N-E-Pre	70.0	115.3	132.9	7.51	8.30	1.11	Separation of concrete side cover
c-C-E-Pre	72.0	129.0	160.6	8.14	10.14	1.25	Flexural cracks → Separation of concrete side cover

Notes: P_c – cracking load, P_u – peak load, δ_u – deflection at P_u, $\delta_{0.8u}$ – deflection at a descending load level corresponding to 0.8 P_u, D – displacement ductility parameter.

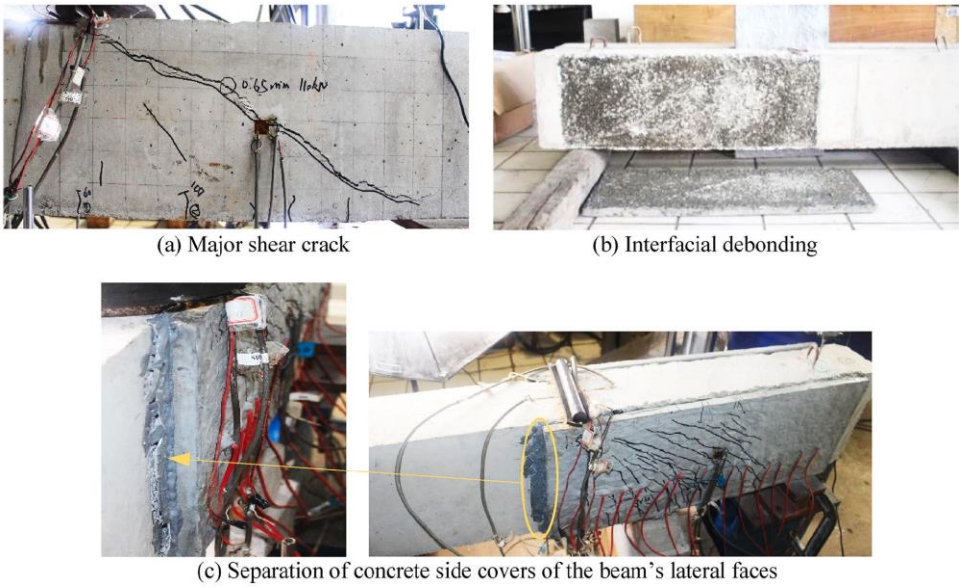

(a) Major shear crack (b) Interfacial debonding

(c) Separation of concrete side covers of the beam's lateral faces

Figure 3.13 Failure modes of the test specimens. (Yang et al. 2020)

Comparing the load capacity, deformation at failure, and ductility of the beams in each group, the authors realized that the matrix type, FRP type, and installation method had different effects on each group. In group A, the matrix type had no influence on load capacity and deformation at failure, but the ECC matrix had a ductility factor of D=1.49 compared to the PMM's D=1.08, while the prefabricated layers caused higher load capacities and deformations at failure than the cast-in-place ones. In group B, the ECC matrix led to 147.6 kN (33.2 kip) load capacity and 4.03 mm (3/16") deformation at failure, compared to the 114.6 kN (25.8 kip) and 2.93 mm (1/8") of the PMM matrix, while both of them having similar ductility factors. According to the authors, that is an indication that the FRP grids are better utilized by the ECC

matrix. Additionally, in group B, the BFRP grids slightly outperformed the CFRP grids in load capacity, deformation at failure, and ductility. In group C, all beams had lower load capacity and deformation than their counterparts in other groups, while the prefabricated layers contributed to 54.4% and 91.6% higher load capacity and deformation at failure respectively, compared to the cast-in-place layers.

After analyzing all the data, the authors concluded that FGREM is a viable material for shear strengthening RC beams, that can increase shear load capacity in a range between 51-161%. They also determined that the prefabricated installation method is more efficient than the cast-in-place one due to its superior failure mode, higher load capacity, and higher deformation at failure, while using BFRP grids is more efficient than using CFRP grids due to their better performance and lower cost.

3.4 SUMMARY

This chapter has presented seven innovative techniques for the flexural and shear rehabilitation of RC beams. In sub-chapter 3.2, flexural rehabilitation techniques, involving FRP and wood, Externally Bonded Basalt FRP sheets, Carbon FRCM, and Bottom and Side NSM CFRP bars, are presented, capable of increasing capacities up to 130%, with BFRP reinforcement having the side effect of causing a 30% reduction in ductility. In sub-chapter 3.3, shear rehabilitation techniques involving the use of Carbon FRP sheets, Carbon, Glass, and PBO FRCM, and Carbon and Basalt FRP Grid Reinforced ECC Matrices (FGREM), are presented, capable of increasing capacities by up to 200% and deformations at failure up to 900%.

Of the flexural rehabilitation techniques reviewed in this chapter, the FRP and wood, as well as the Bottom and Side NSM CFRP bar ones performed the best, while the CFRP sheet technique for shear rehabilitation performed significantly better than the FRCM and FGREM techniques. These results showcase the well-known fact that CFRP is a highly compatible material for RC beam rehabilitation, as well as that cheaper materials, such as wood, can compete with and even outperform more expensive materials in the flexural rehabilitation of RC beams.

4 REHABILITATION TECHNIQUES FOR RC COLUMNS

4.1 INTRODUCTION

RC columns are structural elements most commonly loaded in axial compression due to dead and live loads, as well as in shear and flexure due to lateral loads caused by earthquakes and wind. They guarantee an entire structure's stability by carrying its loads safely to the foundation, and a column failure could lead to the collapse of the entire structure and the loss of life. As such, modern RC building design follows the concept of strong columns-weak-beams to guarantee that in the case of a design-level phenomenon such as an earthquake, the beams are the first elements to fail and absorb most of the seismic energy through the formation of a plastic hinge near the beam-column joint area.

However, not all existing RC buildings are designed with modern design practices and some buildings are repurposed or expanded, leading to increased column loads. Adding to that the possibility of RC columns being damaged or their steel reinforcement having corroded, shows that the development of effective and efficient RC column rehabilitation techniques is highly important.

RC column rehabilitation techniques usually involve the addition of material on the perimeter of the column, utilizing the compressive load capacity of the added material, as well as the confinement effect it creates on the column's concrete, to increase the column's axial compressive capacity and its resistance to lateral loads. According to Gkournelos et al. (2021), RC and steel jacketing are the oldest methods for seismic strengthening of RC members, with more modern methods involving FRP, Fiber Reinforced Cementitious Materials (FRCM), or Textile Reinforced Mortar (TRM) jacketing. A recent study by Murcia-Delso et al. (2020) evaluated the effectiveness of the rehabilitation measures applied to buildings in Mexico after the 1985 earthquake, which were mostly RC and steel jacketing of columns and beams, against the 2017 Mexico earthquake. By studying four RC buildings that were both rehabilitated after the 1985 earthquake and affected by the 2017 earthquake, and by comparing their performance in the two earthquakes, they found that the rehabilitated buildings sustained only minor damages in

the 2017 earthquake and that the old rehabilitation methods are effective for seismic strengthening even today.

While the effectiveness of RC and steel jacketing is not lacking, newer methods attempt to provide higher effectiveness as well as cost-efficiency and ease of installation. Column confinement via Externally Bonded (EB) FRP sheet wrapping is one of the most popular modern RC column rehabilitation techniques, providing significant increases in load capacities and energy dissipation for an insignificant increase in column cross-section, with the drawbacks of a high cost and a reduced performance in high temperatures. A cheaper and better performing in high temperatures alternative to FRP, are FRCM or TRM, which use cementitious materials as a matrix for fibers. Koutas et al. (2019) in their state-of-the-art review mention that TRM jacketing increases stiffness, ductility, and energy dissipation for columns, but is 10%-80% less effective than FRP jacketing depending on the quality of the mortar used. Additional cementitious materials that are considered for use in modern RC column rehabilitation techniques include Ultra-High Performance Fiber Reinforced Concrete (UHPFRC) and Engineered Cementitious Composites (ECC).

In this chapter, seven innovative rehabilitation techniques concerning the seismic rehabilitation and the repair and axial strengthening of RC columns will be presented.

4.2 SEISMIC STRENGTHENING OF RC COLUMNS

4.2.1 SEISMIC STRENGTHENING OF CONCRETE COLUMNS BY ULTRAHIGH-PERFORMANCE FIBER-REINFORCED CONCRETE JACKETING (HONG ET AL. 2021)

Hong et al. (2021) studied the behavior and shear strength of RC columns jacketed by ultrahigh-performance (steel) fiber-reinforced concrete (UHPFRC) with the addition of textile reinforcement, under cyclic lateral loading, by testing it in six different configurations. The authors were motivated to study UHPFRC jacketing due to its advantages over normal RC jacketing, which include a 50% reduced jacketing thickness requirement (Beschi et al. 2011), the elimination of the splitting failure mode in splice regions, and the elimination of longitudinal rebar buckling (Dagenais and Massicotte 2015).

For the purpose of this study, seven 300x300x1260 mm RC columns were tested in cyclic lateral loading: two with UHPFRC jacketing of 30 and 45 mm thickness, two with carbon fiber reinforced UHPFRC jacketing of 30 mm (1 1/8") and 45 mm (1 6/8") thickness, two with glass fiber reinforced UHPFRC jacketing of 30 mm (1 1/8") and 45 mm (1 6/8") thickness, and one reference plain RC column (Figure 4.1). Of the materials used in this test, the UHPFRC had a compressive strength of 172 MPa (25 ksi) and a Young's Modulus of 45,000 MPa (6.5 msi), the carbon fibers had a tensile strength of 4000 MPa (580 ksi), a Young's Modulus of 250 GPa (36.2 msi), and cross-sectional area/m of 141.02 mm^2/m, and the glass fibers had a tensile strength of 1700 MPa (246.5 ksi), a Young's Modulus of 72 GPa (10.4 msi), and a cross-sectional area/m of 105.67 mm^2/m.

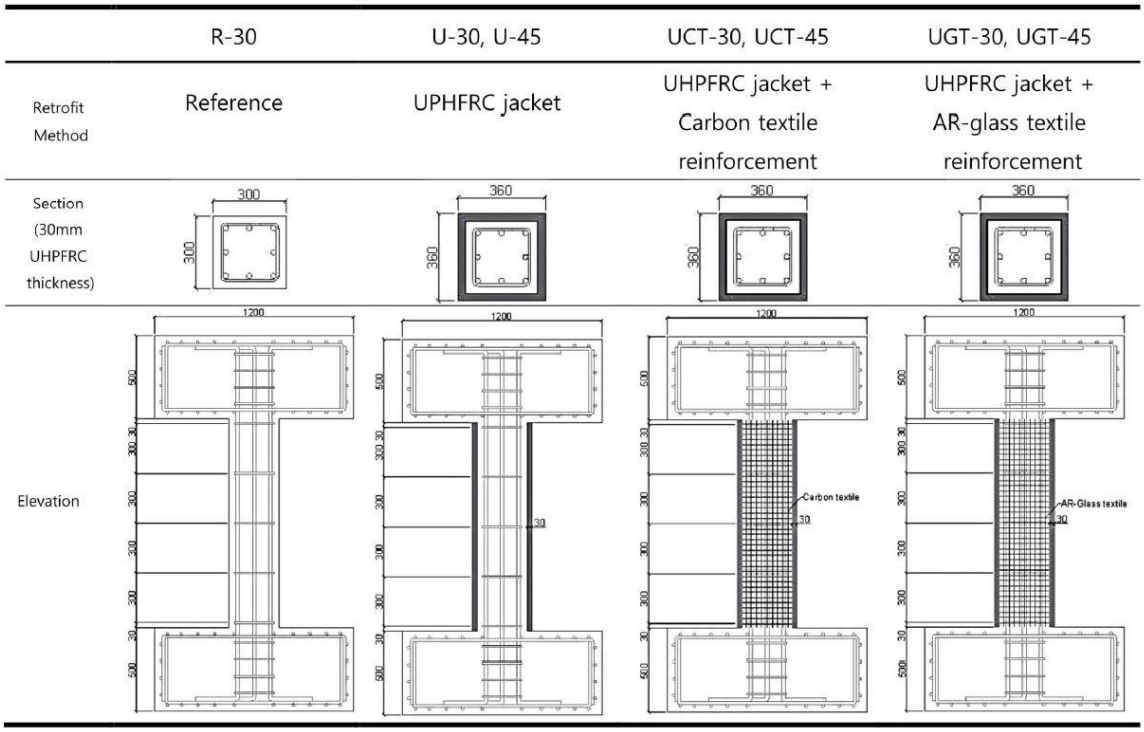

Figure 4.1 Dimensions and reinforcement configurations for the test specimens (Choi et al. 2018)

The test results showed a significant increase in lateral load capacity in all jacketed columns compared to the reference one, as well as the change of the failure mode in some cases, from shear to flexural. Additionally, the inclusion of textile reinforcement caused an increase in ductility, with little difference between the carbon and glass fibers. After testing the columns, the authors developed a formula for calculating the shear strength of UHPFRC jacketed columns and compared it with the results of the tests (Table 4.1).

Table 4.1 Test and prediction results for lateral load capacity (Choi 2018)

		Test result		Prediction		Required shear strength for flexural failure	Strength ratio		
				Shear strength, V_n (kN)			V_u/V_n		
Specimen	Failure mode	V_u (kN)	Initial stiffness (kN/mm)	$\gamma = 0.3$	$\gamma = 0.5$	V_{nf} (kN)	$\gamma = 0.3$	$\gamma = 0.5$	V_u/V_{nf}
R-30	Shear	239	27.6	188	194	330	1.23	1.23	0.72
U-30	Shear	419	34.9	409	437	462	1.03	0.96	0.91
UCT-30	Flexural shear	466	36.5	459	487		1.01	0.96	1.01
UGT-30	Flexural	461	36.5	441	469		1.04	0.98	0.99
U-45	Shear	490	70.1	489	511	508	1.00	0.96	0.96
UCT-45	Flexural shear	538	67.6	539	561		1.00	0.95	1.06
UGT-45	Flexural shear	512	69.2	521	543		0.98	0.94	1.01

The authors concluded that UHPFRC jacketing with textile reinforcement is a viable method of improving a column's axial, flexural, and shear strength without significantly increasing its cross-sectional area, while also increasing its ductility and possibly changing its failure mode from shear to flexural.

4.2.2 EXPERIMENTAL INVESTIGATION OF SEISMIC STRENGTHENING OF REINFORCED CONCRETE SHORT COLUMNS USING EXTERNALLY BONDED REINFORCEMENT, NEAR SURFACE MOUNTED, AND HYBRID TECHNIQUES (KARGARAN AND KHEYRODDIN 2019)

Kargaran and Kheyroddin (2019) investigated the effectiveness of two new techniques for the seismic strengthening of RC short columns, involving the use of externally bonded (EBR) carbon fiber reinforced polymer (CFRP) sheets and Near Surface Mounted (NSM) glass fiber-reinforced polymer (GFRP) and CFRP bars. Of the above two techniques, EBR involves wrapping a member horizontally, vertically, or diagonally with FRP sheets, while NSM involves cutting horizontal, vertical, or diagonal grooves in a member, laying reinforcement bars inside, and filling the grooves with epoxy.

They tested, under lateral cyclic loading, a total of ten short RC 200x200x600 mm (7 7/8"x7 7/8"x1'-11 5/8") columns, consisting of one reference column, five EBR reinforced columns, and four NSM columns, with different configurations, including a hybrid configuration with both EBR and NSM reinforcement (Figure 4.2). The two new configurations investigated by the authors are EBRD+EBR1, which involves full horizontal CFRP wrapping with the addition of diagonal CFRP wrapping, and NFB+EBR1, which involves full horizontal CFRP wrapping with the addition of NSM diagonal GFRP bars.

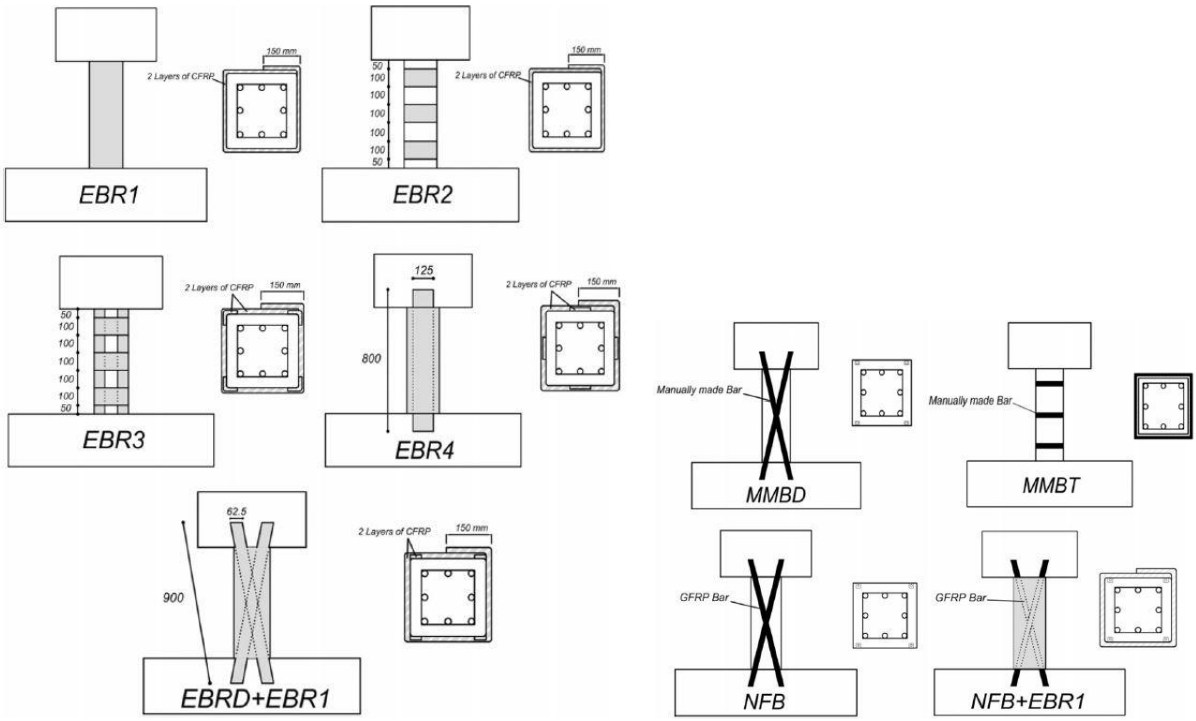

Figure 4.2 EBR configurations with the use of CFRP sheets and NSM configurations with the use of GFRP bars and manually made CFRP bars (Kargaran and Kheyroddin 2019)

Of the materials used in this test, the concrete used for the columns had a compressive strength of f'_c = 30 MPa (4.3 ksi), the steel rebar was of S500 quality (f_y = 500 MPa or 72 ksi), the CFRP sheets were made of fibers with 0.17 mm (1/128") thickness, tensile strength f_t = 3900 MPa (566 ksi) and ultimate strain of 1.7%, while the GFRP bars were of 12 mm (#4) diameter, tensile strength f_t = 1000 MPa (145 ksi), and ultimate strain of 1.5%.

Based on the results of the tests, which can be seen in Table 4.2, the authors came to the following conclusions:

1. Of the NSM configurations, the GFRP bars performed better than the manually made CFRP bars, while between the two CFRP bar configurations, the horizontal one performed better than the diagonal one.
2. Configurations EBR1, EBR4, EBRD+EBR1, and NFB+EBR1, which included full column wrapping with CFRP sheets changed the type of column failure from shear to flexural and delayed the debonding and rupture of FRP compared to the partially wrapped configurations, that exhibited shear column failure (Figure 4.3).

3. The EBR configurations were more ductile, dissipated more energy, and failed at higher drift ratios than the NSM configurations.
4. The two new, hybrid techniques EBRD+EBR1 and NFB+EBR1 led to the highest maximum load capacities, at 41% and 48% higher than the reference column, and had a good overall performance.

Figure 4.3 Damage and cracking patterns of specimen EBR2. (Kargaran and Kheyroddin 2019)

Table 4.2 Test results (Kargaran and Kheyroddin 2019)

Group	Specimen	Failure mode	F_y (kN)	F_{max} (kN)	F_u/FuR	Δ_y (mm)	Δ_u (mm)	Δ_{max} (mm)	μ	μ/μ_R	A (kN.mm)	A/A_R
–	R	Shear	41	71.4	1	9.696	11.58	7.8	1.194	1	4.4562×10^3	1
ERB	EBR1	Flexural	140	155.5	2.18	18.6	34.62	27.3	1.86	1.56	2.9142×10^4	6.54
	EBR2	Shear	120	136.5	1.91	13.7	31.5	17.16	2.29	1.92	2.0956×10^4	4.7
	EBR3	Shear-flexural	92.8	142.3	1.99	17.63	35.58	21.45	2.02	1.69	2.1138×10^4	4.75
	EBR4	Flexural	146	163	2.28	17.8	67.43	37.2	3.79	3.17	5.903×10^4	13.24
	EBRD + EBR1	Flexural	114	172.2	2.41	23.5	73.46	56.2	3.125	2.62	4.5853×10^4	10.29
NSM	MMBD	Shear	77.9	90	1.26	5.05	13.88	7.94	2.74	2.29	3.878×10^3	0.87
	MMBT	Shear	111.4	112.5	1.57	10.61	21.33	17.25	2.01	1.68	9.2192×10^3	2.07
	NFB	Shear	60.5	99	1.39	7.25	21.39	10.92	2.95	2.47	8.3373×10^3	1.87
	NFB + EBR1	Flexural	145.5	177	2.48	21.8	34.91	33.1	1.6	1.34	1.5876×10^4	3.56

F_{max}: maximum load carrying capacity; Δ_{max}: maximum displacement; F_y: elastic load carrying capacity; μ: ductility; Δ_u: ultimate displacement; A: dissipated energy; Δ_y: elastic displacement.

4.2.3 A NOVEL SEISMIC STRENGTHENING METHOD OF RC COLUMNS CONFINED BY DIRECT FASTENING STEEL PLATES (SHAN ET AL. 2020)

Noting the disadvantages of most column jacketing methods, which are section enlargement and time and labor costs for concrete jacketing, low fire resistance for FRP jacketing, and difficulty of installation and possible damage to the column for steel jacketing, Shan et al. (2020) proposed a new technique for steel jacketing of columns by directly fastening steel plates to the faces of columns.

The new rehabilitation method can be applied to a column by following the below steps:

1. Fabrication of four steel plates, one for each face of the column, and welding steel angles at each of their ends.
2. Application of the steel plates to the column and fastening to the top and bottom concrete (beam and slab) with anchor bolts.
3. Clamping of the steel plates to eliminate gaps between them and the column and use of G-clamps to temporarily connect two adjacent steel plates together.
4. Connection of adjacent steel plates by direct fastening and steel angles, with the number of fasteners per angle and spacing of angles determined in design.

A schematic and a photograph of a column strengthened by the proposed method can be seen in Figure 4.4.

To determine the optimal number of fasteners and spacing of the steel angles, the authors tested eight 150x150x640 mm (5 7/8”x5 7/8”x2’-1 2/8”) RC columns reinforced with different configurations of steel plate reinforcements under cyclic lateral loading. Regarding the materials used for this test, the longitudinal reinforcement was comprised of 10 mm diameter (#4) steel bars with yield strength f_y=586 MPa (85 ksi), the concrete compressive strength, f'_c, varied between 26 MPa (3.7 ksi) and 36.6 MPa (5.3 ksi) and the steel plates and steel angles had approximate yield strength f_y=300 MPa (43.5 ksi) With the exception of two reference plain RC columns, the columns were reinforced with steel plates with thickness varying between 3 mm (1/8”) and 5 mm (2/8”) and steel angles with dimensions of 70x70x5 mm (2 6/8”x2 6/8”x2/8”) and 60 mm (2 3/8”) length, their spacing varying between 60 (2 6/8”) and 100 mm (3 7/8”), and the number of fasteners per angle varying between 2 and 4.

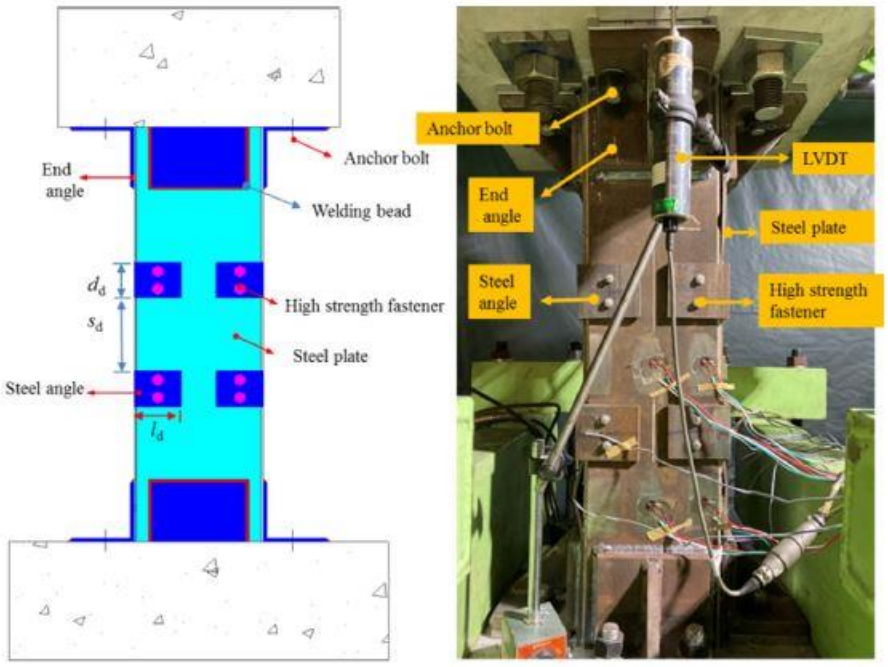

Figure 4.4 Schematic and photograph of a column strengthened by the proposed method. (Shan et al. 2020)

The authors then developed a method for estimating the flexural and shear capacity of columns strengthened by steel plates and validated it with the results of the test (Table 4.3).

Table 4.3 Ultimate drift ratio, shear capacity, and experimental and theoretical lateral load results, with all load values in (kN) (Shan et al. 2020)

Specimen	Experimental lateral load (V_{exp})	Experimental lateral load that considers second moment (V_{exp}')	Axial load (kN)	Ultimate drift ratio	Shear capacity (V_o)	Theoretical lateral load (V_{theo})	V_{theo}/V_o	V_{theo}/V_{exp}'
C-0.16	13.0	14.7	155	2.0	47.5	15.9	0.28	1.08
S-0.16-3-100-2	33.9	37.6	177	2.6	89.1	35.7	0.37	0.95
S-0.16-4-100-2	42.4	47.9	207	2.8	105.5	45.1	0.41	0.94
S-0.16-5-100-2	47.9	55.3	227	3.6	119.4	53.2	0.42	0.96
S-0.16-4-60-4	44.0	49.2	277	3.2	234.4	48.9	0.2	0.99
S-0.16-4-100-4	41.3	46.2	215	3.0	161.2	45.6	0.27	0.99
C-0.3	11.2	12.6	267	1.2	51.7	14.7	0.28	1.17
S-0.3-4-100-2	31.8	37.2	375	1.8	97.2	40.0	0.36	1.08
Mean								1.02
COV								0.1

Note: V_{exp} is the experimental lateral load and V_{exp}' is the experimental lateral load that considers the second moment; V_o is the shear capacity; and V_{theo} is the theoretical lateral load.

Notably, all eight columns exhibited flexural failure, with plastic hinge regions developing near the base of the reference columns and shifting upwards for the strengthened columns. Based on the results of the test, the authors concluded that (a) the steel plate reinforcement significantly increased the flexural capacity and ultimate drift ratio of RC columns, with the thickness of the plate being the most influential parameter and the number of fasteners having almost no influence (b) reducing the spacing between the steel angles increased

the column's energy dissipation, possibly by delaying the buckling of the steel plates; (c) the connection of the RC column and the steel plates through the steel angles was stable and robust throughout the loading process, regardless of the number of fasteners used.

4.2.4 SHEAR STRENGTHENING OF RC SHORT COLUMNS WITH ECC JACKET: CYCLIC BEHAVIOR TESTS (DENG ET AL. 2018)

Reinforced concrete buildings with short columns are at increased risk of collapse during earthquakes, due to short columns being prone to brittle shear and flexural shear failures when affected by lateral cyclic loading. Column strengthening methods commonly involve the jacketing of materials such as FRP and steel, which provide increased ductility but are expensive, and concrete and ferrocement, which are not ductile materials. Engineered Cementitious Composites (ECC) are a type of cement mixture, which includes a low volume of fibers and achieves significantly higher strength and ductility compared to concrete, as well as a strain hardening behavior in tension and shear. In order to enrich the literature on the use of ECC jacketing for strengthening structural elements, Deng et al. (2018) studied the behavior of seven RC short columns with different configurations of ECC jacketing, under reversed cyclic loading.

The seven short columns had a cross-section of 250x250 mm, a height of 600 mm, and an effective height of 500 mm (1'-7 5/8") due to the application of the cyclic load being 100 mm (3 7/8") below the top of the columns. They were constructed using f'c=30 MPa (4.3 ksi) concrete, six longitudinal 16 mm diameter (#5) bars and 8 mm diameter (#3) ties at 100 mm (3 7/8") spacing, made of f_y=400 MPa (58 ksi) (Figure 4.5). Columns C1 to C7 were strengthened with different configurations and had different axial loads applied to them as can be seen in Table 4.4. Essentially, column C2 had ferrocement jacketing, column C3 had unreinforced ECC jacketing, columns C4, C6, and C7 had ECC jacketing reinforced with a steel mesh, while C1 and C5 were control columns. Additionally, columns C1 to C4 were loaded with a constant 572 kN (128.6 kip) axial load, while columns C5 to C7 were loaded with a 715 kN (160.7 kip) axial load.

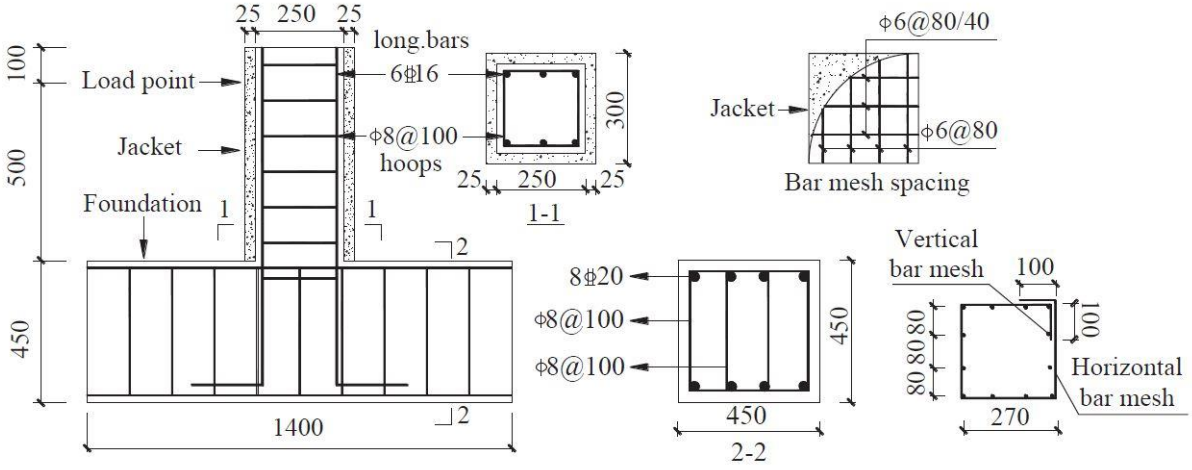

Figure 4.5 Dimensions and reinforcement details for the column specimens. (Deng et al. 2018)

Table 4.4 Main parameters of column specimens. (Deng et al. 2018)

Specimen	Jacket matrix	Mesh spacing h × v (mm)	Jacket scheme	Axial load N (kN)	n_t	n_d
C-1	–	–	–	572	0.35	0.80
C-2	Mortar	80 × 80	Ferrocement	572	0.22	0.47
C-3	ECC	–	0-ECC	572	0.21	0.47
C-4	ECC	80 × 80	B-ECC	572	0.21	0.47
C-5	–	–	–	715	0.43	1.00
C-6	ECC	80 × 80	B-ECC	715	0.26	0.58
C-7	ECC	40 × 80	B-ECC	715	0.26	0.58

The ECC and ferrocement used for strengthening had 59 MPa (8.5 ksi) and 54.9 MPa (7.9 ksi) compressive strength respectively, while the ECC included 1.5% per volume Polyvinyl alcohol (PVA) fibers which led to ECC having a tensile strength of 5 MPa (725 psi). The jacketing was applied manually with a trowel in two layers and had a total thickness of approximately 25 mm (1”). After casting, the jackets were water cured for 28 days and then cured naturally until the tests were conducted. The columns were tested under reversed cyclic loading, with 20 kN (4.5 kip) increments until the steel yielding point, after which the loading became displacement controlled, with 2 mm (3/32”) increments. The tests were terminated when the columns degraded to 85% of their peak lateral strength.

The results showed that the columns strengthened with ECC, in general, had a better performance than the control columns and the ones strengthened with ferrocement.

- In terms of failure modes, the control columns C1 and C5 failed in shear, the ferrocement strengthened C2 failed in brittle flexural shear, the ECC strengthened columns C3, C4,

and C6 failed in ductile flexural shear, while column C7, that had additional horizontal mesh bars, failed in flexure.

- All ECC strengthened columns had better hysteretic performance, ductility, and energy dissipation than their control columns and the ferrocement reinforced column. More specifically, columns C6 and C7 had 41.7% and 85.6% higher ductility compared to control column C5 while also having 258% and 549% higher energy dissipation respectively. Notably, column C3 strengthened with unreinforced ECC exhibited better hysteretic performance than ferrocement strengthened column C2, indicating that unreinforced ECC can be a viable method for quickly strengthening short columns.
- All jacketed columns achieved a higher peak lateral load than their respective control beams, in the range of 44.6% and 48.7% however, indicating that any differences in the strengthening configuration had minimal impact on lateral load capacity.
- After reaching the peak lateral load, the stiffness degradation of the ECC strengthened columns was slower compared to their control beams, with column C7 having the slowest stiffness degradation and the highest amount of loading cycles. While the increased axial load sped up degradation in control column C4 compared to C1, columns C4 and C6, which had identical strengthening schemes and different axial loads, had almost identical stiffness degradation, possibly due to the strain hardening properties of ECC.

The authors concluded that ECC jacketing is a viable and easily applied method for strengthening short RC columns, that provides a significant increase in ductility and energy dissipation that can change the column's failure mode from shear to flexure, and an increase in lateral load capacity comparable to that provided by ferrocement jacketing.

4.3 REPAIR AND AXIAL STRENGTHENING OF RC COLUMNS

4.3.1 REPAIRING AND STRENGTHENING OF DAMAGED RC COLUMNS USING THIN CONCRETE JACKETING (TAYEH ET AL. 2019)

Ultra-High Performance Fiber Reinforced Concrete (UHPFRC) is concrete that includes steel fibers among other materials. It is made with a higher volume of cement and a lower volume of water than Normal Strength Concrete (NSC) and is able to achieve compressive strengths greater than 100 MPa (14.5 ksi), as well as high tensile strengths and ductile behavior.

Tayeh et al. (2019) studied the efficiency of Self-Consolidating UHPFRC (UHPFRSCC) and of NSC in repairing and strengthening damaged RC columns, by testing under uniaxial compression 45 small scale RC columns strengthened with jackets of different thicknesses, made of UHPFRSCC and NSC, and utilizing different methods for improving interfacial adhesion.

The core of the 45 RC columns had a 100x100 mm (3 7/8"x3 7/8") cross-section and a 300 mm (11 6/8") height (Figure 4.6), was made with f'_c=25 MPa (3.6 ksi) concrete, and reinforced with four 8 mm (#3) longitudinal bars of f_y=360 MPa (52 ksi) steel and three 2.5 mm (3/32") ties of f_y=240 MPa (34.8 ksi). In summary, of the 45 columns,

- 3 were control columns with no additional strengthening (UC),
- 6 were also control columns with the same amount of reinforcement but with larger cross-sections of 150x150 mm (5 7/8"x5 7/8") and 170x170 mm (6 6/8"x6 6/8") (MC1, MC2),
- 18 were strengthened by NSC-4.75 jacketing of 25 mm (1") and 35 mm (1 3/8") thickness, compressive strength of f'_c=25 MPa (3.6 ksi), and additional steel reinforcement of four 8 mm (#3) longitudinal bars and three 2.5 mm (3/32") ties (Groups A and B), and
- 18 were strengthened by UHPFRSCC jacketing of 25 mm (1") and 35 mm (1 3/8") thickness, compressive strength of f'_c=120 MPa (17.4 ksi), and the same additional steel reinforcement as the previous groups (Groups X and Y)

The strengthening jackets were installed with three different surface roughening methods: (a) mechanical wire brushing, (b) mechanical scarification, where cuts 3 - 6 mm (1/8" – 2/8") wide and 6-7 mm (2/8") deep were made on the concrete surface, and (c) shear studs, where 4 mm (1/8") diameter, 40 mm (1 4/8") long studs were placed in 6 mm (2/8") diameter, 25 mm (1") deep holes drilled in the concrete surface, along with a bonding material. Of the 15 different column types tested in this study, each type had three representatives, and the final results were calculated as the average. A detailed description of the characteristics of the columns tested can be seen in Table 4.5. In order to simulate the damaged condition of the columns, the authors generated hairline cracks on the column cores before strengthening them, by loading them at 90% of their capacity without them reaching failure. The columns were tested under uniaxial loading at increments of 6 kN/s (1.34 kip/s) with a 20 kN (4.5 kip) starting load.

Figure 4.6 Test specimens. (Tayeh et al. 2019)

Table 4.5 Details of the column specimens (Tayeh et al. 2019)

#	Description		Notation	Column core (mm)	Overall cross section (mm)	Jacket thickness (mm)	Number of samples
1	UC unjacketed reference column		UC	100 × 100	Cross-sectional dimensions of UC and MC reference columns are fixed		3
2	MC monolithically cast reference columns		MC1	150 × 150			3
3			MC2	170 × 170			3
4	NSC-4.75 jacket, [A-B]	Roughening surface by mechanical wire brushing	A-W	100 × 100	150 × 150	25	3
5			B-W	100 × 100	170 × 170	35	3
6		Roughening surface by mechanical scarification	A-C	100 × 100	150 × 150	25	3
7			B-C	100 × 100	170 × 170	35	3
8		Bonding by using shear studs	A-S	100 × 100	150 × 150	25	3
9			B-S	100 × 100	170 × 170	35	3
10	UHPFRSCC jacket, [X-Y]	Roughening surface by mechanical wire brushing	X-W	100 × 100	150 × 150	25	3
11			Y-W	100 × 100	170 × 170	35	3
12		Roughening surface by mechanical scarification	X-C	100 × 100	150 × 150	25	3
13			Y-C	100 × 100	170 × 170	35	3
14		Bonding by using shear studs	X-S	100 × 100	150 × 150	25	3
15			Y-S	100 × 100	170 × 170	35	3

The results of the test can be seen in Table 4.6. Concerning the NSC strengthened columns, their axial load capacity was double that of the UC column and the same as their corresponding MC. The increase in capacity was proportional to the increase in jacket thickness, while the deformation at failure was similar to the one observed for the UC and MC columns. On the other hand, the UHPFRSCC strengthened columns achieved four times the axial capacity of the UC column, two times that of their corresponding MC columns, and 100% higher deformation at failure than the control columns. Additionally, for all NSC and UHPFRSCC strengthened columns, the ones using shear studs slightly outperformed the ones using mechanical wire brushing and mechanical scarification.

Table 4.6 Summary of results for all columns (Tayeh et al. 2019)

#	Description		Notation	P_u (kN)	Axial displacement (mm)
1	UC unjacketed reference column		UC	331	0.972
2	MC monolithically cast reference columns		MC1	478	0.99
3			MC2	751	1.02
4	NSC-4.75 jacket, [A-B]	Roughening surface by mechanical wire brushing	A-W	517	0.99
5			B-W	713	1.11
6		Roughening surface by mechanical scarification	A-C	642	1.02
7			B-C	812	1.14
8		Bonding by using shear studs	A-S	653	1.05
9			B-S	859	1.2
10	UHPFRSCC jacket, [X-Y]	Roughening surface by mechanical wire brushing	X-W	883	1.908
11			Y-W	1224	1.989
12		Roughening surface by mechanical scarification	X-C	956	1.92
13			Y-C	1280	2.001
14		Bonding by using shear studs	X-S	1030	1.98
15			Y-S	1356	2.04

The authors concluded that repairing and strengthening damaged RC columns with NSC and UHPFRSCC jacketing can increase the load capacity of the columns proportionately to the thickness of the jacket. Additionally, jacketing with UHPFRSCC is further able to increase the ductility and the deformation of the column at failure due to the steel fibers present in UHPFRSCC, while also being able to reduce the total thickness of the jacket since it can flow better than NSC in narrow sections. Finally, they determined that among mechanical wire brushing, mechanical scarring, and shear studs, shear studs are the best method for surface roughening and improving adhesion.

4.3.2 TEXTILE REINFORCED CONCRETE FOR STRENGTHENING OF RC COLUMNS: A CONTRIBUTION TO RESOURCE CONSERVATION THROUGH THE PRESERVATION OF STRUCTURES (ORTLEPP AND ORTLEPP 2017)

While CFRP jacketing is a popular strengthening method worldwide, utilizing confinement to strengthen RC columns, in Germany, most RC column strengthening is achieved through the concrete jacketing method, which utilizes the load capacity of the added material. Textile Reinforced Concrete (TRC) or Textile Reinforced Mortars (TRM) jacketing is a strengthening method that can utilize both the compressive strength of concrete as well as the tensile strength of the textiles, to increase confinement and column load capacity. In order to determine the viability of TRC jacketing for strengthening RC columns, Ortlepp and Ortlepp (2017) studied the behavior of 13 slender columns with different configurations of steel reinforcements and TRC jacketing under axial compression.

The 13 columns were divided into three series of four columns each, with one unstrengthened control column and three columns fully wrapped with different amounts of TRC layers, while the 13th column was partially wrapped at the top and bottom ends. In short, series A columns had no steel reinforcement, series B columns and the 13th column had steel reinforcement with 26.5 mm (1") concrete cover, and series C columns had steel reinforcement with 20 mm (6/8") concrete cover. The details of the column specimens can be seen in Table 4.7.

Table 4.7 Details of column specimens (Ortlepp and Ortlepp 2017)

Column No.	Cross section	Longitudinal bars	Stirrup leg	Concrete cover	Strengthening type	No. of textile layers
1.1	Plain concrete	–	–	–	–	–
1.2	Plain concrete	–	–	–	Full	2
1.3	Plain concrete	–	–	–	Full	4
1.4	Plain concrete	–	–	–	Full	6
2.1	Reinforced type 1	4 Ø8 mm	87 mm	26.5 mm	–	–
2.2	Reinforced type 1	4 Ø8 mm	87 mm	26.5 mm	Full	2
2.3	Reinforced type 1	4 Ø8 mm	87 mm	26.5 mm	Full	4
2.4	Reinforced type 1	4 Ø8 mm	87 mm	26.5 mm	Full	6
3.1	Reinforced type 2	4 Ø8 mm	100 mm	20 mm	–	–
3.2	Reinforced type 2	4 Ø8 mm	100 mm	20 mm	Full	0
3.3	Reinforced type 2	4 Ø8 mm	100 mm	20 mm	Full	1
3.4	Reinforced type 2	4 Ø8 mm	100 mm	20 mm	Full	2
4	Reinforced type 1	4 Ø8 mm	87 mm	26.5 mm	Partial	6

The slender column specimens had a cross-section of 140x140 mm (5 4/8"x5 4/8") and a length of 2000 mm (6'-6 6/8"). They were made of f'_c=30 MPa (4.3 ksi) concrete and reinforced by four 8 mm (#3) longitudinal bars and 6 mm (#2) ties at 60 mm (2 3/8") apart in critical sections and 100 mm (3 7/8") apart in the mid-section, made of B500C steel (f_y=500 MPa or 72 ksi). The TRC jacket was made with fine grain concrete with f'_c=73 MPa (10.6 ksi) and bi-directional glass fiber textiles with tensile strength f_u=1232 MPa (178.7 ksi) and Young's modulus E_f=74.45 GPa (10.8 msi), leading to TRC layers with a tensile strength varying between 535 - 644 MPa (77.6 - 93.4 ksi). The TRC layers were 2 mm (3/32") thick each and were manually applied one by one, with the exception of one column of series C, which was strengthened with a single 8.5 mm (3/8") fine grain concrete layer without the use of textiles. The tests were conducted with the use of a 6 MN (1350 kip) compression test machine, and a load rate of 0.5 kN/s (0.11 kip/s) for series A columns, and 1 kN/s (0.22 kip/s) for series B and C columns.

The results showed an increase of up to 85% in axial load capacity, with the increase in capacity being similar to the increase in the number of textile layers used in the TRC jackets. While the unstrengthened control columns and the fully wrapped columns all failed near the load introduction area, the partially wrapped column failed in the mid-section due to buckling, after

having achieved a 34% increase in load capacity compared to its control column. The fully wrapped columns failed due to debonding of the TRC at the column head, followed by rupture of the glass fiber textiles. The details of the results can be seen in Figure 4.7.

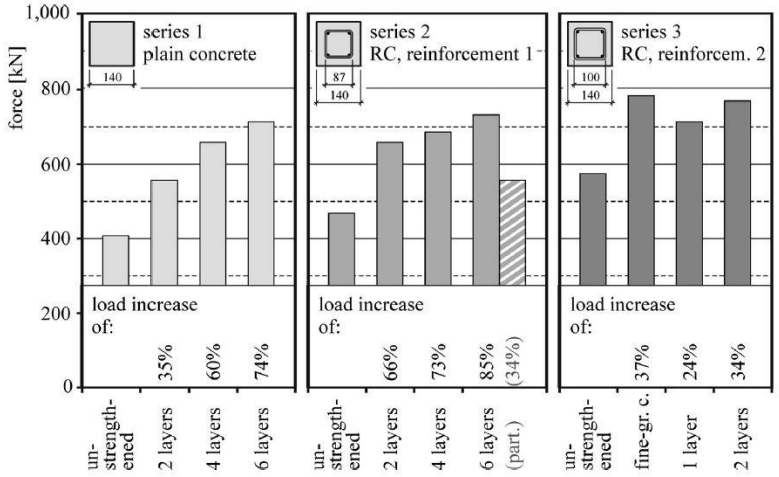

Figure 4.7 Results of the axial compression test (Ortlepp and Ortlepp 2017)

The authors also observed that the TRC jackets used in this study were unable to fully utilize their confining capabilities and failed by tearing at the column edges due to the uneven loading in rectangular column cross-sections. At the sides of the column, due to the low stiffness of the glass fibers used in this study, a larger lateral expansion of the concrete column would have been required in order to activate the confining capabilities of TRC, while at the corners of the column, the TRC jacket was locally compressed, leading to local failures and tearing. In order to improve TRC jacket confining performance in rectangular beams, they advise the use of fibers stiffer than the ones used in this study, such as Carbon fibers, and recommend smoothing column edges before applying the TRC jacket layers.

The authors concluded that TRC is a suitable material for RC column strengthening, capable of improving the axial capacity of columns proportionately to the number of textile layers used. While TRC as a material is able to utilize both its significant compressive and tensile load capacities, the authors recommend the use of stiff carbon fibers and smoothing out column edges to better utilize TRC's confining capabilities.

4.3.3 PERFORMANCE OF HIGH MODULUS NEAR-SURFACE-MOUNTED FRP LAMINATES FOR STRENGTHENING OF CONCRETE COLUMNS (KHORRAMIAN AND SADEGHIAN 2018)

Near Surface Mounted (NSM) FRP reinforcement is a strengthening technique for RC members, alternative to External Bonding (EB) or jacketing, that involves the cutting of shallow grooves on the concrete surface and the insertion of longitudinal FRP rebars. While EB reinforcement for RC columns has been studied extensively, NSM has not been sufficiently studied. One reason for that is that several studies, as well as building codes, recommend not using FRP in compression due to the material's low compressive capacity compared to its tensile capacity, as well as the possibility of micro-buckling of fibers due to imperfections during manufacturing. On the other hand, other studies have found that high stiffness NSM FRP strips have been able to effectively strengthen RC columns. Khorramian and Sadeghian (2018), motivated by the conflicting results of previous studies as well as the limited amount of research on the subject of NSM reinforcement for RC columns, studied the behavior of 14 short concrete columns with NSM CFRP reinforcement under the effect of axial load applied with varying amounts of eccentricity.

The 14 medium-scale short concrete columns used in this study had a cross-section of 150x150 mm (5 7/8"), a height of 500 mm (1'-6 5/8"), and they were constructed with the use of f'_c=37 MPa (5.4 ksi) concrete and with no steel reinforcement. The decision not to include steel reinforcement in the column specimens was made in order to determine the effect of NSM strengthening in fully corroded RC columns. Of the 14 column specimens, nine were strengthened with NSM CFRP strips, and five were made of plain concrete, while the load eccentricities considered in the study were 0 (concentric), 10, 20, and 30% of the width of the cross-section (Table 4.8). The NSM strengthened columns were reinforced with four CFRP strips with a 1.2x10 mm (1/32"x4/8") cross-section applied two each on two opposite sides of the column specimens (Figure 4.8), and had a compressive strength of f_{uc}=1031 MPa (150 ksi), a compressive modulus of E_{fc}=156.1 GPa (22.6 msi), and a compressive strain at failure of ε_{fc}=0.66%. The column specimens were wrapped with two EB Basalt FRP layers at both ends, to avoid localized failures at the load application area, and they had steel caps installed at the top

and bottom ends, with notched plates welded on them in different locations, to provide different amounts of eccentricity.

Table 4.8 Test specimen properties (Khorramian and Sadeghian 2018)

No.	Specimen ID	Eccentricity ratio, e/h (%)	Eccentricity, e (mm)	Reinforcement
1	N-e0-1	0	0	CFRP
2	N-e0-2	0	0	CFRP
3	N-e10-1	10	15	CFRP
4	N-e10-2	10	15	CFRP
5	N-e10-3	10	15	CFRP
6	N-e20-1	20	30	CFRP
7	N-e20-2	20	30	CFRP
8	N-e30-1	30	45	CFRP
9	N-e30-2	30	45	CFRP
10	P-e0-1	0	0	None
11	P-e0-2	0	0	None
12	P-e10-1	10	15	None
13	P-e10-2	10	15	None
14	P-e10-3	10	15	None

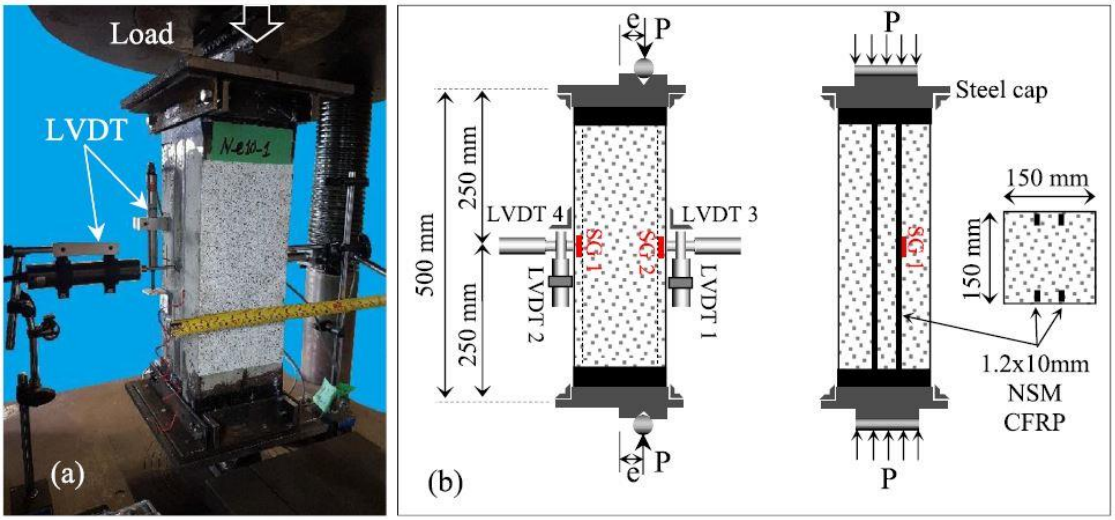

Figure 4.8 Test setup details (a) Testing machine and instrumentation, (b) Schematic with the test setup and NSM reinforcement details (Khorramian and Sadeghian 2018)

The results showed that the column specimens all failed with a combination of four different failure modes: (a) Concrete Spalling, (b) Concrete Crushing, (c) Compressive FRP Crushing, and (d) Tensile FRP Rupture, without the occurrence of CFRP debonding or buckling. More specifically, the concentrically loaded columns failed due to concrete spalling, the 10% eccentrically loaded columns failed due to concrete spalling followed by compressive FRP crushing, the 20% eccentrically loaded columns failed due to FRP crushing followed by concrete spalling, and the 30% eccentrically loaded columns failed due to tensile FRP rupture followed by

concrete spalling and FRP crushing. Notably, all FRP failures occurred after peak loading. The strengthened columns achieved a 7.7% and a 10.9% higher load capacity than the unstrengthened columns at concentric and at 10% eccentric loading.

In addition to the experimental results, the authors created an analytical model of their proposed strengthening method using MATLAB and conducted a parametric study. The parametric study considered an axial load applied at 20% eccentricity, as well as different NSM CFRP reinforcement ratios and different concrete strengths. When considering double and triple the amount of reinforcement used in the experiments, which amounted to 0.43% and 0.64% compared to 0.21% used in the experiments, an increase of 4.32% and 8.61% in axial capacity was noted, respectively. When using 25, 35, and 45 MPa (3.6, 5, and 6.5 ksi) strength concrete along with 0.21% and 0.64% reinforcement ratios, they observed that the compressive strain of the CFRP strips increased along with the increase in concrete strength and reinforcement ratio but did not exceed 50% of the material's ultimate compressive strain.

The authors concluded that strengthening using NSM CFRP strips is a viable approach for short RC columns with no risk of CFRP buckling or debonding occurring. They note, however, that further study is needed to determine the method's viability for slender columns.

4.4 SUMMARY

This chapter has presented seven techniques for the rehabilitation of RC columns. In sub-chapter 4.2, seismic rehabilitation techniques for RC columns are presented, including UHPFRC jacketing, EB, NSM, and hybrid FRP reinforcement, steel plate fastening, and ECC jacketing, able of providing over 200% increase in lateral capacities and of changing the brittle shear failure mode of control specimens to a ductile flexural failure. In sub-chapter 4.3, repair and axial strengthening techniques for RC columns are presented, including UHPFRC jacketing, TRM jacketing, and NSM FRP, capable of increasing axial capacities by over 100%.

Concerning the seismic rehabilitation techniques, all of them achieved significant ductility and energy dissipation results, but the steel plate fastening and EB and hybrid FRP techniques achieved the highest performance, with both of them having over 200% increase in lateral capacities, while the UHPFRC jacketing had over 100%, and the ECC jacketing had approximately 50% increases. The repair technique using UHPFRC was able to restore and strengthen RC columns by 100% of their axial capacity, and the TRM strengthening technique

achieved up to 85% higher load capacities, while the NSM FRP technique achieved capacity increases of up to 10%.

Overall, these results showcase the significant capabilities of FRP for the confinement of RC columns, as well as their comparatively weak abilities in compression. They also highlight the ability of UHPFRC to perform both in compression and in the confinement of RC beams, due to its high compressive and tensile capacity as well as its ductile behavior.

5 REHABILITATION TECHNIQUES FOR RC BEAM-COLUMN JOINTS

5.1 INTRODUCTION

RC beam-column joints, which for the purposes of this chapter will be referred to as joints, are located at the intersections of RC beams and columns and are defined by ACI as the portion of the column within the depth of the deepest beam that frames into the column. They are a critical component of RC buildings since they are responsible for transferring loads and moments between beams and columns, and their behavior during earthquakes determines the performance of their entire building. According to the concept of strong columns-weak beams followed by modern RC building design, RC frames are able to dissipate more seismic energy if the first failure in their frames, during a design level earthquake, is a plastic hinge formation in the beam-joint interface. Older RC buildings commonly have poor joint reinforcement, leaving them at risk of brittle shear joint failure in the event of a strong enough earthquake. Such buildings are in need of joint rehabilitation measures, capable of increasing their joints' shear capacity and of promoting failure due to the formation of a plastic hinge in the beam-joint interface against any other failure mode.

According to Engindeniz et al. (2005), older methods of RC joint rehabilitation include epoxy injections of damaged joints, removal, and replacement of damaged concrete, and concrete and steel jacketing, while since 1998, most of the research on RC joint rehabilitation has focused on Externally Bonded (EB) FRP. Pohoryles et al. (2019) in their state-of-the-art review mention that multiple EB FRP strengthening schemes have been able to increase joint shear capacities, relocate the formation of plastic hinges away from the joint and towards the beam, and address the weak column problem present in older buildings. However, they also mention that the effectiveness of any FRP retrofit scheme is highly dependent on anchorage, commonly provided by FRP fans and metallic anchors and that anchorage of FRP sheets at the joint area is a challenge that has not been sufficiently studied.

Recent studies on RC joint rehabilitation involve techniques that utilize FRP, as well as Fiber Reinforced Cementitious Materials (FRCM) and Ultra-High Performance Fiber Reinforced

Concrete (UHPFRC). In this chapter, six innovative RC joint rehabilitation techniques will be presented.

5.2 MONOTONIC RESPONSE OF RC EXTERIOR BEAM-COLUMN JOINTS REINFORCED WITH FILLER-MODULES AND FRP COMPOSITE WRAPS/GUSSETS (MAJJIGAPU 2020)

With the goal of developing a simple, economical, and durable RC joint reinforcement scheme, Majjigapu (2020), studied the behavior of joints strengthened by filler-modules and FRP wraps and gussets. In this study, he tested 20 2D RC beam-column joints, designed with pre-1976 standards, and strengthened with different combinations of FRP and filler-module configurations and materials, under monotonic bending loading.

The 20 RC joints consisted of 10”x10” columns and 12”x10” beams made of low-strength concrete of 2600, 3300, and 3800 psi compressive strength and reinforced with 60 ksi steel according to pre-1976 design standards, in order to ensure shear failure at the joint (Figure 5.1).

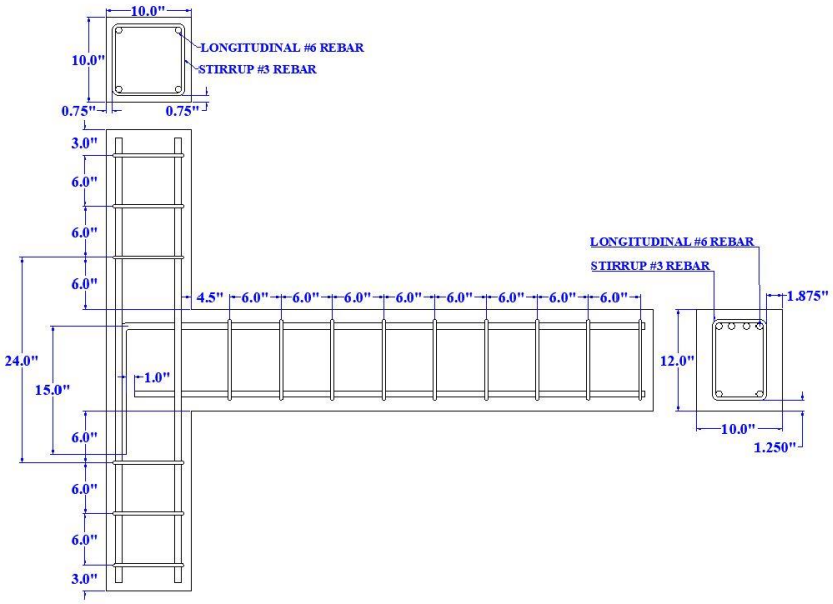

Figure 5.1 Reinforcement details of control joint specimens (Majjigapu 2020)

The filler-modules were made of three different materials: (a) Reinforced Concrete of 3300, 5400, and 9500 psi compressive strength, (b) Parallel Strand Lumber (PSL) with a compressive strength of f_c=2900 psi, and Young’s modulus of E=2 msi parallel to the strand

direction, and (c) Syntactic Foam (SF) with a compressive strength of 4320 psi and Young's modulus of 261 ksi in compression. The FRP wraps and gussets were made of t=0.04" thick layers of either unidirectional CFRP with a tensile strength of f_{fu}=181 ksi and an ultimate strain of ε_{fu}=0.0175 or unidirectional GFRP with a tensile strength of f_{fu}=88.6 ksi and an unknown ultimate strain. Along with the variation in filler-module and FRP material, the joints were also tested with a variation in filler-module shape, which included wedge and curved shapes (Figure 5.2), and with the addition or not of reinforcing dowels (Table 5.1).

Figure 5.2 Specimen with a curve-shaped filler-module, coated with primer prior to the installation of FRP wraps. (Majjigapu 2020)

Table 5.1 Joint specimen testing configuration details, (Majjigapu 2020)
CW: Concrete Wedge, CC: Concrete Curve, SF: Syntactic Foam, D: Reinforcing Dowel

Phase #	Joint	f'_c	CL	Reinforcing scheme
Phase I	JI-1	2639 psi	$0.28f'_cA_g$	Control
	JI-2			CW(3.3 ksi)+D
	JI-3			CW(3.3 ksi)+D+CFRP Wrap+360°-anchor
	JI-4			SF(4.3 ksi)+D+CFRP Wrap+360°-anchor
Phase II	JI-5	2639 psi	$0.18f'_cA_g$	Control
	JI-6			CW(5.5 ksi)+D+CFRP Gusset+U-anchor
	JI-7			CW(5.5 ksi)+D+CFRP Gusset+U-anchor*
	JI-8			CW(9.5 ksi)+D+CFRP Gusset+U-anchor*
Phase III	JIII-1	3866 psi	$0.18f'_cA_g$	Control
	JIII-2			CC(5.5 ksi)+D+GFRP Wrap+no anchor*
	JIII-3			CW(5.5 ksi)+D+GFRP Wrap+no anchor*
	JIII-4			CW(5.5 ksi)+D+GFRP Wrap+U-anchor*
Phase IV	JII-1	3309 psi	$0.21f'_cA_g$	Control
	JII-2			CFRP Wrap
	JII-3			PSL-C+D
	JII-4			PSL-W+D
	JII-5			PSL-C+CFRP Wrap+360°-anchor
	JII-6			PSL-C+D+CFRP Wrap+360°-anchor
	JII-7			PSL-W+D+CFRP Wrap+360°-anchor
	JII-8			PSL-W+D+GFRP Wrap+360°-anchor

Schematics of the strengthening scheme for specimen JI-4, which utilized SF filler-modules and CFRP wraps can be seen in Figure 5.3. The joints were loaded until failure with a monotonically increasing bending load, applied 6” away from the free end of the beam, and with a pre-determined constant axial load applied on the column (Denoted as CL in Table 5.1).

The results showed an increase in strength and ductility of up to 300%, as well as an increase of approximately 1200% in energy dissipation for the strengthened specimens compared to the control ones. Additionally, while all control joint specimens experienced shear failure through diagonal tension in the joint, the strengthened specimens failed either due to flexural failure of the beams or shear failure of the columns, with column and beam rebars having exceeded their yielding point in both cases. More specifically, specimens strengthened by plain FRP wrapping showed an increase in capacity, ductility, and energy dissipation of 69%, 100%, and 223% respectively, while specimens strengthened by plain filler-modules showed a limited increase in the same categories due to premature column failure. Specimens strengthened by both FRP wraps/gussets and filler-modules achieved up to 314%, 300%, and 1188% increase in capacity, ductility, and energy dissipation respectively, due to the relocation of the plastic hinge away from the joint and towards either the beam or the column.

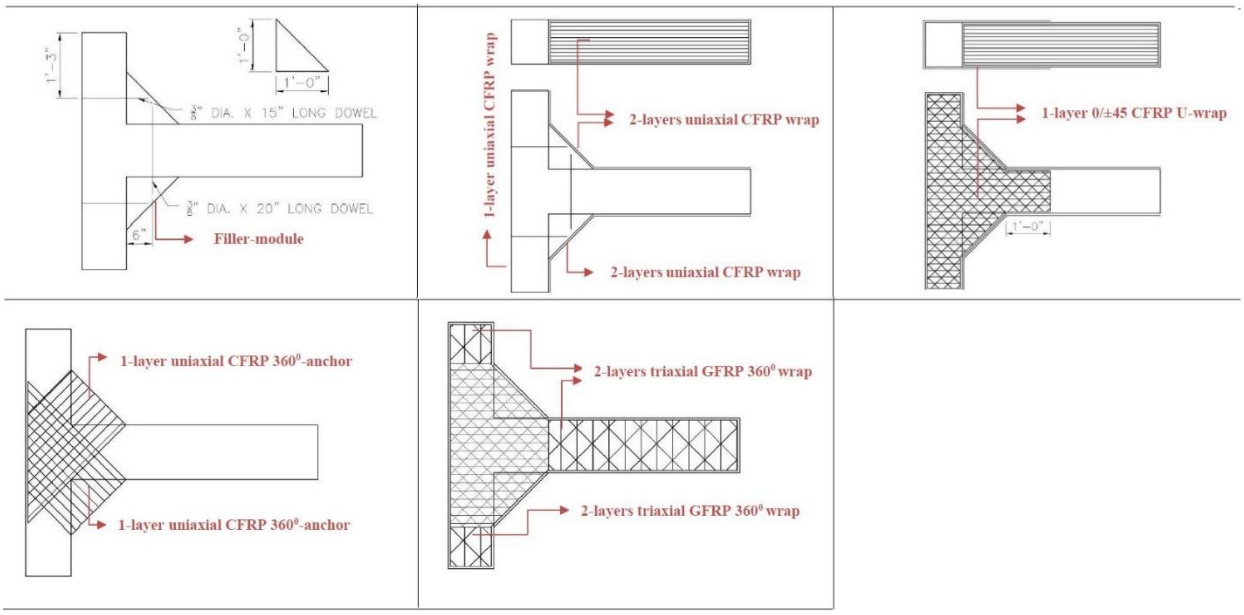

Figure 5.3 Schematics of the strengthening scheme used on specimen JI-4 (Majjigapu 2020)

The presence of reinforcing dowels increased capacity and energy dissipation by 47%, while the shape of the filler-modules had minimal influence on the performance of the

specimens. Finally, specimen JI-4 with the low stiffness SF filler-module and CFRP wraps performed overall best out of all the strengthening configurations, with 314%, 200%, and 1188% increases in capacity, ductility, and energy dissipation respectively (Figure 5.4), while the PSL filler-module with GFRP wraps achieved the highest increase in ductility, with 184%, 300%, and 1074% increases in capacity, ductility, and energy dissipation respectively.

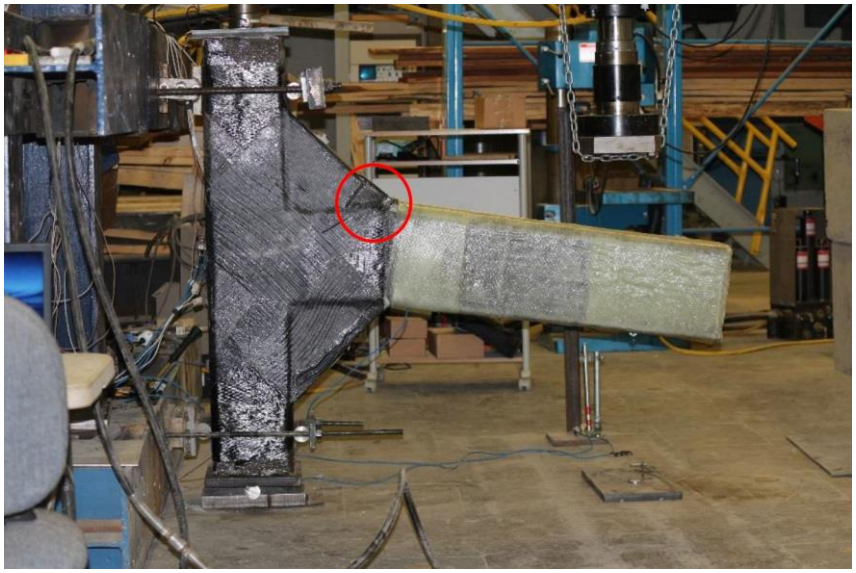

Figure 5.4 Specimen JI-4 at failure. (Majjigapu 2020)

The author concluded that the proposed method, using filler-modules with FRP wraps/gussets, is a viable method for strengthening RC joints under monotonic bending loads. His suggestions for future research include the testing of 3D joints, possibly with the addition of a slab, as well as performing reverse cyclic loading tests in order to evaluate the method's performance under earthquake loads.

5.3 EXPERIMENTAL INVESTIGATION OF THE EFFICACY OF EBROG METHOD IN SEISMIC REHABILITATION OF DEFICIENT REINFORCED CONCRETE BEAM-COLUMN JOINTS USING CFRP SHEETS (MOSTOFINEJAD AND AKHLAGHI 2017)

In many studies concerned with strengthening RC structural members with FRP, debonding of the FRP from the concrete substrate is the most common and undesirable failure mode. In order to avoid the FRP debonding failure, Mostofinejad and Mahmoudabadi (2010) developed an RC strengthening scheme they named Grooving Method and later renamed

Externally Bonded Reinforcement on Grooves (EBROG), according to which, grooves are cut on the surface of the concrete, are filled with epoxy, and have FRP sheets installed within them. Their study showed the ability of the EBROG scheme to increase the flexural capacity of RC beams by 80% compared to the conventional Externally Bonded (EB) scheme while delaying or even avoiding debonding failure. Mostofinejad and Akhlaghi (2017), motivated by the positive performance of EBROG in the flexural strengthening of RC beams, evaluated the effectiveness of EBROG in the seismic rehabilitation of shear deficient RC joints, by testing six RC joint specimens strengthened with different configurations of CFRP wraps according to the EBROG scheme.

The six RC joint specimens consisted of a 250x250x1500 mm (9 7/8”x9 7/8”x4’-11”) column and a 300x250x1500 mm (11 6/8”x 9 7/8”x4’-11”) beam and included one unstrengthened control specimen and five CFRP EBROG strengthened specimens with different amounts of layers, different sheet lengths, different wrapping configurations, and with and without the use of FRP fans for anchoring. The specimens were constructed with f'_c=30 MPa (4.3 ksi) concrete, reinforced by f_y=400 MPa (58 ksi) steel bars, and strengthened by unidirectional CFRP layers 1 mm (1/32”) thick each, with a tensile load capacity of f_u=420 MPa (61 ksi) and Young’s modulus of Ef=33 GPa (4.79 msi). As can be seen in the details of Table 5.2 and the schematics of Figure 5.5, specimens RDS3H75 and RDS3H325 had 3 horizontal CFRP layers extending 75 (3”) and 325 mm (1’-6/8”) towards the beam respectively, specimens RDS3H325F and RDS4H500F had 3 and 4 horizontal CFRP layers extending 325 mm (1’-6/8”) and 500 mm (1’-7 5/8”) towards the beam respectively and had the addition of CFRP dowels, and specimen RDS1X250 had 1 CFRP layer wrapped in the X-shape configuration at a 45° angle relative to the beam.

Table 5.2 Details of the test specimens (Mostofinejad and Akhlaghi 2017)

		CFRP sheet					
Number	Specimen	Configuration	Ply number	Length [L_f (mm)]	Width [w_f (mm)]	CFRP wrap	CFRP fan
1	DCS	—	—	—	—	—	—
2	RDS-3H75	U-shape	3	75	400	—	—
3	RDS-3H325	U-shape	3	325	400	—	—
4	RDS-3H325F	U-shape	3	325	400	—	On beam
5	RDS-4H500F	U-shape	4	500	300	—	On beam
6	RDS-1X250	X-shape	1	—	250	On beam	—

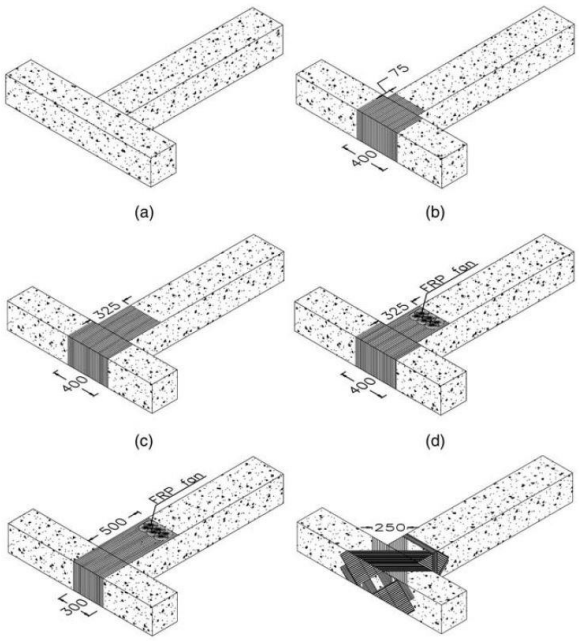

Figure 5.5 Schematics of the different EBROG strengthening configurations used in the study (Mostofinejad and Akhlaghi 2017)

The edges of the rectangular joint sections, where FRP wraps would be applied, were rounded with a minimum radius of 13 mm (4/8”) in order to avoid stress concentrations as per the guidelines of ACI 440.2R-17 (2017). According to the EBROG method, 10x10 mm grooves were cut on all sides of the joint core and adjacent beam and column surfaces where CFRP sheets would be applied, with 30 mm (1 1/8”) spacing between them (Figure 5.6). The grooves were filled with epoxy, and a thin epoxy layer was also placed on the concrete surface before the CFRP sheets were installed. The CFRP fans were made by cutting CFRP sheets to the appropriate length, wrapping them together in strands, keeping a uniform fiber alignment, and bonding their middle portion together with epoxy. The fans were then installed by placing their one end into an epoxy-filled predrilled hole in the concrete surface, and by bonding their other end to the wrapped CFRP sheets. The tests were conducted inside a stiff steel frame, where the specimens were applied a constant 185 kN (41.6 kip) axial vertical load and a reversed cyclic horizontal load at the top of the specimens’ columns. The reversed cyclic loading was done according to ACI Committee 374.1, with three fully reversed cycles for each drift ratio, and an increment of approximately 1% between drift ratios.

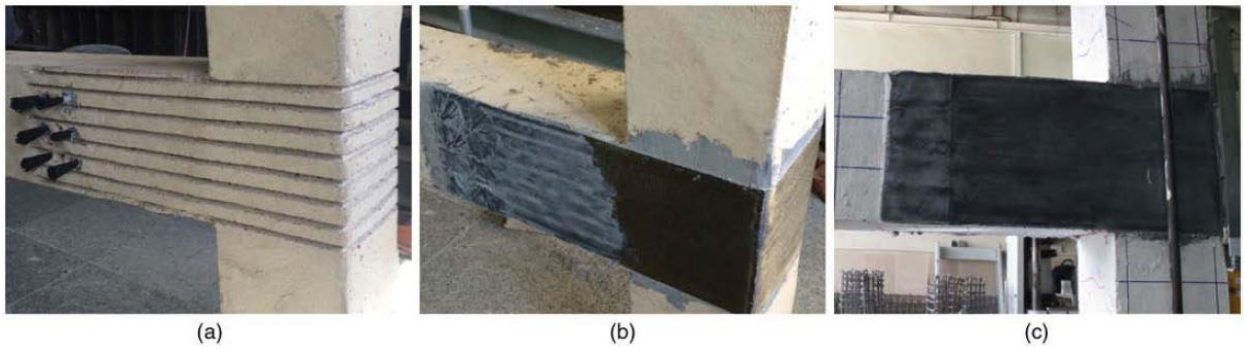

Figure 5.6 Installation procedure for horizontal EBROG CFRP sheets (a) Cutting of grooves and installation of anchoring fans, (b) Application of the first CFRP layer and spreading of the fans, (c) Installation of the final CFRP layer (Mostofinejad and Akhlaghi 2017)

The results showed that the U-wrapped specimens with the combined use of CFRP fans and the X-wrapped specimen successfully avoided FRP debonding failures and achieved a ductile behavior with significant increases in load capacity, ductility, and energy dissipation, as well as reductions in stiffness degradation, while the U-wrapped specimens without CFRP fans failed due to debonding and had a non-ductile behavior, similar to the control specimen (Figure 5.7). More specifically,

- The control specimen achieved a peak capacity of 63.8 kN (14.34 kip) at 2.2% drift ratio and reached a brittle shear failure at 4.5% drift ratio, with 46 kN (10.34 kip) load capacity.
- Specimens RDS3H75 and RDS3H325 exhibited non-ductile behavior after delamination at 2.75% and 3.5% drift ratios respectively.
- Specimen RDS3H325F exhibited a ductile behavior with no FRP debonding and achieved a peak capacity of 86.5 kN (19.4 kip) at 5.2% drift ratio which was 36% higher than the control specimen. It also achieved 68% higher ductility, 140% higher energy dissipation, and 80% lower stiffness degradation compared to the control specimen. Notably, the peak load capacity of this specimen was possibly higher than recorded, since the testing could not exceed 5.2% drift ratio due to limitations of the testing equipment. In the final stages of the test, a plastic hinge started to develop on the beam, around the termination point of the CFRP sheets.
- Specimen RDS4H500F exhibited similar behavior to its 325F counterpart, but with a peak load of 97 kN (21.8 kip) at 4.5% drift ratio which was 52% higher than the control

specimen. It achieved 32.5% higher ductility, 88% higher energy dissipation, and 110% lower stiffness degradation compared to the control specimen. According to the authors, the observed values for ductility and energy dissipation for this specimen are lower than expected due to the yielding of the column's steel rebar during the test.

- Specimen RDS1X250 exhibited a ductile behavior with a peak load of 74.7 kN (16.8 kip) at 4.5% drift ratio, which was 17% higher than the control specimen. At 3.5% drift ratio it experienced partial debonding at the back side of the column, where no grooves had been cut out. However, no debonding was observed in other areas where grooves were cut out. It achieved 72.5% higher ductility, 81% higher energy dissipation, and 61% lower stiffness degradation than the control specimen.

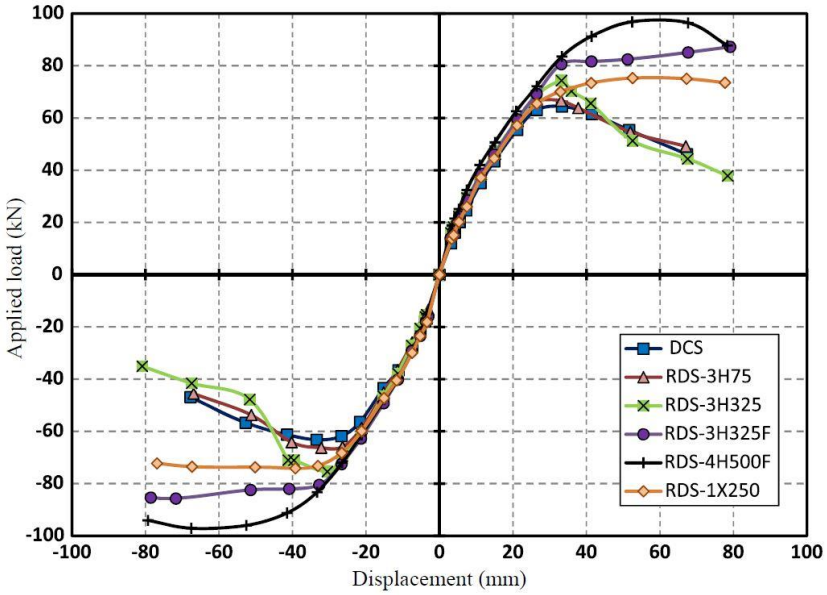

Figure 5.7 Load-displacement curves of test specimens. (Mostofinejad and Akhlaghi 2017)

The authors concluded that using EBROG CFRP with the combined use of CFRP anchoring fans is a viable method for strengthening and seismically rehabilitating shear-critical RC joints. It is capable of eliminating FRP debonding failure, relocating the formation of the plastic hinge away from the joint and towards the beam, and increasing load capacity, ductility, and energy dissipation.

5.4 REPAIR OF SEVERLY-DAMAGED RC EXTERIOR BEAM-COLUMN JOINTS WITH FRP AND FRCM COMPOSITES (FALESCHINI ET AL. 2019)

Externally Bonded (EB) FRP and FRCM are commonly used modern rehabilitation methods for RC joints, however, more research is needed to better understand and accurately predict the effects of their application. Additionally, most current research is focused on the strengthening of undamaged RC joint specimens, while the repair of damaged specimens is relatively understudied. With the goal of enriching the literature concerned with the repair of RC joints with EB FRP and FRCM, Faleschini et al. (2019) studied the behavior of three previously damaged RC joint specimens, repaired with different configurations of EB FRP and FRCM, under the same lateral cyclic loads that caused their original damages.

The three joint specimens consisted of 500x300x2500 mm (1'-7 5/8"x11 6/8"x8'-2 3/8") beams and 300x300x4100 mm (11 6/8"x11 6/8"x13'-5 3/8") columns and were made with different concrete strengths each, with cube compressive strengths of 48.7, 60.6, and 54.9 MPa (7, 8.8, and 7.9 ksi) for specimens 1, 2, and 3 respectively. The equivalent cylindric compressive strength is approximately 40, 50, and 45 MPa (5.8, 7.2, and 6.5 ksi) respectively. They were reinforced with f_y=555 MPa (80.5 ksi) steel longitudinal and f_y=485 MPa (70.3 ksi) steel transverse rebars, similarly to other existing Italian RC buildings of low ductility class (Figure 5.8).

The original specimens were tested under lateral cyclic loading and exhibited a beam and joint failure, with yielding of the beams' longitudinal rebars and severe cracking and spalling in the joint area. The details of the original tests were recorded by Faleschini et al. (2017) and showed a peak strength of 74.7 kN (16.8 kip), 80.0 kN (18 kip), and 80.6 kN (18.12 kip) in the push direction, and 79.2 kN (17.8 kip), 85.0 kN (19.1 kip), and 75.3 kN (16.9 kip) in the pull direction, for specimens 1, 2, and 3 respectively, while all three original specimens exhibited a 30% reduction in strength and a 15% stiffness degradation by the end of the test.

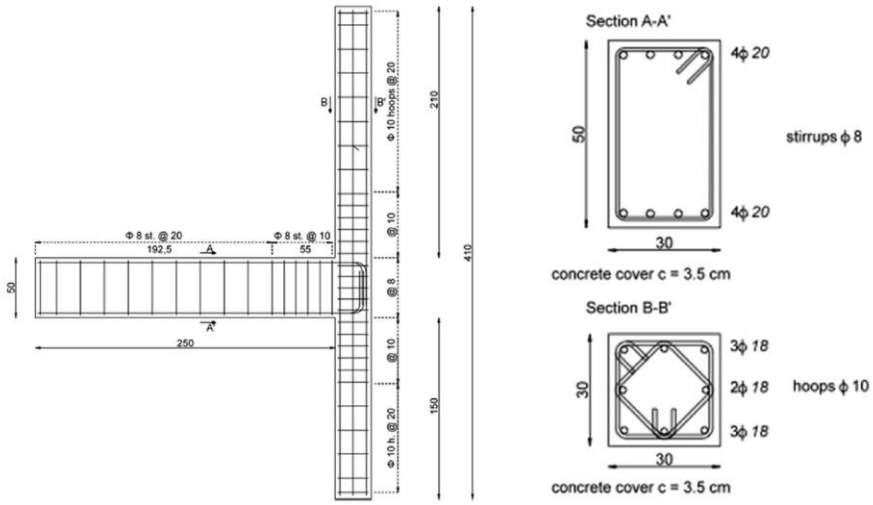

Figure 5.8 Dimensions and reinforcement details of the test specimens. (Faleschini et al. 2019)

For this study, after inspection, the loose concrete of the damaged original specimens was removed, their surfaces were cleaned, and their sections restored to their original dimensions using f'_c=32 MPa (4.6 ksi) concrete, but it was decided that the cracks within the region confined by steel rebar should not be filled, in order to better evaluate the effectiveness of the FRP and FRCM repairs. The repairing schemes of the three specimens can be seen in Figure 5.9, and in short:

- Specimen 1 was repaired with FRCM, using f'_c=32 MPa (4.6 ksi) concrete as the matrix, and using two layers of bidirectional carbon fibers with an ultimate tensile strength of f_u=4700 MPa (682 ksi), Young's modulus of E_f=240 GPa (34.8 msi), and an ultimate strain of ε_f=1.8%. The final thickness of the repairing layer was t=20 mm.
- Specimens 2 and 3 were repaired with FRP, using an unnamed epoxy resin as the matrix and two layers of unidirectional carbon fibers with an ultimate tensile strength of f_u=3000 MPa (435 ksi), Young's modulus of E_f=390 GPa (55.5 msi), and an ultimate strain of ε_f=0.8%.
- Specimen 2 had its fiber layers installed at an angle in the joint area, aligned according to the expected principal stresses, while Specimen 3 had its fiber layers installed horizontally in the joint area and had them extend to the beam's sides.

During the test, a constant 400 kN (89.9 kip) axial load and a reversed cyclic lateral load were applied at the top of the columns, with 13 displacement steps in the lateral cyclic loads and

three full loading cycles for each step, starting at 2 mm (3/32”) and ending at 150 mm (5 7/8”) displacement, which was equivalent to 3.9% drift ratio.

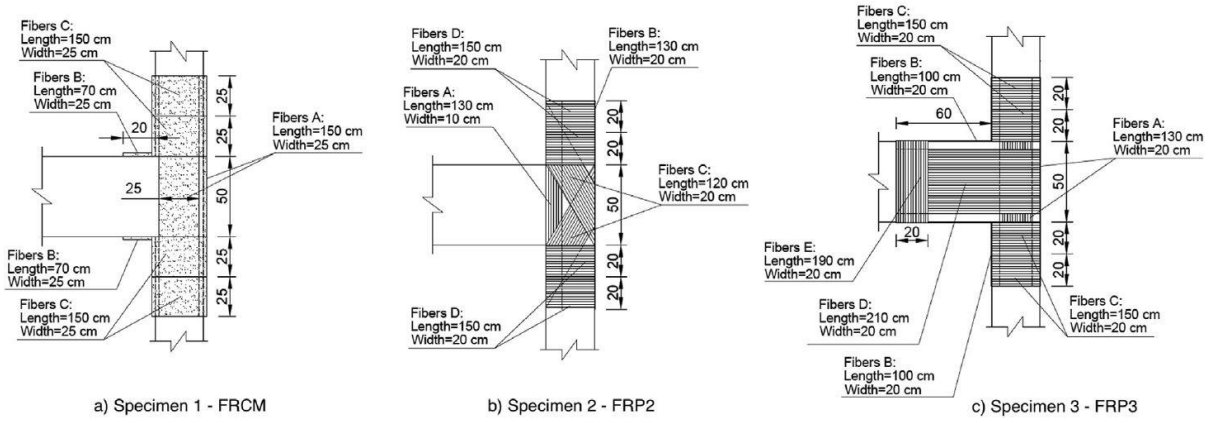

Figure 5.9 Schematics of the three different repair schemes (Faleschini et al. 2019)

The results showed that all three repaired specimens were unable to restore the load capacity to the level of the original specimens. However, it should be noted that the peak loads of the repaired specimens were recorded at the last displacement step which could not be further increased due to limitations of the testing equipment, meaning that the true load capacity of the repaired specimens could be higher than observed. More specifically,

- Specimen 1 achieved 84% and 60% of the original’s peak strength in the push and pull directions respectively, and exhibited new vertical, horizontal, and diagonal cracks in the joint area and wide new vertical cracks in the column area, but no new cracks in the beam area.
- Specimen 2 achieved 79% and 70% of the original’s peak strength in the push and pull directions respectively, with diagonal fibers in the joint area fracturing due to their alignment maximizing their effectiveness.
- Specimen 3 achieved 65% and 76% of the original’s peak strength in the push and pull directions respectively, with concrete crushing at the exterior of the column.

The repaired specimens also exhibited lower ductility and energy dissipation than the original specimens but achieved a final stiffness similar to the originals’ even though their initial stiffness was significantly lower.

The authors concluded that the repair of RC joints using only EB FRP and FRCM is unable to restore a damaged joint's load capacity, ductility, and energy dissipation, but is able to reduce the rate of stiffness degradation, which is a desirable quality in earthquake design. The authors believe that the results of this study emphasize the importance of crack injections in repairing damaged RC joints and suggest further research to focus on the contribution of crack injections to the behavior of repaired joints and their interaction with different EB reinforcements.

5.5 BEHAVIOR OF RC EXTERIOR BEAM COLUMN JOINT RETROFITTED USING UHP-HFRC (SHARMA AND BANSAL 2019)

Ultra-High Performance Hybrid Fiber Reinforced Concrete (UHP-HFRC) is a material that combines the compressive strength of Ultra-High-Performance Concrete with the tensile strength and ductility of steel fibers. Intending to improve knowledge on the effect of different levels of damage on the behavior of rehabilitated RC joints, Sharma and Bansal (2019) tested four RC joints, previously damaged to predetermined levels and retrofitted with UHP-HFRC, under quasi-static reverse cyclic loading.

The four joint specimens consisted of 225x125x950 mm (8 7/8"x4 7/8"x3'-1 3/8") beams and 225x125x1000 mm (8 7/8"x4 7/8"x3'-3 3/8") columns, constructed with f'_c=20 MPa (2.9 ksi) concrete and reinforced with f_y=415 MPa (60 ksi) steel as can be seen in Figure 5.10 (Left). The level of damage dealt to the specimens was determined with the Park-Ang damage model, according to which, values of a dimensional index D are assigned to damaged members, with D>1 meaning complete, 0.6<D<0.8 severe, 0.4<D<0.6 moderate, 0.2<D<0.4 slight, and D=0 meaning no damage. The columns of the specimens were loaded at 10% of their axial load capacity, while the beams were loaded at their free ends with a vertical reversed cyclic load at incremental steps of 5 mm (2/8") displacements until they achieved the desired level of damage for each specimen, that was D=1 (complete or CD), D=0.75 (severe or SED), D=45 (moderate or MD), and D=0.3 (slight or SD). After the initial loading procedure, the damaged specimens had the concrete cover around their joint area removed (Figure 5.10 Right) and replaced with UHP-HFRC that included both steel micro-fibers of 15 mm (5/8") length and steel macro-fibers of 60 mm (2 3/8") length and had a cubic compressive strength of 125.4 MPa (18.2 ksi) which is equivalent to approximately 100 MPa (14.5 ksi) cylindric strength. After casting and curing, the

rehabilitated specimens were then tested until failure with the same procedure as the original specimens.

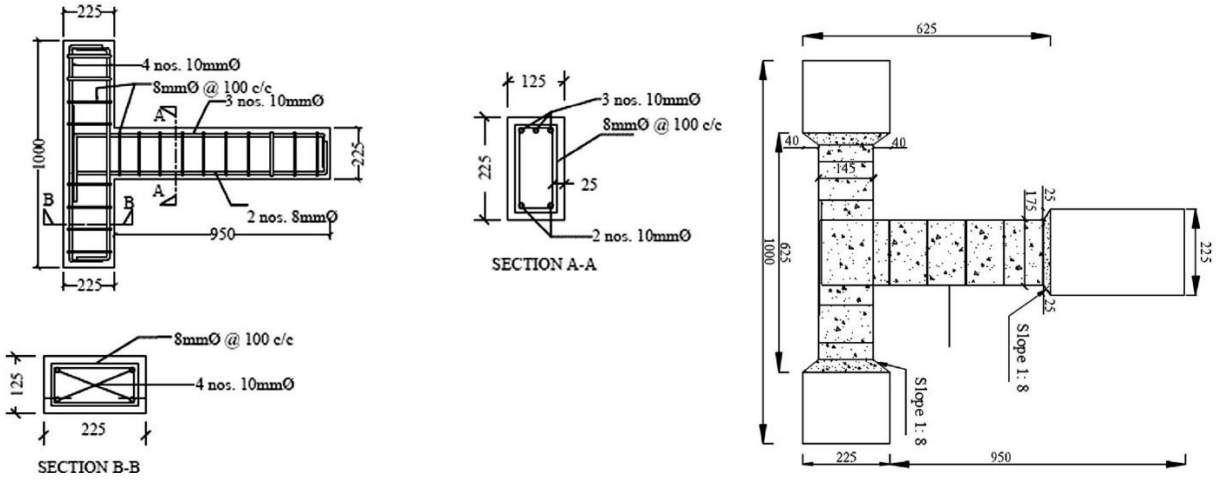

Figure 5.10 Left: Dimensions and reinforcement details of the specimens. Right: Schematic showing the concrete area removed from the damaged specimens. (Sharma and Bansal 2019)

The results showed that the control specimen reached complete damage level (D=1) at 35 mm (1 3/8”) displacement at approximately 8 kN (1.8 kip) and 21 kN (4.7 kip) peak loads in the compression and tension face respectively, with steel yielding and concrete cracking in the joint area of the compression face of the beam due to it having less steel reinforcement than the tension face. Similarly, the rehabilitated CD specimen (RCD) exhibited a sudden drop in capacity at 10 mm (3/8”) displacement, due to the steel rebar in the compression face having previously yielded and failed by concrete cracking in the joint area of the compression side of the beam at 25 mm (1”) displacement. In contrast, specimens RSED, RMD, and RSD failed in flexure at 35 mm (1 3/8”), 40 mm (1 5/8”), and 40 mm (1 5/8”), respectively, due to a plastic hinge forming in the beam-joint area, with RSED having a sudden drop in capacity at 25 mm (1”) displacement and RMD and RSD having a stable reduction in strength throughout the loading procedure. The authors also noticed that the micro and macro fibers were successful in resisting hairline and wider cracks in the plastic hinge area up until the highest drift ratios.

The peak loads of the rehabilitated specimens were 10 kN (2.25 kip), 26 kN (5.85 kip), 27 kN (6.07 kip), and 27 kN (6.07 kip) at the compression face and 42 kN (9.44 kip), 26 kN (5.85 kip), 28 kN (6.3 kip), and 31 kN (6.97 kip) at the tension face for specimens RCD, RSED, RND, and RSD respectively, showing a more than 200% increase in the compression face and a

24%-48% increase in the tension face for all specimens except RCD. Their initial stiffness was approximately three times higher and degraded at a lower rate than that of the control specimen, while the ductility of the rehabilitated specimens was 20%, 21.17%, 40.29%, and 43.29% higher, and the cumulative energy dissipation was 1.14, 1.58, 2.08, and 2.48 times larger than the control specimen for specimens RCD, RSED, RMD, RSD respectively.

The authors concluded that UHP-HFRC jacketing of RC joints is a viable repair and rehabilitation method capable of restoring the load capacity, stiffness, ductility, and energy dissipation of the joint area of completely and severely damaged members while improving the aforementioned parameters for moderately and slightly damaged members.

5.6 SEISMIC PERFORMANCE OF REINFORCED CONCRETE BEAM-COLUMN JOINT STRENGTHENING BY FRP SHEETS (ATTARI ET AL. 2019)

Considering the high strength and stiffness of Carbon FRP (CFRP) along with its brittle behavior in failure and comparing it to the lower strength, lower stiffness, and relatively higher ductility of the cheaper Glass FRP (GFRP), Attari et al. 2019 aimed to evaluate the effectiveness of CFRP, GFRP, and of a hybrid Carbon-Glass FRP in seismically rehabilitating possibly damaged RC joints. For that purpose, they studied the behavior of 10 RC joints with different levels of damage, strengthened with different configurations of FRP materials, under reverse cyclic loading.

The 10 RC joint specimens were constructed in 1/3 scale and consisted of 100x150 mm (3 7/8”x5 7/8”) beams and columns made of f'_c=39 MPa (5.6 ksi) concrete and reinforced with f_y=500 MPa (72.5 ksi) steel, with the reinforcement details shown in Figure 5.11. The materials used for strengthening the specimens and their ultimate strength (f_u), Young’s modulus (E_f), ultimate strain (ε_f), and thickness (t) are listed below:

- A unidirectional CFRP: f_u=403 MPa (58.4 ksi), E_f=43.5 GPa (6.3 msi), ε_f=0.95%, t=1.5mm (1/16”)
- A unidirectional GFRP: f_u=325 MPa (47.1 ksi), E_f=19.2 GPa (2.78 msi), ε_f=1.7%, t=2mm (3/32”)
- A bidirectional Carbon-Glass hybrid FRP: f_u=218 MPa (31.6 ksi), E_f=27 GPa (3.9 msi), ε_f=0.85% t=2mm (3/32”)

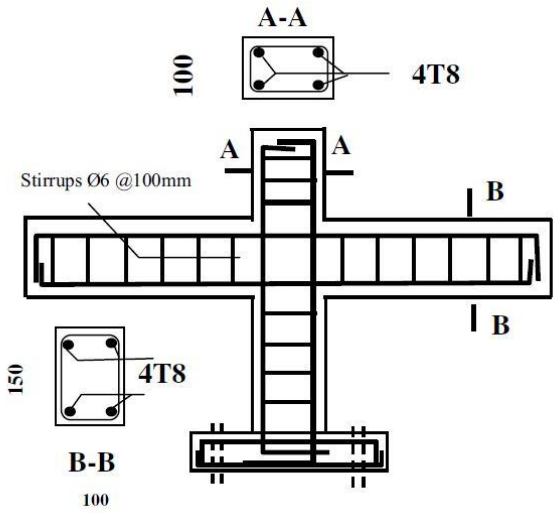

Figure 5.11 Reinforcement details for all specimens except NC2. Specimen NC2 had additional beam shear reinforcement in the joint area (Attari et al. 2019)

The details of the RC joint specimens and the strengthening configurations used on them can be seen in Table 5.3. In summary, specimens NC1 and NC2 are unstrengthened control specimens, with NC2 having additional stirrups in the joint area. Specimens NA2 and NA3 had L-shaped wrapping configurations at the four joint corners as well as wrapping on the beams and compared the effectiveness of CFRP with the hybrid FRP. Specimens NB4 and NB5 used a strengthening configuration more viable for joints with slabs, that included L-shaped wraps at the joint corners and long FRP layers covering the bottom part of the sides of the beams and were used to compare the effectiveness of GFRP and hybrid FRP. Specimens NC1R and NC2R were the rehabilitated versions of the completely damaged control specimens NC1 and NC2 that had their steel reinforcement yield, while specimens NR1 and NR2 were new specimens that were damaged to sustain 0.2 mm (1/128”) wide cracks at their joints without yield of their steel reinforcement.

Table 5.3 Details of the specimens and their strengthening configurations (Attari et al. 2019)

No	state		Specimen	Details
1	Control		NC1	Without stirrups in the joint
2			NC2	With stirrups in the joint
3	Strengthening	Series A	NA2	4 × 1 L CFRP fabric wrap 0° + 1 CFRP fabric wrap 90° (See Fig. 5)
4			NA3	4 × 2 L HFRP fabric wrap 0° + 2 Hexcel-HFRP fabric wraps 90° (See Fig. 5)
5		Series B	NB4	4 × 1 L CFRP fabric wrap 0° + 2 GFRP (on the bottom of the beam) (See Fig. 6)
6			NB5	4 × 1 L HFRP fabric wrap 0° + 2 Hexcel-HFRP fabric wraps (on the bottom of the beam) (See Fig. 6)
7	Repairing		NC1R	4 Pultruded Carbon + 4 L GFRP + 2 U GFRP fabric 90° (See Fig. 7)
8			NC2R	4 × 1 L CFRP + GFRP fabric 0° + 2 U GFRP 90° (See Fig. 8)
9			NR1	4 Pultruded Carbon + 4 × 1 L GFRP fabric wrap
10			NR2	4 × 2 L GFRP fabric wrap + 2 GFRP (on the faces of the beam) (See Fig. 10)

The rehabilitated specimens had their damaged areas cleaned, their cracks filled with epoxy, and their sections strengthened with a combination of long FRP layers on the top and bottom of the beams, L-shaped wraps at the joint corners, U-wraps at the bottom of the beams, and long wraps that covered the two sides of the beams. In addition, all specimens had column confinement near the joints with one layer of GFRP (Figure 5.12). The specimens were tested under a constant vertical 100 kN (22.5 kip) axial load on the column and a vertical reverse cyclic load, applied at the free ends of the beams, with incremental displacement steps of 0.25 mm (1/128") increasing until failure and with five full cycles per step.

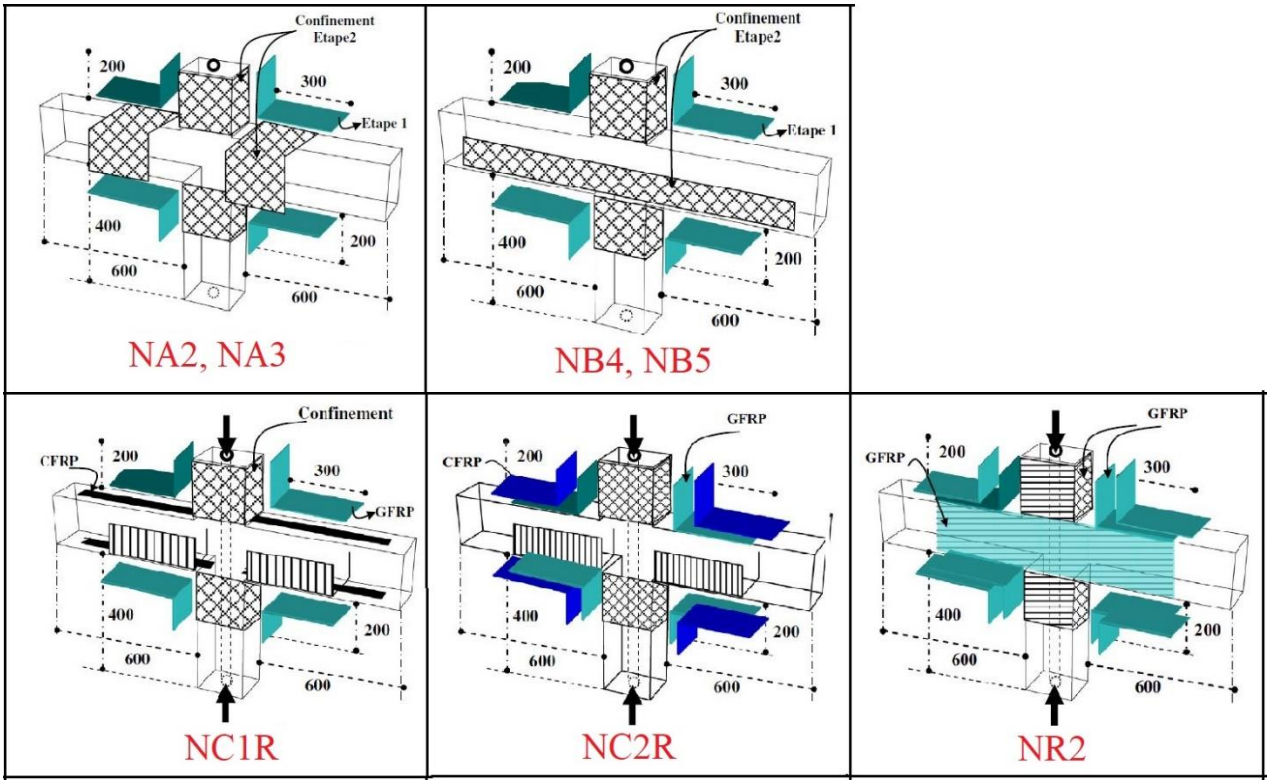

Figure 5.12 Strengthening schemes for the joint specimens (Attari et al. 2019)

The results showed that all specimens failed due to the formation of vertical cracks at the beam-joint interface, with all rehabilitated specimens except the completely damaged NC1R and NC2R showing various degrees of performance improvements, and the GFRP and hybrid FRP performing as well as CFRP. More specifically,

- The control specimens NC1 and NC2 achieved a peak load of 12.57 kN (2.82 kip) and 12.83 kN (2.88 kip) with a 7.64 mm and 8.22 mm (approximately 5/16”) deformation at failure respectively.
- Specimens NA2 and NA3 achieved peak loads of 14.3 kN (3.21 kip) and 13.2 kN (2.97 kip) respectively with an 8.9 mm (3/8”) and 8.36 mm (5/16”) deformation at failure. The specimens dissipated the same amount of cumulative energy, showcasing the hybrid FRP’s ability to compete with CFRP.
- Specimens NB4 and NB5 had an asymmetric behavior due to having more reinforcement at the top of the beams than at the bottom and had different displacements at the top and bottom sides of the beams. The specimens achieved peak loads of 15 kN (3.37 kip) and 15.4 kN (3.46 kip), and deformation at failure at the bottom of 13.5 mm and 13.8 mm (4/8”) respectively, while they both had deformation at failure at the top of 9 mm (3/8”). Specimen NB4 dissipated 78% more energy than the control specimens due to its ductile GFRP flexural reinforcement.
- Specimens NC1R and NC2R were unable to restore the specimens’ original performance due to the steel reinforcement at the top of their beams having yielded before testing. They achieved peak loads of 10.6 kN (2.38 kip) and 6.13 kN (1.38 kip) respectively, with 6.77 mm (2/8”) and 2.01 mm (3/32”) deformations at failure.
- Specimens NR1 and NR2 achieved significant increases in strength and stiffness, achieving peak loads of 18.4 kN (4.13 kip) and 23 kN (5.17 kip) respectively while having 7.5 mm (5/16”) and 13.6 mm (4/8”) deformations at failure. Specimen NR2 specifically had an 89% increase in peak load, while its increased deformation at failure allowed it to dissipate 350% more energy compared to the control specimens.

The authors concluded that when strengthening RC joints with FRP, hybrid and Glass FRP can have results similar to Carbon FRP with the benefit of a lower cost, with GFRP able to provide the highest increase to the joint’s ductility. The strengthening schemes employed in their study were able to increase the specimens’ load capacities by up to 89% and their energy dissipation by up to 350%, while their attempt at restoring the performance of a fully damaged RC joint using only FRP wrapping was unsuccessful.

5.7 A COMBINATION OF GFRP SHEETS AND STEEL CAGE FOR SEISMIC STRENGTHENING OF SHEAR-DEFICIENT CORNER RC BEAM-COLUMN JOINTS (ESMAEELI ET AL. 2017)

The use of Externally Bonded FRP for strengthening RC members is a commonly used modern solution, with FRP premature debonding being one of its most common and undesirable forms of failure. Additionally, its application for joints is further complicated due to the existence of beams and slabs not allowing the wrapping of three or four sides of the joint, and the solution of anchoring and extending FRP on the faces of beams may increase the beams' flexural strength and lead instead to shear failure in the joint. Esmaeeli et al. (2017) propose a novel rehabilitation method for RC joints, that aims to utilize the full strength of GFRP wrapping by anchoring it to a steel cage. For that purpose, the authors studied the behavior of two full-scale 3D external joints, strengthened by the proposed method, under reverse cyclic loading.

The two similar 3D full-scale RC joint specimens represented external joints, which are the weakest type of joint against lateral loads, and one of them was strengthened with the proposed method while the other was not strengthened and acted as the control specimen. They were built using f'_c=30 MPa (4.3 ksi) concrete and reinforced by f_y=500 MPa (72.5 ksi) longitudinal and f_y=365 MPa (53 ksi) transverse steel rebars, with no stirrups in the joint area to ensure shear failure in the joint (Figure 5.13).

The strengthening configuration included GFRP wrapping, applied according to Figure 5.14, with four layers of bidirectional Glass fibers of tensile strength f_f=3400 MPa (493 ksi), tensile modulus E_f=73 GPa (10.6 msi), strain at failure ε_f=4.5% and thickness t=0.067 mm (1/512"), and an epoxy of tensile strength f_m=76.1 MPa (11 ksi) and tensile modulus E_m=2789 MPa (404.5 ksi). The steel cage was made of steel angles, placed at the corners of the column as can be seen in Figure 5.15, and tied to each other with steel threaded rods of 10 mm (3/8") diameter and nuts applying 10 N.m (7.37 ft-lb) torque.

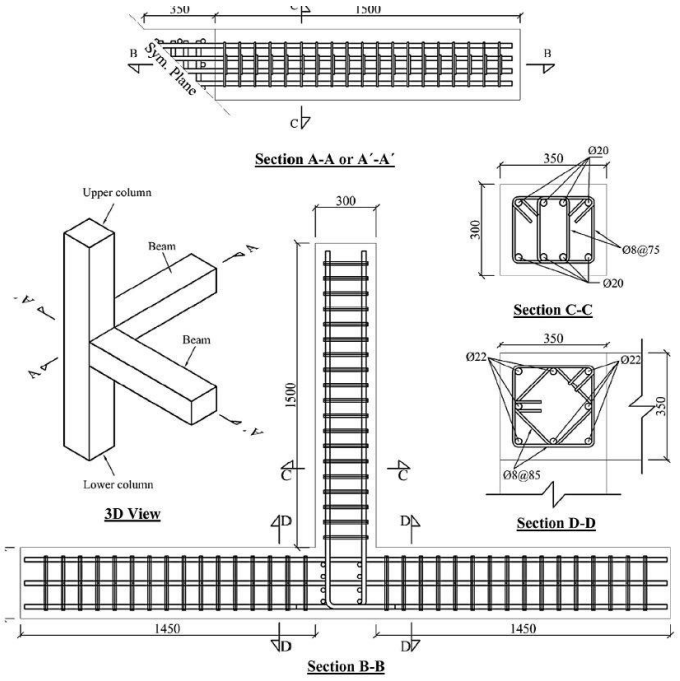

Figure 5.13 Dimensions and reinforcement details of the specimens (Esmaeeli et al. 2017)

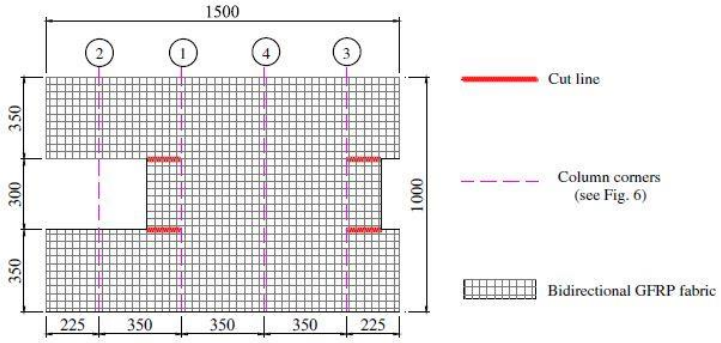

Figure 5.14 Configuration of the bidirectional GFRP sheets (Esmaeeli et al. 2017)

During the test, a constant 370 kN (83.2 kip) axial load, representing 10% of the columns' capacity was applied to the columns, while both beams were loaded with a quasi-static reverse cyclic load at the beams' free ends, with incremental displacement steps of 0.4% drift angle, and two full loading cycles for each step. The tests terminated at 30% of strength loss for each specimen.

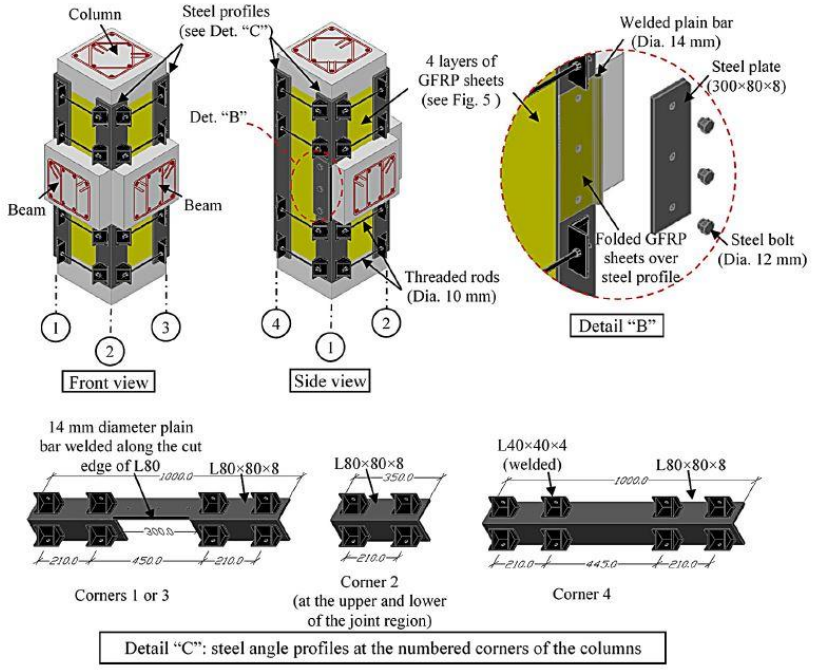

Figure 5.15 Details of the steel cage (Esmaeeli et al. 2017)

The results showed that the control specimen reached its peak load at 1.6% and failed at a 2% drift angle due to inclined shear cracks at the joint, without beam or column steel reinforcement yielding. On the other hand, the strengthened specimen reached its peak load at 2% and dropped 30% of its strength at a 6% drift angle, with the beams' steel rebars having yielded, flexural cracks having formed on the beams, and the GFRP sheets being undamaged.

After the test, the authors removed the steel cage and GFRP wraps at the joint area and observed that the concrete in the joint area was uniformly crushed, with the proposed strengthening configuration having successfully prevented the beams' flexural cracks from penetrating the joint area. Additionally, the strengthened specimen achieved a 60% higher load capacity with a 25% higher drift angle at peak load, a 28% increase in ductility, a 14% higher initial stiffness with a 40% higher stiffness at a 2% drift angle, and 10.7 times higher energy dissipation. The strengthened specimen exhibited a sudden post-peak drop of 9% in strength at a 2% drift ratio, followed by a plateau in strength until 3.6%, after which, its strength steadily dropped to 70% of its peak strength at a 6% drift ratio. This excellent ductile behavior is responsible for the significant increase in energy dissipation and can be observed in the shear load versus drift angle diagram of Figure 5.16.

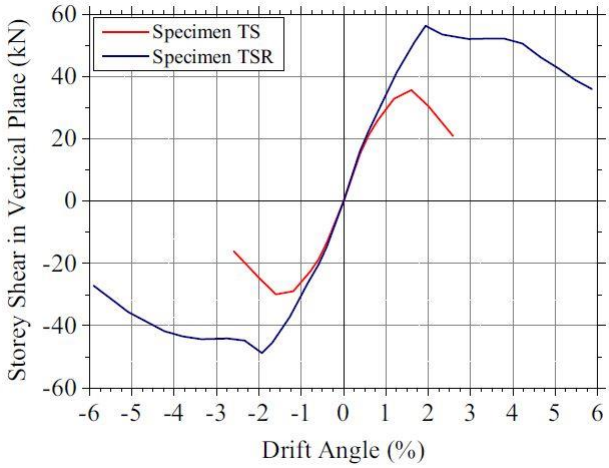

Figure 5.16 Shear load versus drift angle diagram for the control (TS) and strengthened (TSR) specimens (Esmaeeli et al. 2017)

The authors concluded that their proposed method is an effective way of seismically rehabilitating shear deficient RC joints, capable of increasing their load capacity, initial stiffness, ductility, and energy dissipation, decreasing their stiffness degradation, and changing their brittle shear failure into a ductile failure mode while providing ease of installation for any type of RC joint, without the need to drill through concrete to provide anchorage.

5.8 SUMMARY

This chapter has presented six techniques for the rehabilitation of RC joints, utilizing (a) a combination of filler-modules and FRP wraps, (b) the EBROG method with CFRP sheets, (c) FRP and FRCM for the repair of damaged joints, (d) UHP-HFRC, (e) a combination of CFRP, GFRP, and hybrid FRP sheets, and (f) a combination of GFRP sheets and steel cage. The studies under which the techniques were developed, varied in the types of joint specimens they used, as well as the types of loading they applied to their specimens, with most studies using 2D joints and specimens with one beam, and testing their specimens under reverse cyclic loading. The exceptions were studies (f) which used 3D joints, (e) and (f) which used specimens with two beams, and (a) which tested its specimens under monotonic loading. While the developed techniques cannot be directly compared, the following are some interesting takeaways.

- Neither (c) FRCM and FRP, (e) Glass and hybrid FRP, nor (d) UHPFRC jacketing techniques were able to sufficiently repair damaged RC joint with yielded longitudinal beam rebars, with FRCM, FRP, and Glass and hybrid FRP jacketing unable to restore the

specimens' load capacity, and even though UHPFRC jacketing was able to do so, it was unable to restore the specimens' deformation capacity.

- The (b) EBROG CFRP, (d) UHPFRC, (e) Glass and hybrid FRP, and (f) GFRP with steel cage methods were successful in strengthening RC joints by increasing their load capacities up to 89% in the case of Glass and hybrid FRP and energy dissipation up to 1070% in the case of GFRP with a steel cage.
- The efficiency of GFRP and hybrid Glass-Carbon FRP in rehabilitating RC joints was proven to be comparable and even superior to the more expensive CFRP.
- The (a) filler-module with FRP wraps method achieved a 314% increase in load capacity and an 1188% increase in energy dissipation when tested under monotonic loading, but needs to be tested under cyclic loading to prove its effectiveness in seismic rehabilitation.

6 CONCLUSIONS AND RECOMMENDATIONS

6.1 CONCLUSIONS

This problem report has presented a literature review on innovative techniques for the rehabilitation of Reinforced Concrete buildings, focusing on techniques developed after 2017. The techniques were presented in categories based on their scope, which is either global (structural level) or local (element level), and their target, which is either RC beams, RC columns, or RC beam-column joints. The following conclusions have been derived from the literature review:

- Building rehabilitation is gaining relevance in recent years due to the high cost of new construction and is especially important in the life cycle of RC buildings.
- While older rehabilitation methods remain effective even by today's standards, newer techniques utilizing modern materials can provide greater effectiveness and efficiency.
- Innovative global seismic rehabilitation techniques for RC buildings involve improvements in the use of masonry infill walls, exoskeletons, seismic dampers, and base isolation to upgrade the performance of buildings under earthquake loads.
- Each type of global rehabilitation technique has unique advantages and disadvantages, and the optimal technique depends on the needs of the individual building.
- Innovative RC beam, RC column, and RC beam-column joint rehabilitation techniques involve the use of modern materials, such as FRP, FRCM, ECC, and UHPFRC, as well as the use of traditional materials, such as steel, in novel ways.
- FRP remains the most popular and studied material for local rehabilitation techniques, with the highest performance in strengthening RC members of all types but with a high dependence on sufficient anchorage in order to avoid premature debonding failures.
- FRCM, TRC, and ECC are viable materials for local rehabilitation and can provide significant performance improvements, but not at the level provided by FRP. Their advantages lie in their higher heat resistance and lower cost relative to FRP.
- UHPFRC, in the context of this problem report, was most successful in repairing damaged RC columns and beam-column joints due to its high compressive and tensile strength contributing toward the column's axial load capacity and confinement, as well as

its steel fibers resisting the propagation of cracks. However, it was at most, able to come on par with FRP when used for strengthening undamaged RC members.

- Innovative techniques utilizing steel for rehabilitating RC columns and beam-column joints can provide significant performance improvements, showing that steel is capable of keeping up with newer materials.

6.2 RECOMMENDATIONS

- With building rehabilitation becoming more relevant in recent years, it would be beneficial if more universities worldwide raised awareness by providing relevant undergraduate or graduate courses for Civil Engineers.
- While the amount of research on rehabilitating RC buildings is significant, the types of testing procedures and test specimens vary highly. An effort must be made to standardize the construction and testing of specimens in order to facilitate data analysis and comparison across multiple studies.
- Concerning future research on rehabilitation techniques utilizing FRP, emphasis should be placed on developing techniques for providing sufficient anchorage of FRP and avoiding premature debonding failure.

REFERENCES

ACI 440.2R-17 (2017). “Guide for the Design and Construction of Externally Bonded FRP Systems for Strengthening Concrete Structures.” American Concrete Institute, Farmington Hills, MI.

ASCE/SEI 41-17 (2017). “Seismic Evaluation and Retrofit of Existing Buildings.” American Society of Civil Engineers, Reston, VA.

Attari, N., Y. S. Youcef, and S. Amziane. (2019). “Seismic performance of reinforced concrete beam–column joint strengthening by frp sheets.” Structures, 20: 353–364. https://doi.org/10.1016/j.istruc.2019.04.007.

Beschi, C., A. Meda, and P. Riva. (2011). “Column and joint retrofitting with high performance fiber reinforced concrete jacketing.” J. Earthq. Eng., 15 (7): 989–1014. https://doi.org/10.1080/13632469.2011.552167.

Bilotta, A., F. Ceroni, M. Di Ludovico, E. Nigro, M. Pecce, and G. Manfredi. (2011). “Bond efficiency of EBR and NSM FRP systems for strengthening concrete members.” J. Compos. Constr., 15 (5): 757–772. https://doi.org/10.1061/(asce)cc.1943-5614.0000204.

Bilotta, A., F. Ceroni, E. Nigro, and M. Pecce. (2015). “Efficiency of CFRP NSM strips and EBR plates for flexural strengthening of RC beams and loading pattern influence.” Compos. Struct., 124: 163–175. https://doi.org/10.1016/j.compstruct.2014.12.046.

Choi, Y. (2018). “Shear strengthening of concrete columns by textile reinforced UHPC jacketing.” Master’s Thesis, Dept. of Architecture and Architectural Engineering, Seoul National Univ., South Korea.

Dagenais, M.-A., and B. Massicotte. (2015). “Tension lap splices strengthened with ultrahigh-performance fiber-reinforced concrete.” J. Mater. Civ. Eng., 27 (7). https://doi.org/10.1061/(asce)mt.1943-5533.0001169.

De Domenico, D., and G. Ricciardi. (2018). “An enhanced base isolation system equipped with optimal tuned mass damper inerter (TMDI): An enhanced base-isolation system equipped with optimal tuned mass damper inerter (TMDI).” Earthq. Eng. Struct. Dyn., 47 (5): 1169–1192. https://doi.org/10.1002/eqe.3011.

De Luca, A., and L. G. Guidi. (2019). “State of art in the worldwide evolution of base isolation design.” Soil Dyn. Earthq. Eng., 125. https://doi.org/10.1016/j.soildyn.2019.105722.

Deng, M., Y. Zhang, and Q. Li. (2018). “Shear strengthening of RC short columns with ECC jacket: Cyclic behavior tests.” Eng. Struct., 160: 535–545. https://doi.org/10.1016/j.engstruct.2018.01.061.

Di Lorenzo, G., E. Colacurcio, A. Di Filippo, A. Formisano, A. Massimilla, and R. Landolfo. (2020). “State-of-the-art on steel exoskeletons for seismic retrofit of existing RC buildings.” Ingegneria Sismica, 37 (1): 33–50.

Duic, J., S. Kenno, and S. Das. (2018). “Flexural rehabilitation and strengthening of concrete beams with BFRP composite.” J. Compos. Constr., 22 (4). https://doi.org/10.1061/(asce)cc.1943-5614.0000851.

Eldin, M. N., A. J. Dereje, and J. Kim. (2020). “Seismic retrofit of RC buildings using self-centering PC frames with friction-dampers.” Eng. Struct., 208. https://doi.org/10.1016/j.engstruct.2019.109925.

Engindeniz, M., L. F. Kahn, and A.-H. Zureick. (2005). “Repair and strengthening of reinforced concrete beam-column joints: State of the art.” ACI Struct. J., 102 (2): 187–197. https://doi.org/10.14359/14269.

Esmaeeli, E., F. Danesh, K. F. Tee, and S. Eshghi. (2017). “A combination of GFRP sheets and steel cage for seismic strengthening of shear-deficient corner RC beam-column joints.” Compos. Struct., 159: 206–219. https://doi.org/10.1016/j.compstruct.2016.09.064.

Faleschini, F., J. Gonzalez-Libreros, M. A. Zanini, L. Hofer, L. Sneed, and C. Pellegrino. (2019). “Repair of severely-damaged RC exterior beam-column joints with FRP and FRCM composites.” Compos. Struct., 207: 352–363. https://doi.org/10.1016/j.compstruct.2018.09.059.

Faleschini, F., L. Hofer, M. A. Zanini, M. dalla Benetta, and C. Pellegrino. (2017). “Experimental behavior of beam-column joints made with EAF concrete under cyclic loading.” Eng. Struct., 139: 81–95. https://doi.org/10.1016/j.engstruct.2017.02.038.

FEMA356 (2000). “Prestandard and Commentary for the Seismic Rehabilitation of Buildings.” Federal Emergency Management Agency, Washington, D.C.

Gkournelos, P. D., T. C. Triantafillou, and D. A. Bournas. (2021). “Seismic upgrading of existing reinforced concrete buildings: A state-of-the-art review.” Eng. Struct., 240. https://doi.org/10.1016/j.engstruct.2021.112273.

Grazide, C., E. Ferrier, and L. Michel. (2020). “Rehabilitation of reinforced concrete structures using FRP and wood.” Constr. Build. Mater., 234. https://doi.org/10.1016/j.conbuildmat.2019.117716.

Hamakareem, M. I. (2019). “Seismic dampers - types, working mechanism, and components.” *The Constructor*. Accessed October 21, 2022. https://theconstructor.org/earthquake/seismic-dampers/8332/.

Hong, S.-G., J.-H. Lee, Y. Choi, and I.-Y. Gu. (2021). “Seismic strengthening of concrete columns by ultrahigh-performance fiber-reinforced concrete jacketing.” J. Struct. Eng. (N. Y.), 147 (10). https://doi.org/10.1061/(asce)st.1943-541x.0003111.

Hur, M.-W., Y. Lee, M.-J. Jeon, and S.-H. Lee. (2022)a. “Seismic strengthening of RC structures using wall-type Kagome damping system.” Buildings, 12 (1). https://doi.org/10.3390/buildings12010041.

Hur, M.-W., Y. Lee, M.-J. Jeon, and S.-H. Lee. (2022)b. “Seismic strengthening of RC structures using wall-type Kagome damping system.” Buildings, 12 (1): 41. https://doi.org/10.3390/buildings12010041.

Javidan, M. M., and J. Kim. (2019). “Seismic retrofit of soft-first-story structures using rotational friction dampers.” J. Struct. Eng. (N. Y.), 145 (12). https://doi.org/10.1061/(asce)st.1943-541x.0002433.

Kadhim, A. M. H., H. A. Numan, and M. Özakça. (2019). “Flexural strengthening and rehabilitation of reinforced concrete beam using BFRP composites: Finite element approach.” Adv. Civ. Eng., 2019: 1–17. https://doi.org/10.1155/2019/4981750.

Kargaran, A., and A. Kheyroddin. (2020). “Experimental investigation of seismic strengthening of reinforced concrete short columns using externally bonded reinforcement, near surface mounted, and hybrid techniques.” J. Compos. Mater., 54 (9): 1177–1195. https://doi.org/10.1177/0021998319874499.

Khorramian, K., and P. Sadeghian. (2019). “Performance of high-modulus near-surface-mounted FRP laminates for strengthening of concrete columns.” Compos. B Eng., 164: 90–102. https://doi.org/10.1016/j.compositesb.2018.11.064.

Kim, Y. Y., H.-J. Kong, and V. C. Li. (2003). “Design of engineered cementitious composite suitable for wet-mixture shotcreting.” ACI Mater. J., 100 (6): 511–518. https://doi.org/10.14359/12958.

Koutas, L., S. N. Bousias, and T. C. Triantafillou. (2015). “Seismic strengthening of masonry-infilled RC frames with TRM: Experimental study.” J. Compos. Constr., 19 (2). https://doi.org/10.1061/(asce)cc.1943-5614.0000507.

Koutas, L. N., Z. Tetta, D. A. Bournas, and T. C. Triantafillou. (2019). “Strengthening of concrete structures with textile reinforced mortars: State-of-the-art review.” J. Compos. Constr., 23 (1). https://doi.org/10.1061/(asce)cc.1943-5614.0000882.

Lundqvist, J., H. Nordin, B. Täljsten, and T. Olofsson. (2005). “Numerical analysis of concrete beams strengthened with CFRP -a study of anchorage lengths.” Proceedings of international symposium on bond behaviour of FRP in structures, Hong Kong China, December 7-9, 2005. p. 239–46.

Majjigapu, P. K. R. (2020). “Monotonic response of RC exterior beam-column joints reinforced with filler-modules and FRP composite wraps/gussets.” Ph.D. Dissertation, Wadsworth Department of Civil and Environmental Engineering, West Virginia University, Morgantown, WV.

Manfredi, V., and A. Masi. (2018). “Seismic strengthening and energy efficiency: Towards an integrated approach for the rehabilitation of existing RC buildings.” Buildings, 8 (3). https://doi.org/10.3390/buildings8030036.

Manfredi, V., A. Masi, G. Ventura, L. Chiauzzi, A. Digrisolo, and G. Santarsiero. (2018). “Rafforzamento sismico degli edifici esistenti in c.a. una soluzione innovativa per interventi integrati e sostenibili.” Structural, 215.

Manfredi, V., G. Santarsiero, A. Masi, and G. Ventura. (2021). “The high-Performance Dissipating Frame (HPDF) system for the seismic strengthening of RC existing buildings.” Sustainability, 13 (4). https://doi.org/10.3390/su13041864.

Mhanna, H. H., R. A. Hawileh, and J. A. Abdalla. (2019). “Shear strengthening of reinforced concrete beams using CFRP wraps.” Procedia struct. integr., 17: 214–221. https://doi.org/10.1016/j.prostr.2019.08.029.

Mostofinejad, D., and A. Akhlaghi. (2017). “Experimental investigation of the efficacy of EBROG method in seismic rehabilitation of deficient reinforced concrete beam–column joints using CFRP sheets.” J. Compos. Constr., 21 (4): 04016116. https://doi.org/10.1061/(asce)cc.1943-5614.0000781.

Mostofinejad, D., and E. Mahmoudabadi. (2010). “Grooving as alternative method of surface preparation to postpone debonding of FRP laminates in concrete beams.” J. Compos. Constr., 14 (6): 804–811. https://doi.org/10.1061/(asce)cc.1943-5614.0000117.

TMS 402/602-16 (2016). “Building Code Requirements and Specification for Masonry Structures.” Masonry Standards Joint Committee.

Murcia-Delso, J., S. M. Alcocer, O. Arnau, Y. Martínez, and D. Murià-Vila. (2020). “Seismic rehabilitation of concrete buildings after the 1985 and 2017 earthquakes in Mexico City.” Earthq. Spectra, 36: 175–198. https://doi.org/10.1177/8755293020957372.

Nobili, A., and F. O. Falope. (2017). “Impregnated carbon fabric–reinforced cementitious matrix composite for rehabilitation of the finale Emilia hospital roofs: Case study.” J. Compos. Constr., 21 (4). https://doi.org/10.1061/(asce)cc.1943-5614.0000780.

Oinam, R. M., and D. R. Sahoo. (2017). “Seismic rehabilitation of damaged reinforced concrete frames using combined metallic yielding passive devices.” Struct. Infrastruct. Eng.: Maint. Manage. Life-Cycle Des. Perform., 13 (6): 816–830. https://doi.org/10.1080/15732479.2016.1190766.

Oinam, R. M., D. R. Sahoo, and R. Sindhu. (2014). “Cyclic response of non-ductile RC frame with steel fibers at beam-column joints and plastic hinge regions.” J. Earthq. Eng., 18 (6): 908–928. https://doi.org/10.1080/13632469.2014.916239.

Ortlepp, R., and S. Ortlepp. (2017). “Textile reinforced concrete for strengthening of RC columns: A contribution to resource conservation through the preservation of structures.” Constr. Build. Mater., 132: 150–160. https://doi.org/10.1016/j.conbuildmat.2016.11.133.

Pardalopoulos, S. I., S. J. Pantazopoulou, and G. E. Thermou. (2020). “Seismic rehabilitation of substandard R.c. buildings with masonry infills.” J. Earthq. Eng., 24 (2): 298–327. https://doi.org/10.1080/13632469.2018.1453397.

Pohoryles, D. A., C. Maduta, D. A. Bournas, and L. A. Kouris. (2020). “Energy performance of existing residential buildings in Europe: A novel approach combining energy with seismic retrofitting.” Energy Build., 223. https://doi.org/10.1016/j.enbuild.2020.110024.

Pohoryles, D. A., J. Melo, T. Rossetto, H. Varum, and L. Bisby. (2019). “Seismic retrofit schemes with FRP for deficient RC beam-column joints: State-of-the-art review.” J. Compos. Constr., 23 (4). https://doi.org/10.1061/(asce)cc.1943-5614.0000950.

Raoof, S. M., L. N. Koutas, and D. A. Bournas. (2017). “Textile-reinforced mortar (TRM) versus fibre-reinforced polymers (FRP) in flexural strengthening of RC beams.” Constr. Build. Mater., 151: 279–291. https://doi.org/10.1016/j.conbuildmat.2017.05.023.

Reggio, A., L. Restuccia, L. Martelli, and G. A. Ferro. (2019). “Seismic performance of exoskeleton structures.” Eng. Struct., 198. https://doi.org/10.1016/j.engstruct.2019.109459.

Sabau, C., C. Popescu, G. Sas, J. W. Schmidt, T. Blanksvärd, and B. Täljsten. (2018). “Strengthening of RC beams using bottom and side NSM reinforcement.” Compos. B Eng., 149: 82–91. https://doi.org/10.1016/j.compositesb.2018.05.011.

Shan, Z. W., D. T. W. Looi, and R. K. L. Su. (2020). “A novel seismic strengthening method of RC columns confined by direct fastening steel plates.” Eng. Struct., 218. https://doi.org/10.1016/j.engstruct.2020.110838.

Sharbatdar, M. K., and A. Tajari. (2021). “Experimental in-plane seismic strengthening of masonry infilled reinforced concrete frames by engineered cementitious composites (ECC).” Constr. Build. Mater., 293 (123529): 123529. https://doi.org/10.1016/j.conbuildmat.2021.123529.

Sharma, R., and P. P. Bansal. (2019). “Behavior of RC exterior beam column joint retrofitted using UHP-HFRC.” Constr. Build. Mater., 195: 376–389. https://doi.org/10.1016/j.conbuildmat.2018.11.052.

Siddika, A., M. A. A. Mamun, R. Alyousef, and Y. H. M. Amran. (2019). “Strengthening of reinforced concrete beams by using fiber-reinforced polymer composites: A review.” J. Build. Eng., 25. https://doi.org/10.1016/j.jobe.2019.100798.

Taraithia, S. S., Sahoo, D. R., Madan, A. (2013). “Experimental study of combined yielding metallic passive devices for enhanced energy dissipation of structures.” Proceedings of Pacific Structural Steel Conference, Singapore.

Tayeh, B. A., M. A. Naja, S. Shihada, and M. Arafa. (2019). “Repairing and strengthening of damaged RC columns using thin concrete jacketing.” Adv. Civ. Eng., 2019: 1–16. https://doi.org/10.1155/2019/2987412.

“The seismic assessment of existing buildings, Part C, C7” (2017). New Zealand Society for Earthquake Engineering, Christchurch, New Zealand.

Thermou, G. E., and S. J. Pantazopoulou. (2011). “Assessment indices for the seismic vulnerability of existing R.C. buildings.” Earthq. Eng. Struct. Dyn., 40 (3): 293–313. https://doi.org/10.1002/eqe.1028.

Yang, X., W.-Y. Gao, J.-G. Dai, and Z.-D. Lu. (2020). “Shear strengthening of RC beams with FRP grid-reinforced ECC matrix.” Compos. Struct., 241. https://doi.org/10.1016/j.compstruct.2020.112120.

Younis, A., U. Ebead, and K. C. Shrestha. (2017). “Different FRCM systems for shear-strengthening of reinforced concrete beams.” Constr. Build. Mater., 153: 514–526. https://doi.org/10.1016/j.conbuildmat.2017.07.132.